Dissertation

submitted to the

Combined Faculties of the Natural Sciences and Mathematics
of the Ruperto-Carola University of Heidelberg, Germany

for the degree of

Doctor of Natural Sciences

by

Dipl.-Phys. **Sascha Zöllner**
born in Magdeburg, Germany

Final exam:

July 17, 2008

One-dimensional Few-boson Systems in Single- and Double-well Traps

Referees:

Prof. Dr. Peter Schmelcher
Priv.-Doz. Dr. Thomas Gasenzer

Eindimensionale Wenig-Bosonen-Systeme in Einzel- und Doppel-Topffallen. Gegenstand dieser Arbeit sind eindimensionale Systeme weniger Bosonen in einfach-harmonischen und Doppeltopf-Fallen. Dabei liegt der Schwerpunkt auf dem Übergang von schwachen Wechselwirkungen hin zum Grenzfall starker Abstoßung, in dem das Bose-Gas auf ein ideales Fermi-Gas abgebildet werden kann. Zur Beschreibung dieses *Fermionisierungs*-Übergangs dient eine hier entwickelte Exakte Diagonalisierung und eine numerisch exakte Quantendynamik-Methode (MCTDH). Der Übergangs-Mechanismus für den *Grundzustand* besteht in der Ausbildung eines Zweiteilchen-Korrelationsloches und der anschließenden Lokalisierung der einzelnen Teilchen, sobald diese sich hinreichend stark abstoßen. Dies schlägt sich nieder in der Verringerung der Kohärenz. Es wird gezeigt, wie der konkrete Verlauf des Fermionisierungs-Übergangs abhängt von der Fallen-Geometrie, der räumlichen Modulation der Wechselwirkung sowie der Teilchenzahl. Darüber hinaus untersuchen wir die niedrigsten *Anregungen* des Systems. Deren Verständnis erweist sich als wesentlich für die Untersuchung der *Tunnel-Dynamik* weniger Bosonen. Diese ändert ihren Charakter mit zunehmender Wechselwirkung von Einteilchen-Tunneln hin zu fragmentiertem Paar-Tunneln. Durch eine zusätzliche Potential-Differenz zwischen den Töpfen lassen sich zudem einzelne Tunnel-Resonanzen ansteuern. Dies ermöglicht die kontrollierte Entnahme einzelner Atome.

****

One-dimensional Few-boson Systems in Single- and Double-well Traps. This thesis studies the one-dimensional Bose gas in harmonic and double-well traps from a few-body perspective. The main emphasis is on the crossover from weak interactions to the fermionization limit of infinite repulsion, where the system maps to an ideal Fermi gas. To explore the structure as well as the quantum dynamics throughout that crossover, we both develop an exact-diagonalization approach and resort to a multi-configurational time-dependent method (MCTDH). The basic mechanism of the fermionization crossover for the *ground state* is shown to consist in the formation of a correlation hole in the two-body density, which culminates in a localization of the individual particles for strong repulsion. This is accompanied by a reduction of coherence. We demonstrate how the concrete pathway depends on the trap geometry, on the shape of the interaction, as well as on the atom number. By extension, we also investigate the lowest *excitations*, whose understanding is a base for studying the impact of the fermionization crossover on the *tunneling dynamics* in a double well. In symmetric wells, a pathway from single-particle to fragmented-pair tunneling shows up. By energetically offsetting the two wells, tunnel resonances become accessible, which may be used to extract single atoms.

Contents

Introduction

Ultracold atoms

In recent years, the research field of ultracold atoms has become highly popular, with an outreach extending far beyond atomic physics [1–3]. This is because ultracold atoms by now are an incredibly flexible toolbox. For one thing, it has become possible to *cool* atoms (chiefly, but not only, alkali gases) down to the regime of nano-Kelvin temperatures, where the de-Broglie wavelength exceeds the inter-particle distance to the extent that the quantum-mechanical wave features become crucial. This has been done drawing on a combination of different techniques such as laser or evaporative cooling [1, 4]. Moreover, exploiting the atoms' interaction with electromagnetic fields, both their *external* and *inter-particle* forces may be designed experimentally. For instance, the atoms can be stored in trapping environments such as the textbook harmonic potential; but also the seeming toy model of a ring-shaped trap has been realized [5]. By extension, it is possible to generate "optical lattices" via lasers, or to make the trap strongly anisotropic so as to confine the system to lower dimensions. Likewise, the effective interactions nowadays can be tuned almost at will via Feshbach resonances [6], so one can go all the way from switching off interactions completely to artificially creating strongly correlated systems.

This impressive toolbox has been applied to a variety of problems. A central aspect is that of quantum simulators, where the atoms are used to realize paradigmatic quantum systems. The seminal example here is Bose-Einstein condensation [1, 2, 4] – not only as it had been a longstanding prediction of statistical quantum mechanics, but also because the route toward its experimental realization opened up the door to exploring many other effects. Currently, cold atoms often serve as some kind of Rosetta stone for puzzles ranging from condensed-matter physics (e.g., superfluidity, superconductivity, magnetism, and disorder), nonlinear optics, and fundamental quantum problems (like vortices or tunneling) – to name but a few [7]. Other applications, such as sensoring via matter-wave interferometry [8] or, somewhat more visionary, quantum-information processing [9], draw on the high degree of coherence of Bose-Einstein condensates.

Few vs. many atoms

Bose-Einstein condensates—the core piece of most experiments—are typically produced with large particle numbers, say $N \sim 10^5$. By contrast, recent years have seen a trend toward the study of few-atom systems. For one thing, many *experiments* have undergone persistent miniaturization, so studying only few atoms is becoming a realistic perspective. Today there is a broad range of techniques allowing for the extraction, the controlled one-by-one transport and positioning of atoms via laser fields [10, 11] and storing small ensembles on a so-called atom chip [12]. It is also feasible to image them with up to microscopic resolution, both *in situ* (via fluorescence imaging [10] or impact ionization [13], where the signal may also be enhanced simply by producing an array with many different copies of the system as in [14]) or in time-of-flight measurements. On the other hand, studying few-body systems is fascinating from a *theoretical* standpoint. Apart from often being surprisingly rich in their own right—as exemplified in the exotic three-body Efimov states [15, 16]—few-body systems provide a "bottom-up" perspective on processes also underlying larger systems. This is facilitated by the fact that small systems are more amenable to *ab initio* calculations, which do not rely on any uncontrolled approximations, or in a few instances even afford analytic solutions, as in the case of two atoms in an isotropic [17] and, more generally, anisotropic harmonic trap [18].

1D Bose gas

One example where the combined potential of ultracold few-atom systems as quantum simulators has proven particularly expedient is the one-dimensional (1D) Bose gas. Since the old days of quantum mechanics—well, not quite the Paleolithic, rather the Middle Ages—this model system has allured researchers for its sometimes counterintuitive features. We are used to thinking of bosonic and fermionic particles as very disparate – bosons are often said to be "sociable" in allusion to the fact that they tend to condense into the same single-particle state at low temperatures, whereas fermions are in a way more aloof in that they obey Pauli's exclusion principle. Strikingly, in 1D there is a way to actually connect these two very different pictures – that is, to make bosons behave almost like fermions, or *vice versa*. More precisely, already in 1960 it has been proven by Girardeau that bosons with infinitely repulsive point interactions map one-to-one to an ideal Fermi gas [19]. In particular, the ground state is given simply by the absolute value of the fermionic one, the Slater determinant with all orbitals filled up to the Fermi edge. This makes it tempting to think of the exclusion principle as mimicking the effect of the hard-core repulsion, which is why this limit is termed *fermionization*. That general theorem was confirmed later on by Lieb and Liniger [20], who solved the special problem of the homogeneous Bose gas with periodic boundary conditions (i.e., on a ring of length L) exactly for arbitrary interaction strength in the thermodynamic limit ($N, L \to \infty$ with $n \equiv N/L$ fixed). The Lieb-Liniger solution was able to reproduce the fermionization prediction by letting the interaction strength tend to infinity.

The quest for fermionization

Thrilling as it was as a theoretical conception, this fermionization limit long remained an exotic toy model. It was not before the availability of ultracold atoms that its experimental realization came within reach. A cornerstone was set by Olshanii, who suggested that bosons under strong cylindrical confinement—such that the transverse motion were essentially frozen and the particles could move only in the longitudinal direction—would experience an effective 1D interaction strength that might depend very strongly on the transverse confinement [21]. This so-called confinement-induced resonance opened up the prospect of tuning the effective coupling so as to reach the fermionization limit. That two-body prediction was complemented by estimates of the parameter regimes necessary for its realization in a many-body system, requiring, amongst others, low densities and temperatures small compared to the transverse-excitation energy [22–24]. In 2004, eventually experimental evidence of fermionization was given virtually simultaneously by two groups [14, 25]. Sparked also by this experimental realization, there has recently been a proliferation of works focusing on that topic. Altogether these have given a fairly broad image of fermionized bosons, including their ground state in a harmonic trap [26, 27] and in a periodic potential [28], the self-similar expansion and breathing dynamics [29–31], fermionized dark solitons [32, 33], their coherence in interference experiments [34], Bragg reflections off optical lattices [35], and non-exponential decay behavior [36]

– a list which is nowhere near exhaustive.

Crossover to fermionization

Compared to that, little is known about the exact *transition* between the two borderline cases of the familiar weakly interacting Bose "condensate" and the above fermionization limit of infinite repulsion. As insinuated above, the thermodynamic Lieb-Liniger solution in principle describes the entire crossover and is consistent with the Bose-Fermi map. While their seminal paper was concerned solely with the energy spectrum, it has served as a base for some closer considerations on the crossover [22, 23]. A first step to take into account finite-size effects was taken via Monte-Carlo simulations [37] and later by extending the analytic Lieb-Liniger approach to finite systems [38]. However, in experiments, periodic boundary conditions are hard to impose. This naturally brings up the question of the impact of external traps, which render the system nonintegrable except in the simple case of two atoms in a harmonic trap [17, 39]. Here, a first indication of the onset of the characteristic fermion-like density profile upon confining the 3D system to quasi-1D was given by Monte-Carlo studies [40, 41]. Soon after, the fermionization transition was revisited from a multi-orbital mean-field perspective, which suggested to interpret it as a crossover from a "condensate" (where all particles occupy the same delocalized single-particle state) to an N-fold "fragmented" state, in the sense that each particle resides in a localized orbital [42]. However, by the time this thesis was started, the understanding of the crossover to fermionization was still somewhat patchy; and it has only been very recently that a complete picture has started to emerge [43–50].

This thesis

The goal of this thesis is to contribute to a systematic picture of the crossover to fermionization in trapped few-body systems. To tackle this numerically, two approaches have been pursued (Ch. 2): First, an exact-diagonalization approach for trapped bosons has been developed. However, most results in this thesis have been obtained via the numerically exact multi-configurational time-dependent Hartree method, a versatile scheme well known for its efficiency in wave-packet-dynamics applications.

To understand the basic mechanism of the fermionization crossover, we start out in Ch. 3 by studying the ground state in dependence on the atom number N, with a focus on the interplay between external and inter-particle forces [46, 47]. To this end, both the reference case of a harmonic trap as well as a double-well trap are investigated, the latter being a paradigm model for fundamental quantum effects like interferences or tunneling. Moreover, the role of the interaction is illuminated by considering also the situation where the interaction potential is inhomogeneous, in that the coupling constant is spatially modulated between the left and the right-hand side of the trap.

Chapter 4 extends that investigation to the low-lying excitations [48]. This way it bridges the gap between the ground state and the quantum dynamics studied in Ch. 5, which deals with the impact of the fermionization crossover on the tunneling dynamics in double-well traps [49, 50].

To keep this thesis largely self-contained, the reader is introduced to the theoretical background in Ch. 1. After reviewing some basic concepts and notations of many-body quantum mechanics, the effective model Hamiltonian for the ultracold, quasi-1D Bose gas is derived. This is complemented by a concise introduction to the analysis of many-body states in terms of correlation functions, as well as an overview of some salient soluble models in the context of the 1D Bose gas.

Chapter 1

Theoretical background

The objective of this thesis is a theoretical study of ultracold few-atom systems in traps. Here our focus is not on the structure of the individual atoms but on the interplay of *interatomic* and *external* trapping forces. After giving a concise but coherent review of the mathematical language of many-body physics and its Fock-space formulation in Sec. 1.1, we will set out to model the system. To this end, both the interaction of atoms with external electromagnetic fields (Sec. 1.2.1) and between atoms (Sec. 1.2.2) needs to be encoded in an effective Hamiltonian. Furthermore, in Sec. 1.2.3 we derive an effective description for quasi-one-dimensional systems, which arise in the limit of strong transversal confinement. After an interlude on density matrices (Sec. 1.3), which constitute an important tool to visualize correlations in many-particle systems, in Sec. 1.4 we present three simple models for which there exist analytic solutions. This provides a link to the investigation of concrete many-body systems.

1.1 Fock-space formulation of many-body physics

The subject of this thesis are systems of few interacting bosons. Despite the word *few* (in this context signifying $N < 10$), we are actually interested in treating the particle number as just another parameter, rather than exploiting *a priori* that our system contains exactly two atoms (or perhaps three or four) and tailor our treatment to account for just that fact. In light of this remark, the appropriate language is that of *many-body* physics—the so-called Fock-space formulation of quantum mechanics, also referred to as quantum field theory. Reviewing its concepts and, along the way, introducing some widely used notations will be the goal of this section.

Here we will follow the standard route in the context of *non-relativistic* field theory, which goes by the name of *Second Quantization*, indicating that it takes a detour over the ‘first quantization’ of *one-body* observables. Starting from the corresponding one-body states, the many-body states will be constructed ‘on top’, as it were. This is a very constructive and technical scheme, as opposed to the canonical approach that starts from a classical field theory and quantizes it directly.

1.1.1 Identical particles

To begin with, let us recapitulate the quantum mechanics of N identical particles [51, 52]. The indistinguishability postulate demands that, under any permutation of the particles $i = 1, \dots, N$, every physical state Ψ should change according to

$$U(P)\Psi = (\pm 1)^{\mathrm{inv}(P)}\,\Psi.$$

Here $P \in S_N$ is a member of the symmetric group, with its representation U on the Hilbert space and $\mathrm{inv}(P)$ denoting the minimum number of transpositions into which P can be decomposed. $U(P)$ is an invariant of the system, as it commutes with the Hamiltonian H (and with every observable, for that matter); hence its eigenvalues may be used to classify the corresponding eigenspaces: Particles obeying the $+$ sign are called *bosons*, while the alternating representation refers to *fermions*. Given that consideration, the above requirement asserts that Ψ lives only in *those* subspaces of the full (direct-product) space $\mathbb{H}_1^{\otimes N}$ that are invariant subspaces under the fully (anti-)symmetric representations of S_N, $U(P)$. In symbolic form,

$$\Psi \in \mathbb{H}_N^{\pm} \equiv \{\Psi \mid S_\pm \Psi = \Psi\},$$

where $S_\pm = \frac{1}{N!}\sum_{P\in S_N} (\pm 1)^{\mathrm{inv}(P)}\,U(P)$ denotes the orthogonal projectors onto the subspaces.

As an illustration, consider the (manifestly permutation-symmetric) single-body Hamiltonian $H_1 = \sum_{i=1}^N h(p_i, x_i)$, with eigenstates $(h - \epsilon_a)\phi_a = 0$. Were the particles distinguishable, the Hilbert space would most naturally be constructed as

$$\mathbb{H}_1^{\otimes N} = \mathrm{span}\{\Phi_{\boldsymbol{a}} \equiv \phi_{a_1} \otimes \cdots \otimes \phi_{a_N}\}.$$

The product state $\Phi_{\boldsymbol{a}}$ (using the convenient multi-index $\boldsymbol{a} \in \mathbb{Z}^N$) describes a configuration where particle $\#i$ occupies orbital ϕ_{a_i}. Symmetrizing it amounts to averaging $\boldsymbol{a}$ over all permutations,

$$\Phi_{\boldsymbol{n}}^{\pm} := \frac{S_\pm \Phi_{\boldsymbol{a}}}{\|S_\pm \Phi_{\boldsymbol{a}}\|} = \frac{1}{\sqrt{N!\boldsymbol{n}!}} \sum_{P\in S_N} (\pm 1)^{\mathrm{inv}(P)}\,\Phi_{P(\boldsymbol{a})}. \tag{1.1}$$

This needs some clarification: As we have wiped out the memory of *which* particle sits in *which* orbital, the only information we are left with is by *how many* particles each orbital ϕ_b is occupied:

$$n_b := \#\{i \mid a_i = b\} \equiv \sum_{i=1}^N \delta_{a_i,b}.$$

These *occupation numbers* for all orbitals $\{\phi_b\}$ are again collected in a multi-index[1] $\boldsymbol{n} = (n_0, n_1, \dots)$, which thus unambiguously characterize the *(occupation-)number state* $\Phi_{\boldsymbol{n}}^{\pm}$. The latter ones are normalized to one,

$$\langle \Phi_{\boldsymbol{n}'}^{\pm} | \Phi_{\boldsymbol{n}}^{\pm} \rangle = \delta_{\boldsymbol{n}',\boldsymbol{n}},$$

---

[1] We abide by the usual notation $\boldsymbol{n}! = \prod_a n_a!$ and $|\boldsymbol{n}| = \sum_a n_a$. Clearly $|\boldsymbol{n}| = N$ by conservation of the particle number.

which is secured by retaining $\|S_\pm \Phi_{\boldsymbol{a}}\|^2 = \frac{1}{N!}\boldsymbol{n}!$ in (1.1).

1.1.2 Fock-space formulation

By now, it has become apparent that this procedure, on top of being somewhat cumbersome, is unsatisfactory from a fundamental standpoint: For a system with a symmetry $U(P)$, we first create some symmetry-broken —i.e., unphysical— solution (such as $\Phi_{\boldsymbol{a}}$), and then go to great lengths to reinstate that symmetry by averaging over all equivalent solutions. This is highly redundant. Drawing on our key insight that we need not keep track of individual particles, but rather what states are occupied, we now devise a more efficient description encoding just that information.

The essential idea how to do this is to treat the particle number N not as an *a priori* parameter of the system, but solely as an observable, this way rendering the whole problem formally N-independent. As so often, a problem is solved by looking at it from a higher (and seemingly more complicated) ground: A state now lives on the Fock space

$$\mathbb{F} := \bigoplus_{N\in\mathbb{N}_0} \mathbb{H}_N \text{ , with } \mathbb{H}_0 \equiv \mathbb{C}$$

as opposed to the 'smaller' N-body Hilbert space.[2] Note that the trivial zero-body Hilbert space, spanned by the *vacuum* $|0\rangle \in \mathbb{H}_0$, is included for completeness. Concordantly, any Fock-space vector now is a denumerable collection $\Psi^{\mathbb{F}} = (\Psi^{(0)}, \Psi^{(1)}, \dots)$ of states with $N = 0, 1, \dots$ particles. Endowed with the canonical scalar product

$$\langle \Psi^{\mathbb{F}} | \Phi^{\mathbb{F}} \rangle := \sum_N \langle \Psi^{(N)} | \Phi^{(N)} \rangle,$$

$\mathbb{F}$ can be promoted to a Hilbert space.

Representing states

The task now is to express states as well as operators on Fock space. Here one resorts to a basis-specific construction: Choosing an arbitrary one-body basis, $\mathbb{H}_1 = \operatorname{span}\{\phi_a\}$, we found that $\mathbb{H}_N$ can be spanned by the symmetric product states (1.1) labeled solely by the occupation numbers n_a. Embedded in Fock space, we will now refer to these number states as $|\boldsymbol{n}\rangle \in \mathbb{F}$. However, irrespective of their physical meaning, the number states have the same mathematical structure as those of a simple harmonic oscillator: There, also all states were enumerated by a simple number $n = 0, 1, \dots$ —which could be recovered as an eigenvalue of some 'number operator' $\hat{n}$ defined as the absolute squared of a non-hermitian ladder operator $\hat{c}$. Recalling that this was footed on a very general algebraic structure and largely detached from the details of the harmonic oscillator, it is appealing to introduce just that structure in our context.[3] So define

---

[2] For now we suppress the superscript ± and, for simplicity, focus on the bosonic sector. There is no loss of generality, as only some signs differ, such as later on in the (anti-)commutation relations (1.2).

[3] Obviously, the difference here is that we have many occupation numbers n_a, instead of just one. Owing to the orthonormality of the one-body basis, though, the definition carries over to all modes a *separately*.

the *annihilation operator* for mode $\#a$

$$c_a|\boldsymbol{n}\rangle = \sqrt{n_a}|\boldsymbol{n} - \boldsymbol{e}_a\rangle, \qquad [c_a, c_b^\dagger] = \delta_{ab}1, \tag{1.2}$$

where for convenience we have introduced the shorthand

$$(\boldsymbol{e}_a)_b \equiv \delta_{ab}.$$

The familiar relations from the harmonic-oscillator model are obvious corollaries of this; just to touch on a few:

- the *creation operator* $c_a^\dagger|\boldsymbol{n}\rangle = \sqrt{n_a + 1}|\boldsymbol{n} + \boldsymbol{e}_a\rangle$
- the *number operator* $\hat{n}_a := c_a^\dagger c_a \geq 0$, with $\hat{n}_a|\boldsymbol{n}\rangle = n_a|\boldsymbol{n}\rangle$
- the vacuum: $c_a|0\rangle = 0$.

Most importantly, this puts us in a position to algebraically construct arbitrary number states (and thus a basis for the whole Fock space) via

$$|\boldsymbol{n}\rangle = \left(\prod_a \frac{1}{\sqrt{n_a!}}(c_a^\dagger)^{n_a}\right)|0\rangle.$$

In particular, the one-particle states can be embedded as $c_a^\dagger|0\rangle = 1|1_a\rangle \sim \phi_a$, and by iteration this goes for arbitrarily complicated $\Phi_{\boldsymbol{n}}^{\pm}$.

Before moving on, let us state that a unitary basis transformation $\varphi_b = \sum_a \langle\phi_a|\varphi_b\rangle\,\phi_a$ —invoking the above identification $C_b^\dagger|0\rangle = |1_b\rangle \sim \varphi_b$ —induces a unitary transform for the mode operators,

$$C_b = \sum_a \langle\varphi_b|\phi_a\rangle\,c_a,$$

which by unitarity leaves the commutation relations invariant. Academic though it may sound, this opens the door to a more intuitive description resembling the conventional field-theoretical one: Take the continuum limit $|\varphi_b\rangle \equiv |\mathbf{x}\rangle$, then this defines the *field operator*

$$\psi(\mathbf{x}) = \sum_a \phi_a(\mathbf{x})c_a, \quad \text{or} \quad c_a = \int d\mathbf{x}\,\phi_a^*(\mathbf{x})\psi(\mathbf{x}), \tag{1.3}$$

which obeys the continuum commutation relations $[\psi_{\mathbf{x}}, \psi_{\mathbf{x}'}^\dagger] = \delta(\mathbf{x} - \mathbf{x}')$.[4] Its meaning becomes clear from $\psi^\dagger(\mathbf{x})|0\rangle \sim |\mathbf{x}\rangle$: it is responsible for creating (destroying) a particle at position $\mathbf{x}$. The corresponding number operator becomes a density in the continuum limit, $\hat{n}(\mathbf{x}) = \psi^\dagger(\mathbf{x})\psi(\mathbf{x})$, which is normalized to the total number operator $\hat{N} = \int \psi^\dagger\psi$. To get a feeling for its appeal, consider the many-body position eigenstate

$$|\mathbf{x}_1, \dots, \mathbf{x}_N\rangle \equiv \psi^\dagger(\mathbf{x}_1)\cdots\psi^\dagger(\mathbf{x}_N)|0\rangle.$$

---

[4] Mathematically, this defines an operator-valued distribution via $\psi[\phi] := \int d\mathbf{x}\,\phi^*(\mathbf{x})\psi(\mathbf{x}) \equiv \langle\phi|\psi\rangle$, so strictly the ensuing commutation relations make sense only upon integration.

Applying the density operator $\psi^\dagger(\mathbf{x})\psi(\mathbf{x})$ yields, after some straightforward commutator algebra,

$$\hat{n}(\mathbf{x})|\mathbf{x}_1,\ldots,\mathbf{x}_N\rangle = \sum_{i=1}^{N}\delta(\mathbf{x}-\mathbf{x}_i)|\mathbf{x}_1,\ldots,\mathbf{x}_N\rangle.$$

This makes it tempting to think of the particles as point particles (represented by the field ψ), a notion that would seem somewhat awkward from the usual quantum-mechanics perspective of 'smeared-out' wave packets. Of course, these are but two different viewpoints of one and the same quantum theory: After all, $\psi(\mathbf{x})$ etc. are operators, and only their expectation values are meaningful—this is where the field theory links to standard quantum mechanics.

Representing operators

After having found a natural description of many-body *states* on Fock space, let us seek representations of *operators*. Of course, any operator on $\mathbb{H}_N$ can be trivially embedded in $\mathbb{F}$; more generally a Fock-space operator can even be a sum of N-body operators, $A^{\mathbb{F}} = \sum_N A_N$. Indeed, this is the special case if it commutes with the particle number, $[A^{\mathbb{F}}, \hat{N}]$, in which case all N-body sectors can be treated separately. Still there is a very general expansion theorem for any operator in terms of the mode operators $\{c_a\}$ (tacitly assuming a certain one-body basis):

$$A^{\mathbb{F}} = \sum_{N,N'}\sum_{\boldsymbol{a},\boldsymbol{a}'} A^{(N,N')}_{\boldsymbol{a},\boldsymbol{a}'}\left(\prod_{i=1}^{N} c^\dagger_{a_i}\right)\left(\prod_{j=1}^{N'} c^\dagger_{a'_j}\right)^\dagger. \tag{1.4}$$

This seemingly monstrous expression becomes clearer when applied to some prototype operators. Aside from the trivial examples $A^{\mathbb{F}} = 1$ or c_a, these are n-body operators on $\mathbb{H}_N$ ($n \le N$) with

$$A_n = \frac{1}{n!}\sum_{i_1\neq i_2\cdots\neq i_n}\mathcal{A}|_{i_1\ldots i_n}.$$

Here $\mathcal{A}$ operates in $\mathbb{H}_n$, each term acting only on particles $i_1,\ldots,i_n \in \{1,\ldots,N\}$. Then one can show that the expansion coefficients are diagonal in N, $A^{(N,N')}_{\boldsymbol{a},\boldsymbol{a}'} = \frac{1}{n!}\delta_{N,n}\delta_{N',n}\langle\Phi_{\boldsymbol{a}}|\mathcal{A}|\Phi_{\boldsymbol{a}'}\rangle$, and relate directly to n-body integrals

$$\langle\Phi_{\boldsymbol{a}}|\mathcal{A}|\Phi_{\boldsymbol{a}'}\rangle = \langle a_1\cdots a_n|\mathcal{A}|a'_1\cdots a'_n\rangle.$$

As an illustration, let us consider the two by far most frequent cases.

One-body operators Imagine a one-particle operator $H_1 = \sum_i h(\mathbf{p}_i,\mathbf{x}_i)$, with h operating in $\mathbb{H}_1$. Expanding it in terms of some basis $\{\phi_a\}$, the corresponding Fock-space operator takes the form

$$H_1^{\mathbb{F}} = \sum_{a,b}\langle a|h|b\rangle c_a^\dagger c_b.$$

If the basis diagonalizes h, this becomes simply $H_1 = \sum_a \epsilon_a \hat{n}_a$. This has a simple meaning: If we think of h as a one-particle Hamiltonian with spectrum $\{\epsilon_a\}$, then the eigenstates of the corresponding many-body operator will consist of number states $|\boldsymbol{n}\rangle$ of the one-body eigenstates φ_a; so the many-body spectrum is easily constructed by counting how many particles n_a

are in orbital $\#a$. We have thus obtained nothing but the analog of the Hilbert-space operator $H_1 = \sum_i h(\mathbf{p}_i, \mathbf{x}_i)$.

Two-body operators Along these lines, let us now consider the operator V on $\mathbb{H}_2$, which can be embedded in $\mathbb{H}_N$ via $H_2 = \sum_{i<j} V(\mathbf{x}_i, \mathbf{x}_j) = \frac{1}{2}\sum_{i\neq j} V(\mathbf{x}_i, \mathbf{x}_j)$.[5] Following the prescription leads to

$$H_2^{\mathbb{F}} = \frac{1}{2}\sum_{ab,cd} \langle ab|V|cd\rangle c_a^\dagger c_b^\dagger c_d c_c,$$

where $\langle ab|V|cd\rangle = \int d\mathbf{x}_1 d\mathbf{x}_2 \phi_a^*(\mathbf{x}_1)\phi_b^*(\mathbf{x}_2)V(\mathbf{x}_1, \mathbf{x}_2)\phi_c(\mathbf{x}_1)\phi_d(\mathbf{x}_2)$.

The one-body basis $\{\phi_a\}$ we had chosen is arbitrary. If we make the particular choice of the localized continuous basis $|\mathbf{x}\rangle$ with field operators $\psi(\mathbf{x})$, then the N-body Hamiltonian $H = H_1 + H_2$ becomes

$$H^{\mathbb{F}} = \int d\mathbf{x}\psi^\dagger(\mathbf{x})h(\mathbf{p}, \mathbf{x})\psi(\mathbf{x}) + \frac{1}{2}\int d\mathbf{x}_1 d\mathbf{x}_2 \psi^\dagger(\mathbf{x}_1)\psi^\dagger(\mathbf{x}_2)V(\mathbf{x}_1, \mathbf{x}_2)\psi(\mathbf{x}_2)\psi(\mathbf{x}_1). \quad (1.5)$$

This suggests an intuitive interpretation: If we were to treat ψ as a classical field, with density $\varrho \equiv |\psi|^2$, then the first term would simply be the integral over the energy density, $\int \varrho h$, while $\frac{1}{2}\int d\mathbf{x}_1 d\mathbf{x}_2 V(\mathbf{x}_1, \mathbf{x}_2)\varrho(\mathbf{x}_1)\varrho(\mathbf{x}_2)$ is reminiscent of the self-interaction energy of a classical charge distribution. This formulation makes it tempting to think of our system of point particles as a continuous matter-wave field ψ, which spreads out over all space and interacts with itself, much like a classical electromagnetic field substituting the discrete point charges. Its beauty lies in the fact that this description is formally independent of N, with its whole complexity hidden in the many-body states Ψ needed to compute observable quantities. In appealing to this ideology, we have glossed over two qualifications. One, the "matter-wave field" ψ is complex and thus not a proper classical field; in fact, only $|\psi|^2$ has the (commonplace) interpretation of a probability field. This makes clear why we haven't started out with a classical field theory and then quantized it in the first place, though this was really the historical route to relativistic field theory. Second, the field is not classical but quantized, which manifests itself in uncertainty relations going by the name of *quantum fluctuations*.

1.2 Modeling the system

Solving a system of trapped interacting atoms from first principles may seem an exercise in futility: Strictly speaking, the constituents of each atom (nucleus and electrons) interact not only with each other, but by construction with those of all other atoms. On top of that, the whole system couples to the electromagnetic quantum field. In spite of this slightly gloomy perspective, it is actually possible to deduce some kind of effective model that not only describes central aspects of the physics very well, but which is actually amenable to computation. The key is a scale separation characteristic of the physics of ultracold atoms which, roughly speaking, allows one to discard many details of the *realistic* system and retain only a highly reduced description. To anticipate our results, this description will comprise

---

[5] To avoid inessential notation, let us assume that V is a (symmetric) operator function $V(\mathbf{x}_1, \mathbf{x}_2)$ without loss of generality.

1. an effective one-body potential $U(\mathbf{r})$ corresponding to the energy shift of a (two-level) atom due to the electro-magnetic field (Sec. 1.2.1), and
2. a two-body point interaction $V(\mathbf{r}_1 - \mathbf{r}_2)$, encoding the effect of low-energy scattering on the wave function (Sec. 1.2.2).

Finally, in this thesis we will focus on quasi-*one-dimensional* (1D) systems, whose transverse degrees of freedom ($\mathbf{r}_\perp$) are assumed to be energetically well separated so that they can be integrated out, yielding an effective 1D description. This dimensional reduction will be laid out in Sec. 1.2.3.

1.2.1 Trapping potential

One can think of two ways to trap atoms via electromagnetic fields: using the interaction with

- a magnetic field $\mathbf{B}$ — which was the method of choice in the earlier experiments on Bose-Einstein condensation and still underlies the so-called *atom chip* setup;
- an electric (mostly: laser) field $\mathbf{E}$ — a flexible tool many current experiments rely on, in particular the whole subfield dedicated to creating *optical lattices* (viz., periodic trap potentials).

Both are covered extensively in the literature (see, e.g., [1, 4]). While the technical details are not vital for the understanding of this thesis, we would like to give a rough idea of how trapping is achieved on the example of *optical* traps. In either case, since atoms are charge neutral, the key is the *dipole* interaction with the field (or, in principle, higher multipoles). This leads to an energy shift of the (internal) atomic levels, which may be interpreted as an effective potential U.

As a simple model, consider a single atom with just two internal levels $\epsilon_{l=0,1}$ and a single laser mode $\mathbf{E}(\mathbf{r}, t) = \mathrm{Re}\,(\mathbf{e}\mathcal{E}(\mathbf{r})a)$, coupled in the *dipole approximation* by the term $V = -e\mathbf{r} \cdot \mathbf{E}(\mathbf{r}, t)$.[6] Expanding the coupled atom-laser Hamiltonian

$$H = H_{\text{atom}} + H_{\text{L}} + V$$

in terms of the *atomic* SU(2) basis

$$\mathbf{1} = |0\rangle\langle 0| + |1\rangle\langle 1|, \quad \sigma_+ = |1\rangle\langle 0| = \sigma_-^\dagger, \quad \sigma_3 = |1\rangle\langle 1| - |0\rangle\langle 0|$$

leads to

$$H = \frac{1}{2}\omega_{01}\sigma_3 + \omega a^\dagger a + g(\mathbf{r})(\sigma_+ + \sigma_-)(a + a^\dagger), \qquad g(\mathbf{r}) \equiv -e\mathcal{E}(\mathbf{r})\langle 0|\mathbf{e} \cdot \mathbf{x}|1\rangle.$$

The individual matrix elements of the dipole interaction may be thought of as transferring the atom from, say, state $1 \to 0$ (σ_-) while annihilating a photon (a), and so on. From this heuristic standpoint, the terms $\sigma_- a, \sigma_+ a^\dagger$ only correspond to *virtual* processes and thus are commonly discarded (*rotating-wave approximation*). The resulting Hamiltonian, written out in the *photonic* basis $|n\rangle = \frac{1}{\sqrt{n!}}\left(a^\dagger\right)^n|0\rangle$, has the graceful feature that

---

[6] This model is valid as long as (i) the laser frequency ω is quasi-resonant with exactly one atomic excitation frequency, here $\omega_{01} = \epsilon_1 - \epsilon_0$, and (ii) the wavelength of $\mathbf{E}$ is large compared with the atom size.

- $H_{\rm at} + H_{\rm L}$ is trivially diagonal (in the product basis $|l\rangle|n\rangle$)
- $V = g(\mathbf{r})\left(\sigma_+ a^\dagger + \sigma_- a\right)$ couples only pairs of states $|1\rangle|n\rangle$ and $|0\rangle|n+1\rangle$;

hence the truncated H decouples into tridiagonal submatrices

$$H_n = n\omega\mathbf{1} + \frac{1}{2}\begin{pmatrix} \Delta & 2g\sqrt{n+1} \\ 2g\sqrt{n+1} & -\Delta \end{pmatrix},$$

with the *detuning* $\Delta = \omega_{01} - \omega$. These can be readily diagonalized by an $\mathrm{SO}(2)$ transform to the *dressed* (interacting) states $|\ell\rangle_n$:

$$\begin{pmatrix} |0\rangle_n \\ |1\rangle_n \end{pmatrix} = \begin{pmatrix} \cos\vartheta_n & \sin\vartheta_n \\ -\sin\vartheta_n & \cos\vartheta_n \end{pmatrix}\begin{pmatrix} |0\rangle|n\rangle \\ |1\rangle|n\rangle \end{pmatrix},$$

with

$$\tan 2\vartheta_n = \frac{2g\sqrt{n+1}}{\Delta}.$$

Most importantly, the interacting energies are

$$E_{l,n}(g) = n\omega \pm \frac{1}{2}\sqrt{\Delta^2 + (2g\sqrt{n+1})^2}.$$

This simple formula is just what we were looking for: It tells us that the non-interacting ground state is shifted in the presence of the light field by an energy whose nontrivial part is, for large detunings $\Delta \gg g\sqrt{n}$, proportional to $|g(\mathbf{r})|^2/\Delta$. Despite the nontrivial considerations above, recall that this is nothing but the dynamic 'Stark shift' induced by a spatially varying electric field. In pictorial terms, the field induces an electric dipole moment. The energy shift depends on position parametrically through $\mathbf{E}(\mathbf{r})$, and may thus be regarded as an effective potential $\Delta E_{l,n}[g(\mathbf{r})] =: U(\mathbf{r})$ for each atom.

This *conservative* part of the interaction is dominant for not-too-small detunings; for $\Delta \to 0$ in turn, dissipative processes like absorption and spontaneous emission of photons become relevant. Although they can be included phenomenologically by adding an imaginary part $-i\Gamma/2$ to the energy—accounting for the finite lifetimes of excited levels—this is not essential in the framework of this thesis. Suffice it to claim that, for timescales smaller than the lifetime $1/\Gamma$, the conservative potential is indeed a very good description.

1.2.2 Effective interactions

As pointed out before, accounting for the full interactions between all N atoms with each other (as well as with electromagnetic fields in the presence of traps) is essentially impossible to handle. It is thus desirable to derive a reduced description of the interatomic forces which captures the *key* features specific for the low energies and densities considered in the context of ultracold atoms. This has the advantage of being not only more amenable to computation, but also offers a significantly more intuitive view of the essential physics. The detailed road toward such an effective interaction is indeed highly nontrivial, as opposed to the eventual result, so we will only sketch the conceptual steps involved and then go on to focus only on the *two-body* potential interaction.

As a first step, we shall ignore the effect of the electromagnetic field and comment on its implication later on. At that stage, we are left with a set of nuclei surrounded by electrons, which altogether Coulomb-interact with all other atoms. Due to their very different masses, however, the kinetic-energy scales governing the constituents' motions are well separated, as are the time scales. It is therefore rather legitimate to integrate out the fast electronic motion in the spirit of the *Born-Oppenheimer* approximation, which leaves us with an effective Hamiltonian for the *internuclear* coordinates only, depending on the internal degrees of freedom only parametrically. This formulation in terms of interatomic coordinates already takes us very close to representing the atoms as point-like particles. More precisely, if we restrict the many-atom system to just two atoms[7], we will obtain some interatomic potential $V(\mathbf{r} \equiv \mathbf{r}_1 - \mathbf{r}_2)$ which should be computed for any atom species *individually.* Even though it may be arbitrarily complicated—in fact, it is only for very simple atoms (like H) that this can be done to a satisfactory precision—the general structure is universal:

- For short distances, V is expected to behave wildly, incorporating the detailed interaction physics. There will be both an attractive part that supports bound states (signifying the formation of molecules) and a repulsive core as $r \to 0$ due to the fermionic nature of its constituents.
- At larger separations, $V(r)$ falls off very quickly such that the atoms will be asymptotically free, almost as if the potential were box-like.

However, intuition tells us that the detailed structure should become more and more irrelevant for low collision energies, when the de-Broglie wavelength of the scatterer is too large to probe the *short-range* behavior of the true interaction potential. In that limit, the results are expected to become *shape independent* and can be wrapped up in just a small number of parameters which in turn can be determined experimentally. The classic example is that of a Lennard-Jones potential, whose qualitative behavior is modeled on that sketched above, but whose coefficients remain to be fitted. Still, any sufficiently short-ranged V may be approximated in a *systematic* way in terms of δ functions (*point interactions*), which allow an explicit identification of different *partial waves* contributing to the scattering, but also facilitate analytic approaches to the many-body problem.

Derivation of Huang's pseudopotential

The point interaction in the framework of quantum mechanics is usually introduced in the following fashion. Suppose there is some short-ranged two-body interaction[8] V whose asymptotic effect on the relative wave function is concealed in the scattering amplitude f_k (or the phase shifts, alternatively): [53]

$$\psi(\mathbf{r}) \sim \phi(\mathbf{r}) + \frac{e^{ikr}}{r} f_k(\mathbf{e}_r). \tag{1.6}$$

---

[7] Strictly speaking, one would resort to an expansion in terms of n-body interaction potentials. Here we restrict ourselves to the case of two-body interactions ($n = 2$), which correspond to elastic collisions. Three-body collisions ($n = 3$, and higher collision orders) in turn may describe inelastic processes such as recombination. In fact, the true ground state of alkali atoms near zero temperature is a solid rather than a gas (viz., a Bose-Einstein condensate). However, for low enough densities, higher-order collisions are suppressed. Hence the gas phase is metastable and may be modeled reliably by the effective two-body interaction presented below.

[8] For simplicity, we shall restrict the discussion to isotropic potentials $V(r \equiv |\mathbf{r}|)$, so that angular momentum is conserved.

This holds asymptotically (for $r > R$ if the range R is finite). The *zero-range* or *pseudopotential* is now introduced by extending this asymptotic behavior to $\mathbb{R}^3\backslash\{\mathbf{0}\}$ and defining the pseudopotential as the potential with support at zero that generates this asymptotic form.

The most common, if perhaps not the most natural approach to low-energy effective interactions is via partial waves. Huang's derivation [54, 55] starts from the asymptotic wave function in its partial-wave expansion. To delve into a subtlety, it actually does not draw on the asymptotic expansion itself, but rather constructs the *exact* solution of a hard-sphere potential of range R which reproduces the scattering length of the *true* interaction, a_0:

$$\psi = \sum_l (U^\dagger u_l) \otimes Y_{l0},$$

with the unitary transform $(UR)(r) := r\,R(r)$.[9] Inside, Dirichlet boundary conditions apply and $\psi|_{U_R(0)} = 0$. The solution in terms of the Hankel function $h_l(q) \equiv -i(-q)^l(\frac{1}{q}\frac{d}{dq})^l\frac{\exp iq}{q}$ then reads

$$U^\dagger u_l(r) = c_l[h_l^*(kr) + S_l(E)h_l(kr)], \quad (S_l = e^{i2\delta_l}) \tag{1.7}$$

where δ_l is the l-wave phase shift. The idea now is to seek a zero-ranged 'potential' operator (a *pseudo-potential*) such that u_l is an eigenfunction of the pseudo-potential Hamiltonian in *all* of $\mathbb{R}^3\backslash\{\mathbf{0}\}$, that is, including the actual scattering zone. This is achieved using

$$h_l(q) \sim \frac{q^l}{(2l+1)!!} - i\frac{(2l-1)!!}{q^{l+1}} \quad (q \to 0)$$

and exploiting the distribution identity [56]

$$r^l\nabla^2\frac{1}{r^{l+1}} = -4\pi(2l+1)\delta(\mathbf{r}) = -(2l+1)\frac{\delta(r)}{r^2}.$$

Then the radial Hamiltonian $H_l^{(0)}$ applied to u_l about zero formally yields the messy expression

$$(E - H_l^{(0)})u_l(r) \sim \frac{1}{2}c_l(-1 + e^{i2\delta_l(k)})\frac{-i\,(2l-1)!!}{k^{l+1}} \cdot \frac{-(2l+1)\delta(r)}{r^{l+1}} =: v_l u_l(r),$$

whose right-hand side defines the l-wave pseudopotential v_l. To manifest that it is a linear operator (in a distributional sense), note that the Hankel function has a pole about zero and the radial function in that neighborhood can be written as

$$U^\dagger u_l(r) = \alpha r^l + \beta/r^{l+1} \equiv g(r)/r^{l+1}; \quad g(r) = \alpha r^{2l+1} + \beta \text{ being regular}.$$

Hence $\beta = g(0)$ and $\alpha = \frac{1}{(2l+1)!}g^{(2l+1)}(0)$, which by (1.7) implies

$$\begin{aligned} c_l(-1 + e^{i2\delta_l})\frac{-i\,(2l-1)!!}{k^{l+1}} &= \lim_{r\to 0} r^l u_l(r), \text{ or equivalently} \\ c_l(1 + e^{i2\delta_l})\frac{k^l}{(2l+1)!!} &= \lim_{r\to 0}\frac{1}{(2l+1)!}\partial_r^{2l+1}\left[r^l u_l(r)\right]. \end{aligned}$$

---

[9] The unitary transform $U : L^2(\mathbb{R}_+, r^2dr) \to L^2(\mathbb{R}_+, dr)$ merely serves to get rid of the volume-integration weight r^2 so as to 'map out' the radial functions u_l. It is introduced for notational consistency only and should simply be thought of as multiplicator '$r\cdot$' .

In this sense, the l-wave pseudopotential takes on the form

$$\begin{aligned} v_l &= \frac{1}{2}\frac{-(2l+1)\delta(r)}{r} \quad \text{(1st version)} \\ &= \frac{1}{2}\frac{-(2l+1)\delta(r)}{r^{l+1}}\frac{\tan\delta_l(k)}{k^{2l+1}}(2l-1)!!^2\partial_r^{2l+1}r^l \quad \text{(2nd version)}, \end{aligned} \tag{1.8}$$

adding up to the total pseudopotential

$$V_{pp} = \bigoplus_l \left(U^\dagger v_l U\right) \otimes 1.$$

Remarks

1. While the first form is simpler and more natural to arrive at, the second one is what is usually cited in the literature [55] (despite the missing factor of $(2l+1)^{-1}$.) This is possibly due to the fact that the factor

$$\frac{\tan\delta_l(k)}{k^{2l+1}} = -a_l + O(k^2)$$

allows for a simple interpretation of the l-wave scattering length a_l as the 'interaction strength' (at low enough energies.) This has led people to speak of the full series as the *energy-dependent scattering length* [57] $-a_l(k)$.

2. In practice, the pseudopotential turns out to be expedient only for s-waves, in which case the second version reads

$$(U^\dagger v_0 u_0)(r) = \frac{1}{2}\frac{\delta(r)}{r^2}\frac{-\tan\delta_0(k)}{k}(\partial_r u_0)_0 \sim \delta(\mathbf{r})\underbrace{2\pi a_0}_{=:g}\times(\partial_r u_0)_0, \tag{1.9}$$

where g is the interaction strength and ∂_r is referred to as a *regularization* operator. Applied to the total s-wave function $u_0(r)/r$, it amounts to $\partial_r(r\psi)$, which takes care of the $1/r$ singularity of the asymptotic wave; it is merely the identity when it acts on regular states ψ.

3. The *validity* of the s-wave pseudopotential depends on how the wave function (i.e., the scattering amplitude f_k) is reproduced. This generally applies if (i) $f_k(\Omega) \approx f_0(k)$ —which is to say that no higher l contribute significantly—and (ii) even for $l = 0$, $\tan\delta_0(k) \approx -ka_0$, justifying the parametrization solely in terms of the scattering length. Of course (i) depends on whether one is in a low-energy region where s-wave scattering indeed dominates. (Otherwise, higher-ℓ pseudopotentials have to be included, which are considerably more cumbersome.) Criterion (ii) in turn is met when the term $O(k^2)$ in the expansion of δ_0 can be neglected. In terms of the *effective range* r_0 [58], this reads

$$k^2 r_0 \ll |a_0^{-1}|?$$

This amounts to demanding $|ka_0| \ll 1$ if both parameters a_0, r_0 are comparable. In case $r_0 \ll |a_0|$, then the weaker constraint $|kr_0| \ll 1$ suffices.

4. Let us comment on the role played by the presence of *external forces*, such as in the presence of electromagnetic fields. One might jump to the conclusion that the effect

should be drastic, since the trap will not only break the translational invariance of the interaction, but actually undermines the concept of scattering theory as a whole: After all, it makes no longer sense to speak of incoming and outgoing (continuum) states if the whole spectrum is rendered discrete in the presence of confinement. However, the length scale of the short-range physics, a_0, is typically much smaller than that of the trapping potential L. In this sense, the actual scattering physics feels only a locally constant trapping potential $U(\mathbf{r})$. To lowest order in a_0/L, it is therefore legitimate to retain the bare interaction. [59]

5. So far, we have dealt with the two-particle problem. The most natural way to link this to the *many-body* case consists in setting up the interaction part as $\sum_{i<j} V_{\mathrm{pp}}(\mathbf{r}_i - \mathbf{r}_j)$, with the mass now referring to the reduced mass.

Interpretation: Analogy to multipole expansion

In this paragraph, an illustrative alternative perspective on point interactions is presented, which also casts light on the relation between a *true* interaction and its associated pseudopotential. As a motivation, recall that the asymptotic behavior of the scattering wave, $\frac{e^{ikr}}{r} f_k(\mathbf{e}_r)$, is nothing but Green's function G (with an angular modulation), which in turn is an eigenfunction of the pseudopotential Hamiltonian (with a $\delta(\mathbf{r})$ potential):

$$(E - H_0)G = \delta.$$

If we reverse our point of view, then the delta-type pseudopotential is just that potential which generates this asymptotic behavior in an *exact* manner. This is reminiscent of the multipole expansion in electrostatics (but also in the dynamical case): the true, unknown charge density ($\rho \hat{=} V\psi$ here) is replaced by a point source (a point charge, a point dipole etc.) designed to generate the same electric potential asymptotically, i.e., far from the source. Let us take a closer look at this analogy.

In electrodynamics, the density ρ obeys the Poisson equation for the desired potential Φ, $-\nabla^2 \Phi = \rho$, whose solution is given by[10] $\Phi = G * \rho$, in terms of the well-known Green function

$$-\nabla^2 G = \delta \Longrightarrow G(\mathbf{r}) = \frac{1}{4\pi|\mathbf{r}|}.$$

The interpretation is commonplace: G is the potential Φ_0 of a point charge at $\mathbf{0}$, and the *true* potential can be acquired by summing over the potentials of all point charges in the domain of interest. It comes as no surprise that for distances much larger than the diameter of the support of ρ, this can be fairly simplified: the asymptotic behavior $r \gg r'$ is given (in standard multi-index notation) by

$$4\pi G(\mathbf{r}-\mathbf{r}') = 4\pi \sum_{\alpha} \frac{(-1)^{|\alpha|}}{\alpha!} (\partial^\alpha G)(\mathbf{r}) \mathbf{r}'^{\alpha} = \frac{1}{r} - \frac{\mathbf{r}\cdot\mathbf{r}'}{r^3} + \frac{1}{2!}\mathbf{r}' \cdot \left(\frac{3\mathbf{r}\otimes\mathbf{r} - r^2}{r^3} \right) \mathbf{r}' + O\left(\frac{r'}{r}\right)^3.$$

---

[10] Only the particular solution is regarded here.

Carrying out the convolution $\Phi = G * \rho$ yields

$$\Phi(\mathbf{r}) = 4\pi \sum_\alpha \frac{(-1)^{|\alpha|}}{\alpha!} (\partial^\alpha G)(\mathbf{r}) \int d\mathbf{r}' \rho(\mathbf{r}') \mathbf{r}'^\alpha =: \sum_\alpha \frac{4\pi}{\alpha!} (\partial^\alpha G)(\mathbf{r}) q_\alpha.$$

The point is that all the information in $\rho(\mathbf{r})$ is encoded in a set of multipole moments $q_\alpha \in \{q_{(|\alpha|=0)} = \int \rho,\ \mathbf{p}_{(|\alpha|=1)} = \int \rho\mathbf{r}, \dots\}$ (monopole, dipole, etc.)—few of which are ever used. This asymptotic series is solely based on Taylor-expanding the Green function. One can reverse this idea and arrive at the same result by expanding *not* G (the point-charge potential) but the density itself, namely writing

$$\rho(\mathbf{r}) = 4\pi \sum_\alpha \frac{(-1)^{|\alpha|}}{\alpha!} q_\alpha \partial^\alpha \delta(\mathbf{r}) = \left(q - \mathbf{p} \cdot \nabla + \frac{1}{2!} \nabla \cdot Q \nabla + \dots \right) \delta(\mathbf{r}).$$

It goes without saying that this effective multipole density contains all the information on the total (integrated) density wrapped up in the moments $\{q_\alpha\}$, despite its acting only at zero.

These remarks draw a natural line between multipoles and the pseudopotential: in our case, the 'electric potential' is but ψ, while the 'density' (source) is *self-consistently* given by $V\psi$. The exact solution is now obtained by convolving the exact 'density' $V\psi$ with the point-source solution $G(\mathbf{r}) = -\frac{\exp(ikr)}{2\pi r}$. As before, of course, we are interested only in the solution far outside the source, so one would attempt to expand $G(\mathbf{r} - \mathbf{r}')$ for $r \gg r'$. Here the second fundamental difference enters: in scattering theory, the asymptotic Green function usually is *not* derived as a Taylor series as above, but rather approximated by the more convergent expression

$$G(\mathbf{r} - \mathbf{r}') \overset{r \to \infty}{\sim} -\frac{1}{2\pi} \frac{e^{ikr}}{r} e^{-ik\mathbf{e}_r \cdot \mathbf{r}'}.$$

To make the analogy conclusive, let us proceed by expanding in a systematic fashion,

$$G(\mathbf{r} - \mathbf{r}') = \sum_\alpha \frac{(-1)^{|\alpha|}}{\alpha!} (\partial^\alpha G)(\mathbf{r}) \mathbf{r}'^\alpha = -\frac{e^{ikr}}{2\pi r} \left\{ 1 + \left(-\frac{1}{r} + ik \right) \mathbf{e}_r \cdot \mathbf{r}' + O\left(\left(\frac{r'}{r} \right)^2 \right) \right\}.$$

In that case, ignoring convergence, the convolution yields

$$(G * V\psi)(\mathbf{r}) = \sum_\alpha \frac{(-1)^{|\alpha|}}{\alpha!} (\partial^\alpha G)(\mathbf{r}) \int d\mathbf{r}' (V\psi)(\mathbf{r}') \mathbf{r}'^\alpha =: -\sum_\alpha \frac{2\pi}{\alpha!} (\partial^\alpha G)(\mathbf{r}) f_\alpha,$$

where the full source $V\psi$ has been similarly condensed into a set of 'scattering amplitudes' $f_\alpha \in \{f_0 = -\frac{1}{2\pi} \int V\psi;\ \mathbf{f} = -\frac{1}{2\pi} \int d\mathbf{r}' V\psi(\mathbf{r}')\mathbf{r}', \dots\}$, where the monopole term is the low-energy scattering amplitude $f_0 = \lim_{k \to 0} f_k$, $\mathbf{f}$ the low-energy gradient $i\nabla_\mathbf{k} f_k$, and so on. The monopole solution ψ is then the low-energy limit of the usual expansion, followed by a dipole and higher terms reminiscent of multipole radiation.

One can then proceed as in the electrostatic case and put the cart before the horse: Defining a zero-range potential

$$(V_{\mathrm{pp}}\psi)(\mathbf{r}) := -2\pi \sum_\alpha \frac{(-1)^{|\alpha|}}{\alpha!} f_\alpha \partial^\alpha \delta(\mathbf{r}) = (f_0 - \mathbf{f} \cdot \nabla + \dots)\, \delta(\mathbf{r}),$$

we generate the same result in the Lippmann-Schwinger eq. as by expanding Green's function. Note that it is not cast in the same form as (1.8), but rather is non-local in ψ by construction. Also, it is not restricted to a rotation-invariant interaction. In this familiar case, however, we can identify the first coefficient as the scattering length, $f_0 = -a_0$.

Dimensionality aspects

We have so far proceeded on the standard assumption of dealing with $\mathbb{R}^d$, $d = 3$. In this thesis, we are concerned with the case $d = 1$, whose peculiarities are discussed below. (An argument how one can embed this mathematical limit realistically from a three-dimensional perspective will be given in the next subsection.)

Scattering in 1D is conceptually different from that in 3D. While the 3D-scattering wave is a radial one and is usually decomposed into angular-momentum eigenstates, scattering in one dimension can simply go back and forth. This is why one usually writes the asymptotic solution as

$$\psi(x) \sim \left(e^{ikx} + r_k \cdot e^{-ikx}\right)\Theta(-x) + t_k \cdot e^{ikx}\Theta(x)$$

in terms of the reflection and transmission coefficients $|r|^2$ and $|t|^2$, respectively. The essential difference with respect to 3D is that the "unit sphere" is just the disconnected set $\{\Omega \equiv \frac{x}{|x|} = \pm 1\}$. The above asymptotics can be recast into the standard shape (1.6) familiar from 3D scattering: Inserting the 1D-Green function

$$G(x) = -\frac{i}{k} e^{ik|x|} \tag{1.10}$$

in the Lippmann-Schwinger eq. $\psi = \phi + G * V\psi$ yields

$$\psi(x) \sim e^{ikx} + f_k(\Omega) \cdot e^{ik|x|}; \quad 1 + f_k(1) = t_k,\ f_k(-1) = r_k, \tag{1.11}$$

where the scattering amplitude is

$$f_k(\pm 1) = -\frac{i}{k} \int dx' e^{\mp ikx'} (V\psi)(x').$$

The asymptotic form (1.11) can be attained *exactly* by the simple pseudo-potential

$$V_{\mathrm{pp}}(x) = g\delta(x),$$

which imposes a boundary condition on $H_0 = -\frac{1}{2}\frac{d^2}{dx^2}$:

$$\psi'(0^+) - \psi'(0^-) = 2\underbrace{g\psi(0)}_{=ikf_k}. \tag{1.12}$$

The discontinuity in ψ' introduced for $g \neq 0$ is of course an unphysical feature of the effective interaction. This comes as no surprise, given that the contact potential merely serves to get the *asymptotic* behavior right; at distances smaller than the range of the true interaction it should not be taken at face value. A way to make that non-analyticity plausible is to imagine finite-range interaction, which at $r = \pm R$ imposes some boundary condition. Letting the potential shrink to a single point, $R \to 0$, while patching the wave function at $\pm R$, naturally produces a cusp in $\psi(0^\pm)$.

We already argued that the scattering solution has simply the form of $G(x) = -\frac{i}{k}e^{ik|x|}$ by construction. The bound state can be found by analytic continuation to negative energies: In fact, applying the boundary condition (1.12) yields

$$k = -ig,$$

viz., after normalization there is a bound state

$$\psi(x) = \frac{1}{\sqrt{a}}e^{-|x|/a} \quad \text{with } a := -\frac{1}{g}. \tag{1.13}$$

It is in $L^2(\mathbb{R}^1)$ for $a > 0$ only (i.e., $g < 0$); the point spectrum then takes on the universal form $\{-1/2a^2\}$. Irrespective of its sign, $a \equiv -1/g$ is referred to as the one-dimensional *scattering length*. Be aware that, in contrast to 3D, this means that the interaction strength is zero only for $a \to \infty$, which takes some getting used to. Note in passing that this also casts the 1D-scattering amplitude $f_k = -\frac{i}{k}g\psi(0)$ into a suggestive shape: Computing $\psi(0)$ in (1.11) yields

$$f_k = -\frac{i}{k}g\frac{1}{1+\frac{i}{k}g}, \text{ hence } f_k = \frac{-1}{1+ika}. \tag{1.14}$$

1.2.3 Effective one-dimensional description

We have so far been concerned mostly with a truly three-dimensional system. The main focus of this thesis, though, rests on quasi-one-dimensional systems. Here the motion is essentially restricted to one direction (the *longitudinal* one $\|$), while the *transverse* ($\perp$) motion is "frozen" because the energy available is much smaller than the transverse excitation gaps. This situation is encountered, e.g., in "cigar-shaped" traps with strong transverse confinement.

Under these circumstances, it is desirable to integrate out the transverse degrees of freedom so as to attain an effective one-dimensional description. For the trapping potential, this is straightforward and yields a one-dimensional potential $U_\| : \mathbb{R}^1 \to \mathbb{R}$. For the two-body interaction, this is more intricate since the (radially symmetric) interaction couples transverse and longitudinal modes. However, Olshanii constructed a model where this can be done analytically, which shall be presented below [21]. Its idealized setup is modeled by the following Hamiltonian for the *relative* motion,

$$H = h_\| + h_\perp + V,$$

where the realistic three-dimensional system is separated into to a free motion *parallel* to the guide's axis z, and a harmonic-oscillator (HO) potential acting in the *perpendicular* direction:

$$h_\| = \frac{1}{2\mu}p_\|^2, \; h_\perp = \frac{1}{2\mu}\mathbf{p}_\perp^2 + \frac{1}{2}\mu\omega_\perp^2\mathbf{r}_\perp^2 \qquad (\mu \equiv M/2),$$

while the interaction—modeled by the 3D point interaction $V = g\delta(\mathbf{r})\partial_r r$—couples those degrees of freedom. Note that the perpendicular trap frequency $\omega_\perp$ sets the energy scale

$\varepsilon^\perp_N/\hbar\omega_\perp = N+1$ of the 2D-transversal oscillator eigenstates $\varphi_N(\mathbf{r}_\perp)$; accordingly $a_\perp = \sqrt{\hbar/\mu\omega_\perp}$ defines the length scale.

The asymptotic behavior follows straight from the Lippmann-Schwinger equation

$$\psi = \phi + (E - h_\parallel - h_\perp)^{-1} V \psi,$$

where $\phi \equiv |N, k_\parallel\rangle = \varphi_N \otimes |k_\parallel\rangle$ denotes the homogeneous—non-interacting—solution. This readily yields

$$\psi(\mathbf{r}) = \phi(\mathbf{r}) + G(\mathbf{r}, 0) \times g(\partial_r r\psi)_{r=0},$$

but now the Green function $G(\mathbf{r}, \mathbf{r}') = \langle \mathbf{r}|(E - h_\parallel - h_\perp)^{-1}|\mathbf{r}'\rangle$ is *not* $-e^{ikr}/2\pi r$ as in the isotropic (unconfined) case. Nonetheless it can be computed by expanding the resolvent in terms of the non-interacting states ϕ:

$$\begin{aligned} G(\mathbf{r}, \mathbf{r}') &= \sum_N \int dk_\parallel \langle \mathbf{r}|(E - h_\parallel - h_\perp)^{-1}|Nk_\parallel\rangle\langle Nk_\parallel|\mathbf{r}'\rangle \\ &= \sum_N \varphi^*_N(\mathbf{r}'_\perp)\varphi_N(\mathbf{r}_\perp)\mathcal{G}_{E-\varepsilon^\perp_N}(z - z'). \end{aligned}$$

Here $\mathcal{G}_\epsilon = (\epsilon - h_\parallel)^{-1}$ denotes the 1D-Green operator at energy ϵ. At this stage, what is left is to make the solution comparable to the purely 1D scattering case as in (1.11). Assuming that the incident wave $\phi(\mathbf{r}) = \varphi_{N=0}(\mathbf{r}_\perp)e^{ik_\parallel z}$ is in the transversal-HO *ground state*, and that its longitudinal energy is too small to excite any transversally excited states,[11] then we can extract the *longitudinal* wave function using $\varphi_N(\mathbf{0}) = 1/a_\perp\sqrt{\pi}$ and $G_{\epsilon\equiv k^2/2\mu}(z) = -\frac{i\mu}{k}e^{ik|z|}$:

$$\psi(z\mathbf{e}_z) = \frac{1}{a_\perp\sqrt{\pi}}e^{ik_\parallel z} + \frac{g\mu(\partial_r r\psi)_0}{a_\perp^2\pi}\left\{\frac{-i}{k_\parallel}e^{ik_\parallel|z|} + \sum_{0\neq N\in 2\mathbb{N}} \frac{-i}{k_N}e^{ik_N|z|}\right\}.$$

The first term in the bracket ($N = 0$) gives the purely 1D contribution, while the remainder stems from summing over *virtual* states with $k_{N\neq 0} \equiv \sqrt{2\mu(E - \varepsilon^\perp_N)} = i\sqrt{2\mu N\hbar\omega_\perp - k^2_\parallel}$, reflecting the underlying 3D nature of the system. The latter terms vanish asymptotically, but still leave an imprint on the 1D term via $(\partial_r r\psi)_0$, for which a tedious calculation yields

$$(\partial_r r\psi)_0 = \frac{1/\sqrt{\pi}a_\perp}{1 - \frac{g\mu}{a_\perp^2\pi}\left(\frac{-i}{k_\parallel} + \frac{C}{4} + O(k^2_\parallel)\right)} \qquad (C = |\zeta\left(\tfrac{1}{2}\right)| = 1.46\ldots).$$

This admits the asymptotic form to be cast into the familiar shape

$$\psi(z\mathbf{e}_z) \overset{|z|\to\infty}{\sim} \frac{e^{ik_\parallel z} + f_{k_\parallel}e^{ik_\parallel|z|}}{a_\perp\sqrt{\pi}}, \text{ where } f_{k_\parallel} = \frac{-1}{1 + ik_\parallel(\frac{C}{2} - \frac{a_\perp^2\pi}{\mu g}) + O(k^3_\parallel)}.$$

What does this signify when compared to the one-dimensional expression (1.14)? For sufficiently low longitudinal momenta, this indeed resembles the 1D scattering amplitude with $\frac{C}{2} - \frac{a_\perp^2\pi}{\mu g} =: a_{1\mathrm{D}}$. Practically speaking, we can then model an effective 1D interaction $g_{1\mathrm{D}}\delta(z)$,

---

[11] By symmetry, only transitions to symmetric states $N \in 2\mathbb{N}_0$ are allowed. Hence the condition $\langle h_\parallel\rangle < \varepsilon^\perp_2 - \varepsilon^\perp_0 = 2$ is required for quasi-one-dimensionality. Note that this applies even if the transverse motion is frozen in some excited state $N \neq 0$.

in which the coupling strength $g_{1\mathrm{D}} = -\hbar^2/\mu a_{1\mathrm{D}}$ encodes all the relevant information not only on the interaction itself (g), but also on the transverse system that has been integrated out $(a_\perp)$.

If the motion along z is slowed furthermore, $\left|k_\| a_{1\mathrm{D}}\right| \ll 1$, the transmission coefficient

$$|t_{k_\|}|^2 = |1 + f_{k_\|}|^2 \to 0$$

vanishes: the system becomes *impenetrable*. This case corresponds to an infinitely strong repulsion $g_{1\mathrm{D}} \to \infty$, known as the *Tonks-Girardeau* limit, which plays a central role in 1D many-body systems (cf. Sec. 1.4.1).

1.3 Visualizing many-body states: Density matrices

Our goal is to compute N-body states $\Psi \in \mathbb{H}_N$. No matter if these are stationary states or if we are interested in their time evolution, they are quite complex entities already for few particles. This makes it even more vital to make these vectors amenable to interpretation and relate them to physical observables. This is where the concept of *density* operators (or matrices) enters the stage.

1.3.1 Definition and basic properties

As is well known, the knowledge of Ψ is equivalent to that of its density matrix $\rho_N = \mathcal{P}_\Psi \equiv |\Psi\rangle\langle\Psi|$,[12] in the sense that for any operator A

$$\langle A \rangle_\Psi = \mathrm{tr}\,(\rho_N A)\,.$$

By construction, ρ_N constitutes the operator counterpart of a classical probability distribution:

- It is clearly non-negative, $\rho_N \geq 0$ (and even positive unless restricted to the orthogonal complement of $\mathrm{span}\{\Psi\}$).
- It is normalized to unity. More precisely, density operators belong to the trace class $\mathbb{T} = \{\rho \mid \mathrm{tr}(\rho) < \infty\}$, which can promoted to a Banach space via the norm $\|\rho\|_\mathbb{T} = \mathrm{tr}\,|\rho|$. Since $\|\Psi\| = 1$, we naturally have $\|\rho\|_\mathbb{T} = \langle\Psi|\Psi\rangle = 1$.

Its real utility derives from the fact that, if we deal with only an n-body operator $A_n = \frac{1}{n!}\sum_{i_1\neq\cdots\neq i_n} \mathcal{A}|_{i_1\ldots i_n}$, then its expectation value can be boiled down to an n-body expression via

$$\langle A_n \rangle = \binom{N}{n} \mathrm{tr}\,(\rho_n \mathcal{A})\,, \qquad \text{where } \rho_n := \mathrm{tr}_{n+1,\ldots N}(\rho_N)$$

defines the *reduced* n-body density matrix by integrating out all degrees of freedom except $1, \ldots, n$.[13] In particular, to the extent that we study at most two-body observables, it already

---

[12] One of the commonplace advantages of the density-operator formalism is that it readily extends to the case where the system is in an ensemble of states $\{\Psi_m\}$, each with probability p_m, as would be the case for non-isolated systems. Here we consider an isolated system, though.

[13] Trivially, $\rho_0 = 1$, while $\rho_{n=N}$ reproduces the full density matrix. Choosing specific "particle numbers" $1, \ldots, n$ is of course purely conventional owing to permutation symmetry. Moreover, please note that this concept of tracing out naturally extends to any system decomposed into subsystems, whatever their physical meaning.

suffices to consider the two-particle density operator $\rho_2 = \mathrm{tr}_{3\ldots N}|\Psi\rangle\langle\Psi|$, whose diagonal kernel

$$\rho_2(x_1, x_2) \equiv \langle x_1 x_2|\rho_2|x_1 x_2\rangle$$

gives the probability density for finding one particle located at x_1 and any second one at x_2. For this reason, it is also termed *pair-distribution* or *two-body correlation function*.

For any one-particle operator, it would even be enough to know the one-body density matrix $\rho_1 = \mathrm{tr}_2\rho_2$. As an application, observe that the exact many-body energy of $H = \sum_i h_i + \sum_{i<j} V_{ij}$ for any Ψ may be written as

$$E = N\,\mathrm{tr}(\rho_1 h) + \frac{N(N-1)}{2}\mathrm{tr}(\rho_2 V).$$

Similarly to ρ_2, $\rho(x) = \langle x|\rho_1|x\rangle$ represents the probability density for finding a single particle at x. By contrast, the off-diagonal integral kernel $\rho_1(x, x') \equiv \langle x|\rho_1|x'\rangle = \rho_1(x', x)^*$ will be complex in general. It is therefore certainly not an observable in its own right. Nonetheless, it is of some interest as it gives us access to all one-particle quantities, also non-local ones such as the one-body momentum distribution $\tilde{\rho}(k) = 2\pi\langle k|\rho_1|k\rangle$, which can be related to the density matrix via

$$\tilde{\rho}(k) = \int dx \int dx' e^{-ik(x-x')}\rho_1(x, x').$$

It can be understood as the Fourier transform of the integrated 'off-diagonal' density matrix

$$\tilde{\rho}(k) = \int dr e^{-ikr}\bar{\rho}_1(r),$$

with $\bar{\rho}_1(r) := \int dR \rho_1(R + \frac{r}{2}, R - \frac{r}{2})$. [14]

It is common to consider the spectral decomposition of the (hermitian) one-particle density matrix[15]

$$\rho_1 \equiv \sum_a n_a|\phi_a\rangle\langle\phi_a|. \tag{1.15}$$

By non-negativity, all $n_a \in [0, 1]$, while normalization requires that $\mathrm{tr}\rho_1 = \sum_a n_a = 1$. Each n_a is said to be the (relative) population of the *natural orbital* ϕ_a. If all $N_a \equiv n_a N \in \mathbb{N}_0$, then the density may pertain to the (non-interacting) number state $|N_0, N_1, \ldots\rangle$ based on the one-particle basis $\{\phi_a\}$; for non-integer values it extends that concept. In this light, the natural orbitals provide us with sort of an effective one-particle picture which proves helpful in understanding complex interacting situations.

---

[14] At this point, it is worthwhile to mention the relation to the occasionally encountered *Wigner function*, $W(R, k) \equiv \int dr\, e^{-ikr}\rho_1(R + \frac{r}{2}, R - \frac{r}{2})$, which simply replaces the off-diagonal spatial variable in ρ_1 by momentum. It is normalized to $\int dR \int \frac{dk}{2\pi} W(R, k) = 1$, which has led people to consider it as some kind of (non-classical) phase-space density, glossing over the fact that it is complex-valued and thus not a probability.

[15] Similar considerations apply to any density matrix, even though usually the spectral decomposition is carried out only for ρ_1. Note that the expansion (3.2) has the same mathematical structure as a density matrix in thermodynamics representing a mixture of states $\{\phi_a\}$. There, the *reduced* density matrix of some system $\mathcal{A}$ is not in a pure (eigen-)state because the *full* system contains correlations between $\mathcal{A}$ and some "environment" system $\mathcal{B}$. Tracing out $\mathcal{B}$ naturally yields a superposition of $\mathcal{A}$ states. In our case, $\mathcal{A} = \mathbb{H}_n$ comprises particles $1, \ldots, n$; in case of a coupling to the other particles, a "mixed state" of type (3.2) emerges.

1.3.2 Fock-space perspective

We have seen in Sec. 1.1 that the natural language for describing many-body physics is that of Fock space. With this in mind, let us reformulate the few-body density matrices ρ_n. Recall that the field-operator expansion (1.4) asserts that the expectation value of any n-body operator A_n could be expressed as

$$\langle A_n\rangle = \frac{1}{n!}\int dX dX' \langle X|\mathcal{A}|X'\rangle \langle \psi^\dagger(x_1)\cdots\psi^\dagger(x_n)\psi(x'_n)\cdots\psi(x'_1)\rangle, \quad X\equiv(x_1,\ldots,x_n).$$

Comparing this with the standard formula $\langle A_n\rangle = \binom{N}{n}\operatorname{tr}_{1,\ldots,n}(\rho_n\mathcal{A})$, this suggests the natural identification

$$\rho_n(X,X') = \frac{(N-n)!}{N!}\left\langle \psi^\dagger(x_1)\cdots\psi^\dagger(x_n)\psi(x'_n)\cdots\psi(x'_1)\right\rangle$$

as the $\mathbb{F}$ representation of the density matrix (in position space, without loss of generality). Note that $\rho_n(X,X')$ in turn is the expectation value of the Fock-space operator $\psi^\dagger(x_1)\cdots\psi(x'_1)$, which we might come by directly by applying the operator expansion (1.4) to the $\mathbb{H}_n$ operator $\rho_n = |X\rangle\langle X'|$.

For *one-body* operators, $n=1$, we recover the number-density operator

$$\hat{n}(x)\equiv\psi^\dagger(x)\psi(x)$$

already found in Sec. 1.1 by simple considerations. Now we can also assign a meaning to the off-diagonal terms. Taking the average in any state Ψ, we get

$$\langle\Psi|\psi^\dagger(x)\psi(x')|\Psi\rangle = \langle\psi(x)\Psi|\psi(x')|\Psi\rangle.$$

From this perspective, the off-diagonal density matrix tells us the "cross-correlation" between state Ψ with, on the one hand, a particle removed at x and, on the other hand, one particle removed at x'. Put differently,

$$\cos\alpha(x,x')\equiv\frac{\langle\psi(x)\Psi|\psi(x')\Psi\rangle}{\|\psi(x)\Psi\|\,\|\psi(x')\Psi\|} = \frac{\rho_1(x,x')}{\sqrt{\rho(x)\rho(x')}} \tag{1.16}$$

quantifies how different both "hole" states are in a Hilbert-space sense, reflecting the correlation inherent in Ψ between x and x'. This motivates the jargon of $\cos\alpha(x,x') =: g_1(x,x')$ being the *one-body correlation* function. Note that, by the Cauchy-Schwartz inequality, $|g_1|$ is bounded by $+1$ from above ($\rho_1 = |\phi_0\rangle\langle\phi_0|$, with $\rho\equiv|\phi_0|^2$).[16] It is also referred to as the *(first-order) coherence* function and relates to the "visibility" in interference experiments [2].

For *two-body operators*, we recover the *two-body density* (or two-body correlation function)

$$\rho_2(x_1,x_2) = \frac{1}{N(N-1)}\left\langle\psi^\dagger(x_1)\psi^\dagger(x_2)\psi(x_2)\psi(x_1)\right\rangle.$$

---

[16] This equality is also achieved for a "classical" field, where $\psi(x)$ is simply a multiplication operator. However, this should be taken with a grain of salt. The field operator is always a destruction operator and thus $\langle\Psi|\hat{\psi}(x)\Psi\rangle = 0$ for any number-conserving state. However, for large occupations of a certain state, ϕ_0, the above replacement may be understood as a lowest-order *approximation*. For photons, however, particle number is not conserved and such a "coherent state", $\langle\hat{\psi}(x)\rangle = \psi(x)$, is a reasonable assumption for a classical *laser* field.

From this, we can read off two important properties:

- $\rho_2(x_1, x_2) = \frac{1}{N(N-1)} \|\psi(x_2)\psi(x_1)\Psi\|^2$ is given by the norm of Ψ upon subsequently removing particles at x_1, x_2.
- Using the commutation relation, we can relate ρ_2 to the density-density correlations

  $$\langle \psi^\dagger(x_1)\psi^\dagger(x_2)\psi(x_2)\psi(x_1)\rangle = \langle \hat{n}(x_1)\hat{n}(x_2)\rangle - \delta(x_1 - x_2)n(x_1),$$

  which tell us the fluctuation of the atom number in a certain spatial region over repeated measurements.

As a final remark, it is interesting to note again the different conception behind the Fock-space formulation: Rather than starting with the *full* density matrix ρ_N and then step by step integrating out the other particles ("degrees of freedom"), we start with the simplest operator product ($\psi^\dagger\psi$) and iteratively go to higher powers to compute higher-order correlations. Of course, this is only a difference in spirit. For any N-body system, both approaches are entirely equivalent.

1.4 Soluble models

Endowed with an amenable model for our many-body system, and with the appropriate language at hand for describing and analyzing it mathematically, we now have the basic equipment to tackle the physics of few ultracold atoms in traps. Still, before delving into arbitrarily complex systems, it is expedient to first look at simple borderline cases so as to acquire some intuition for the key mechanisms, which help us understand more involved systems. Plus, some of these model examples presented below have become seminal works often referred to in the literature, which makes it even more vital to make their acquaintance.

To classify these simple *soluble* models, let us regard the general (for concreteness, one-dimensional) Hamiltonian

$$H = \sum_{i=1}^{N} h(p_i, x_i) + \sum_{i<j} V(x_i - x_j),$$

where $h(p, x) = \frac{1}{2}p^2 + U(x)$ is the one-body Hamiltonian including kinetic energy and an external (trapping) potential $U(x)$, while $V(x) = g\delta(x)$ is the one-dimensional effective interaction with coupling $g \geq 0$.[17] The following borderline cases should now appear obvious:

- The interaction in the limits $g \to 0$ and $g \to \infty$: The former limit is the trivial ideal gas, in which all bosons condense into the lowest eigenstate of h, ϕ_0. (This single-orbital picture may be carried over to small but nonzero g in a *mean-field* spirit. That leads to the *Gross-Pitaevskii equation* touched upon later on in Sec 2.1.) The nontrivial limit $g \to \infty$ in turn corresponds to a gas of bosons with *hard-core* interactions, which is integrable for any trap U by exploiting the *Bose-Fermi* map (Sec. 1.4.1).

---

[17] To be fair, there are indeed a few soluble many-body models omitted here that do *not* assume point interactions but either other types of interactions or simply encode the interaction directly in the field-operator structure of H.

- As for the trapping potential, the natural candidates are those usual suspects where either U reduces to a pure boundary condition (the *Lieb-Liniger* model examined in Sec. 1.4.2) or it is of quadratic form, in which case it may be solved for $N = 2$ atoms (Sec. 1.4.3).

1.4.1 Bose-Fermi map

The premise of the so-called *Bose-Fermi* mapping is a system of 1D hard-core bosons in an arbitrary trap, a so-called *Tonks-Girardeau gas*. Formally, this amounts to taking $g \to \infty$, even though a more rigorous description is to impose hard-core boundary conditions on the many-body wave function

$$\Psi|_{x_i=x_j} = 0, \qquad i < j. \tag{1.17}$$

Thus we are left with a single-particle Hamiltonian $H_0 = \sum_i h_i$, with the additional constraints of bosonic permutation symmetry and (1.17). The trick now is to recognize that the hard-core boundary condition leads to the same zeroes in Ψ as for (spin-polarized) fermions governed by the same Hamiltonian, only that the cause there is simply the exclusion principle. In fact, one can establish the following theorem first proven by Girardeau [19].

Theorem (*Bose-Fermi map*) For any fermionic solution of the Schrödinger equation $(E - H_0)\Psi_- = 0$, the state

$$\Psi_+ = A\Psi_-, \qquad A(X) := \prod_{i<j} \mathrm{sgn}(x_i - x_j),$$

has bosonic permutation symmetry and satisfies Schrödinger's equation with hard-core boundary conditions (1.17).

Proof: Let us first consider the fundamental domain

$$\mathcal{D} = \left\{X \in \mathbb{R}^N \mid x_1 < x_2 < \cdots < x_N\right\}.$$

If we can show that, on the closure $\bar{\mathcal{D}}$, Ψ_+ is continuous (i) and solves Schrödinger's equation (ii), then we are solely left to demonstrate that it has bosonic permutation symmetry when extended to all of configuration space (iii).

(i) Ψ_+ is continuous in $\mathcal{D}$ since Ψ_- is. On the boundary $\partial\mathcal{D}$, Ψ_- vanishes by the exclusion principle, which proves the continuity of Ψ_+.

(ii) In the interior, Ψ_+ also solves Schrödinger's equation since A is constant there. The correct boundary condition is warranted again by Pauli's exclusion principle.

(iii) Under transposition P_{12} of any two particles, Ψ_+ transforms as

$$P_{12}\Psi_+ = P_{12}A\underbrace{P_{12}^{-1}P_{12}}_{=1}\Psi_- = \underbrace{P_{12}AP_{12}}_{=-A}\underbrace{P_{12}\Psi_-}_{=-\Psi_-} = +\Psi_+,$$

where the antisymmetry of A has been used. This result ensures the bosonic permutation symmetry on the whole configuration space. □

There is a number of neat corollaries of that simple yet powerful theorem, just to name a few:

- The ground state of the hard-core bosons is given simply by the absolute value of the non-interacting fermionic ground state, $\Psi_+^{(0)} = \left|\Psi_-^{(0)}\right|$. This makes it tempting to think of Pauli's exclusion principle as emulating the effect of the repulsive interactions (or vice versa), which is why the limit $g \to \infty$ is commonly referred to as *fermionization*: Just like fermions, the two particles cannot reside on the same spot any longer, although for physically different reasons.
- While being less intuitive, the theorem equally applies to excited states and to time-dependent states. In fact, it even makes a statement about excitation energies: Given some fermionic occupation-number state $|N_0, N_1, \ldots\rangle_-$ in terms of the single-particle orbitals $(h - \epsilon_a)\phi_a = 0$, the corresponding *bosonic* state will have an energy $E = \sum_a N_a \epsilon_a$.
- Since $A^2 = 1$, all local quantities will coincide with those computed from the fermion state. Specifically, this is the case for the density $\rho_N = |\Psi|^2$ and any derived quantities, such as the reduced densities $\rho(x)$ or $\rho_2(x_1, x_2)$. Nonlocal quantities however, particularly the momentum distribution, may differ dramatically from the fermionic ones.

What makes the Bose-Fermi map so useful is the fact that a free fermionic state is simply a "Slater determinant", that is, an (antisymmetrized) product of single-particle orbitals. This reduces a strongly correlated many-body state to a *single-particle* problem. In the rare case where the single-particle orbitals are known analytically, the solution may even be written down explicitly, such as for the ground state of N hard-core bosons in a harmonic trap [26]:

$$\Psi_+(X) \propto e^{-|X|^2/2} \prod_{1 \le i < j \le N} |x_i - x_j|.$$

This result nicely illustrates the interplay of the trapping forces and the two-body interactions: The asymptotics are dominated by the (harmonic) trap, whereas the short-range forces add cusps at all points of collision, $x_i = x_j$.

Remarks:

1. The Bose-Fermi map is restricted to *one* dimension. The reason is somewhat hidden in the succinct statement that it is sufficient to consider the fundamental region $\mathcal{D}$, for configuration space breaks down into disjoint regions obtained by permutations of $\mathcal{D}$. In dimension $d > 1$ the boundary $\{x_i = x_j \mid i < j\}$ actually fails to give disjoint regions. This line of reasoning links to the fact that $\mathbb{R}^{d>1}$ is not ordered, so there is no well-defined *unit antisymmetric function* A.
2. The one-to-one correspondence can in fact be extended to repulsive point interactions of finite strength. The basic idea is to relate a Bose gas with $g \in \mathbb{R}$ to a Fermi gas with a nonlocal "δ'" interaction, which leads to a discontinuity of Ψ rather than its derivative [60]. It is less useful in practice, though, since generally neither solution is known in closed form.

3. The mapping above relies explicitly on the concept of a many-body wave function $\Psi(X)$. However, an alternative Fock-space formulation has been proposed [61], constituting a map between fermionic and bosonic *field operators*:

   $$\hat{\psi}_+(x) = \exp\left[i\pi \int dx' \Theta(x - x')\hat{n}(x')\right] \hat{\psi}_-(x).$$

   This relation is somewhat less intuitive. Indeed, the unitary operator merely serves to reproduce the factors $\mathrm{sgn}(x_i - x_j)$ in the wave function, which are obtained when products of the creation operator are built.

4. As a side note, the map has also been extended to include mixtures of different particle species [62] and spinful bosons [63].

1.4.2 Lieb-Liniger model

The Bose-Fermi map introduced above has the advantage of providing a closed-form solution for a strongly interacting problem, which in principle holds for any external potential. There is one flaw, however: It refers only to the (somewhat unrealistic) limit of infinite repulsion while failing to make a statement about intermediate couplings g. The only model that may claim to have overcome this difficulty is the celebrated *Lieb-Liniger* theory, which deals with an *untrapped* system ($U = 0$) with periodic boundary conditions

$$\Psi(x_1 + L, \dots) = \Psi(x_1, \dots). \tag{1.18}$$

(The periodicity for multiples of L and other coordinates x_i follow by induction and by symmetry, respectively.) Physically, this is the somewhat exotic situation of particles enclosed on a ring of circumference L, which finds its justification in two rationales: (i) it can be solved, (ii) the exact boundary conditions do not matter much for an infinite system—in the thermodynamic limit—which was the original motivation in the seminal paper by Lieb and Liniger [20].

To proceed, the key is again to go to the fundamental domain $\mathcal{D} = \{0 \le x_1 < \cdots < x_N < L\}$, where the full Schrödinger equation $(E - H)\Psi = 0$ reduces to that of a free system unconstrained by permutation symmetry (which enters only when extended to the full configuration space). The periodicity requirement (1.18) and the contact interaction (1.12) enter as boundary conditions on $\partial\mathcal{D}$:

$$\begin{aligned}
\left(\partial_{j+1} - \partial_j\right) \Psi\big|_{x_j = x_{j+1}} &= g\, \Psi\big|_{x_j = x_{j+1}} && (1.19)\\
\partial_1\, \Psi\big|_{x_1 = 0} &= \partial_N\, \Psi\big|_{x_N = L} && (1.20)\\
\Psi(0, x_2, \dots, x_N) &= \Psi(x_2, \dots, x_N, L),
\end{aligned}$$

where the permutation symmetry has been exploited whenever a translation by L would lead out of $\bar{\mathcal{D}}$. We are now ready to state the solution:

Theorem (*Lieb-Liniger gas*) The solution of Schrödinger's equation in $\mathcal{D}$ obeying the boundary conditions (1.20) is given by the *Bethe ansatz*[18]

$$\Psi = \sum_{P \in S_N} a(P)\, U(P) \Phi_{\boldsymbol{k}}, \tag{1.21}$$

where

- $\Phi_{\boldsymbol{k}}(X) \equiv \prod_i e^{ik_i x_i}$ is a direct product of plane waves $|k_i\rangle$ determined implicitly by

$$(k_{j+1} - k_j)L = i \ln \left[\frac{\prod_l H\left(\frac{k_l - k_j}{g}\right)}{\prod_{l'} H\left(\frac{k_{l'} - k_{j+1}}{g}\right)} \right] (\mathrm{mod} 2\pi), \quad \text{with } H(z) \equiv \frac{1 + iz}{1 - iz} \tag{1.22}$$

- the coefficients $a(P)$ for some permutation $P = \prod_\alpha T_{i_\alpha j_\alpha}$ (decomposed in terms of transpositions T_{ij}) must meet

$$a(P) = \prod_\alpha \left(-e^{i\theta_{i_\alpha j_\alpha}} \right), \qquad \theta_{ij} \equiv -2 \arctan\left(\frac{k_i - k_j}{g} \right), \tag{1.23}$$

  where by convention $a(\mathbf{1}) = 1$.

Proof: As the formulas above suggest, the proof is rather technical and less instructive. Since none of its steps are in any way vital for this thesis, let us confine ourselves to the very essence: Irrespective of all the fine print, Bethe's ansatz (1.21) is basically an expansion in terms of plane waves, a most natural approach given that, in the interior of $\mathcal{D}$, plane waves are eigenstates of H_0 with total momentum $K = |\boldsymbol{k}|$ and energy $E = \frac{1}{2} \sum_i k_i^2$.

The physics is captured in the boundary conditions only—which is why this model is soluble in the first place. Specifically, these are the discontinuity condition (1.19), equivalent to the rule for $a(P)$ in (1.23), and the periodicity condition on $\mathcal{D}$ (1.20), which lead to

$$-e^{-ik_j L} = \prod_{i=1}^{N} (-e^{i\theta_{ij}}) \Longleftrightarrow k_j L = -\sum_i \theta_{ij} (\mathrm{mod} 2\pi).$$

Combined with the expression for the $\{\theta_{ij}\}$ obtained before, one infers the implicit equation system (1.22). □

The *full* wave function (and likewise the complete spectrum) again follows from that in the fundamental region by permutation symmetry, and it can be exploited to compute in principle any observables so long as the algebraic equations for the parameters k_j can be solved. This job surely is tedious, but it has been proven feasible for $N = O(10)$ [38]. In fact, the Bethe ansatz has even been extended to derive the ground state with hard-wall boundary conditions [43].

In their seminal paper, Lieb and Liniger did not bother to actually solve the *finite* system (except for $N = 2$), but proceeded directly to the *thermodynamic limit* $N, L \to \infty$ with $n \equiv N/L$ fixed.[19] It turns out that in this limit, the dimensionless coupling $\gamma := g/n$ will be the

---

[18] Bethe's ansatz (1.21), first used in [64], has been a very fruitful tool in a wide range of one-dimensional problems, mostly in the original context of lattice systems.

[19] Note that due to translational invariance (conservation of K), the density is constant for any g, even though of course ρ_1 as well as the correlation function ρ_2 will exhibit interaction effects.

only intensive quantity remaining [20]. The ground state energy $E_0 = Nn^2 e(\gamma)$ thus depends on g only through some universal function $e(\gamma)$, which in turn is computed via a Fredholm-type integral equation not displayed here. Most importantly, it connects the borderline cases

$$\begin{aligned} e(0) &= 0 && \text{(free bosons)} \\ \lim_{\gamma\to\infty} e(\gamma) &= \pi^2/3 && \text{(fermionization).} \end{aligned}$$

The key reasons why this analytic result has become immensely popular even in the seemingly very different context of *trapped* atoms is that one assumes a separation of length scales. Should the density of the *trapped* atoms vary slowly (in the neighborhood of some point x) compared with the length scale of the short-range correlations, it is plausible that *locally* one may take the Lieb-Liniger solution. The trap would then be included only for the *envelope* of the density. This *local-density approximation* is usually carried out by replacing the Lieb-Liniger chemical potential μ_0 by a local potential $\mu(x) \equiv \mu_0 - U(x)$. It is clear that this approach ought to work well wherever the density $n(x)$ is large compared with its change $n'(x)$, which is typically the case where the trap forces are zero (such as in the center of a homogeneous trap), while it fails where $n(x) \simeq 0$.

1.4.3 Two bosons in a harmonic trap

While the Lieb-Liniger model has the invaluable advantage of offering an analytic access to the Bose gas, it would be desirable to also have such a test bed in the case of *trapped* particles. As it turns out, even for the textbook model of harmonic confinement, the external forces break the integrability of the *relative* motion for $N > 2$ atoms. However, already the toy model of two bosons contains the key feature inherent in any trapped many-body system—the interplay between interaction and confining forces—which is what makes this soluble model so essential.

We begin our review with a general observation: In any system of N identical particles with homogeneous two-body interactions $\{V(x_i - x_j)\}$ and harmonic confinement $U(x) = \frac{1}{2}|x|^2$, the center of mass (CM) separates from the relative motion (valid for $x \in \mathbb{R}^d$, in principle). This is easy to see by computing the equations of motion for $R = \frac{1}{N}\sum_{i=1}^N x_i$ and its conjugate momentum $P = \sum_i p_i$, which follow from the CM-transformed Hamiltonian

$$H = h_{\mathrm{CM}} + H_{\mathrm{rel}}, \qquad h_{\mathrm{CM}} \equiv \frac{p_R^2}{2N} + \frac{1}{2}NR^2.$$

One can therefore decompose the Hilbert space $\mathbb{H} = \mathbb{H}_{\mathrm{CM}} \otimes \mathbb{H}_{\mathrm{rel}}$ so as to write the N-body wave function and its energy as

$$\Psi = \phi_{\mathcal{N}} \otimes \psi_{\mathrm{rel}}; \quad E = (\mathcal{N} + \tfrac{1}{2}) + \epsilon_{\mathrm{rel}},$$

where $\phi_{\mathcal{N}}$ is the HO orbital with quantum number $\mathcal{N} = 0, 1, \ldots$. While H_{rel} and thus the equations of motion for the $N-1$ *relative* coordinates will in general be highly coupled and resist an analytic solution, the two-body case reduces to an effective one-body problem for $r \equiv x_1 - x_2$:

$$H_{\mathrm{rel}} = -\partial_r^2 + \frac{1}{4}r^2 + g\delta(r).$$

This may be viewed as a harmonic potential split into halves in the center, i.e., at the point of collision $r = 0$,[20] where the delta function imposes the boundary condition[21]

$$\psi'(0^+) - \psi'(0^-) = g\psi(0). \tag{1.24}$$

This suggests a well-known procedure:

1. In $\mathbb{R}^1\backslash\{0\}$, expand ψ in terms of the standard solutions of the unperturbed differential equation
$$\left[\frac{d^2}{dr^2} - \left(\frac{1}{4}r^2 - \epsilon\right)\right]\psi = 0.$$
Explicitly, these are catalogued in [65] as the *parabolic cylinder functions*
$$U(-\epsilon, r);\; V(-\epsilon, r).$$
2. Impose the correct asymptotic behavior as $|r| \to \infty$, which secures that $\psi \in L^2(\mathbb{R}^1)$. This filters out the U function:
$$\psi_\epsilon(r) = cU(-\epsilon, r). \tag{1.25}$$
3. Apply boundary condition (1.24). Inserting the useful formulas [65]
$$\begin{aligned} \pm U'(-\epsilon, 0^\pm) &= -\frac{\sqrt{\pi}}{2^{-\frac{\epsilon}{2}-\frac{1}{4}}\Gamma\left(\frac{1}{4}-\frac{\epsilon}{2}\right)} \\ U(-\epsilon, 0) &= \frac{\sqrt{\pi}}{2^{-\frac{\epsilon}{2}+\frac{1}{4}}\Gamma\left(\frac{3}{4}-\frac{\epsilon}{2}\right)} \end{aligned}$$
leads us to an implicit equation for $\epsilon(g)$. For pure convenience, let us recast this in terms of the effective quantum number $\nu(g) \equiv \epsilon(g) - \frac{1}{2} \in \mathbb{R}$,
$$\nu(g) \in f_g^{-1}(0): \quad f_g(\nu) := 2^{3/2}\frac{\Gamma\left(\frac{1-\nu}{2}\right)}{\Gamma\left(-\frac{\nu}{2}\right)} + g. \tag{1.26}$$
4. Finally, the normalization constant c is fixed by $\|\psi\| = 1$. This step is conceptually irrelevant and omitted here.

Equations (1.25) and (1.26) determine the solution of the two-particle problem. To get a better understanding of its physical significance, let us detail some of its features.

Asymptotics of ψ

For any value of g, the wave function's behavior at $r = 0$ is determined by the boundary condition (1.24), which imposes a kink, i.e., a discontinuity in ψ'. For positive g, this amounts to a "dip" at $r = 0$ (see Fig. 1.1a), reflecting the particles' tendency to repel each other. In the attractive case $g < 0$, in turn, the dip flips into a peak shaped like $e^{-|gr|/2}$ (Fig. 1.1b,c) –

---

[20] It is clear that a perturbation $\delta(r)$, having support only at $r = 0$, has no effect on fermionic states. There the exclusion principle demands that $\psi(-r) = -\psi(r)$; in other words, these states would have negative parity. We consider bosonic, that is, even functions.

[21] In what follows, the subscript "rel" will be dropped for convenience.

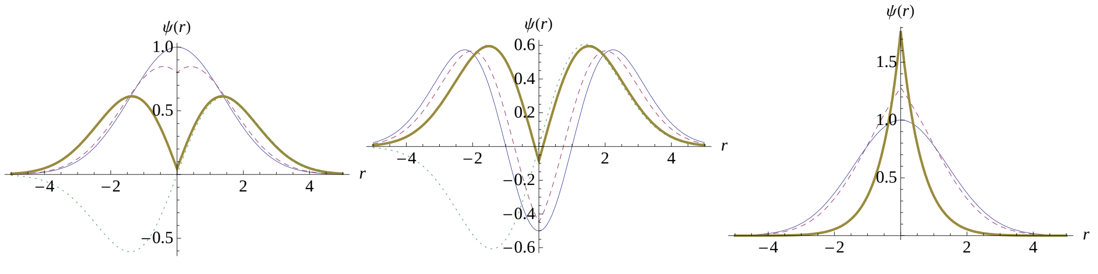

(a) (b) (c)

Figure 1.1: Relative wave function $\psi_\nu(r)$ (in arbitrary units).
(a) *Ground state for repulsive interactions*: The $g = 0$ orbital ($\nu = 0$, thin line) acquires a dip at $r = 0$ for $g > 0$ (cf. $\nu = 0.2$, dashed). As $g \to +\infty$ ($\nu = 0.95$, thick line), this notch reaches almost zero, and the wave function becomes practically indistinguishable (in modulus) from the fermionic ground state $u_1(r) \propto r\, e^{-r^2/4}$ (dotted line).
(b) *Excited states for attractive interactions*: The first bosonic excitation ($\nu = 2$, thin line) picks up a cusp at zero for $g < 0$ (cf. $\nu = 1.7$, dashed). As $g \to -\infty$ ($\nu = 1.1$, thick line), this cusp becomes sharper but, at the same time, is damped out more and more until the wave function's modulus equals the fermionic state $u_1(r) \propto r\, e^{-r^2/4}$ (dotted line).
(c) *Ground state for attractive interactions*: The Gaussian ground state ($\nu = 0$, thin line) becomes peaked for $g < 0$ (cf. $\nu = -0.3$, dashed). Unlike before, this does not saturate but tends to a delta function as $g \to -\infty$ ($\nu = -3$, thick line).

the bound state (1.13) of the pseudopotential in free space. Physically, this corresponds to a molecule strongly localized for very strong attraction $|g|$.

For $r \to \infty$, the wave function falls off like $\psi(r) \sim c e^{-r^2/4} r^\nu$ [65]. Not unexpectedly, the asymptotics is given by that of the HO orbital, but with the generalized quantum number ν. From this, the following picture emerges: An unperturbed HO level is "notched" at $r = 0$ (for $g > 0$), but the effect remains essentially local. Asymptotically, the state behaves almost as if unperturbed, except for the fact that the dip causes the wave function to spread. This reflects in the non-integer exponent (r^ν), leaving an asymptotic imprint of the interaction similar to the concept of phase shifts in scattering theory.

Dependence on g

Equation (1.26) implicitly determines $\epsilon(g) \equiv \nu(g) + \frac{1}{2}$ via the zeroes of f_g. However, it is instructive to get an explicit understanding of how the energy levels evolve as g is varied.

Clearly, at $g = 0$, $f_g(\nu) = 0$ only if the denominator has a pole, $-\frac{\nu}{2} \in -\mathbb{N}$. Hence the non-interacting limit $\nu(g = 0) \in 2\mathbb{N}$ is recovered: the *even* HO levels.

The complementary borderline case $g \to \pm\infty$ is reached for $\nu \in 2\mathbb{N} - 1$. In fact, the solution of (1.26) reveals that these limits are linked as follows (Figs. 1.1, 1.2):

- Starting from a non-interacting level $\nu(0) = 2n$, a small interaction g shifts the energy levels upward (downward) depending on the sign of g: [17]

  $$\epsilon(g) = 2n + \frac{1}{2} + \frac{g}{\sqrt{2\pi}} \binom{n - \frac{1}{2}}{n} + O(g^2),$$

  a result which may be obtained from perturbation theory.

- As g tends to $+\infty$, the next level, $\lim_{g\to\infty} \nu(g) = 2n + 1$, is reached, corresponding to the upper next *fermionic* level. This is a neat illustration of fermionization (Sec. 1.4.1): An even oscillator orbital (say $n = 0$) is notched in the center for $g > 0$ until the dip

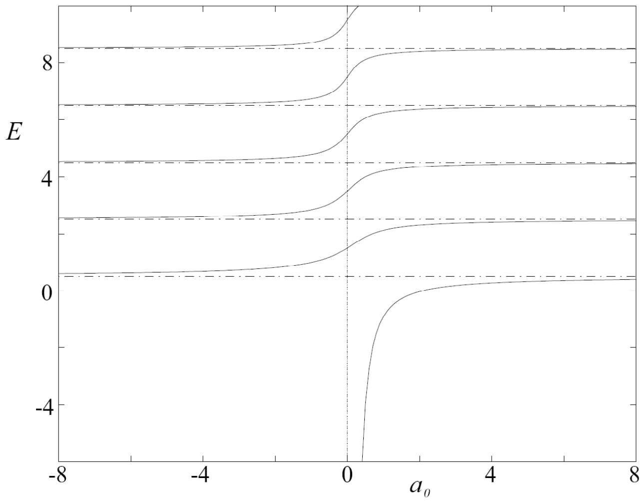

Figure 1.2: Spectrum $\{\epsilon_\nu\}$ of the relative motion as a function of the interaction strength g (Here plotted over $1/a_0 \equiv -g/2$. The plot is taken from [17].)

reaches down to $\psi(0) = 0$ in the limit of fermionization (Fig. 1.1a). In that limit, the wave function equals the first *odd* (fermionic) orbital in density, $\psi = |u_{n=1}|$, whose node at $r = 0$ translates to a dip. The correct bosonic symmetry is restored by multiplying the unit antisymmetric function, $A(r) = \mathrm{sgn}(r)$, which for $n = 0$ amounts to taking the absolute value.

- Conversely, for infinite attraction, the non-interacting level $2n \neq 0$ will be lowered to $\lim_{g\to-\infty} \nu(g) = 2n - 1$. Note that this matches exactly the fermionized level starting from $\nu(0) = 2(n-1)$ – indeed, all energies periodically connect the limits $g \to \infty$ from below to the case $g \to -\infty$. This may be interpreted as some type of fermionization, different from the conventional sense: An unperturbed even level $2n \neq 0$ picks up a kink at $r = 0$ (Fig. 1.1b), which becomes ever sharper and smaller for $g \to -\infty$ until it goes over to the dipped fermionized orbital corresponding to $2(n-1)$.
  For the ground state $n = 0$, such a mechanism simply is not available: The unperturbed Gaussian u_0 will be turned into a single peak $e^{-|gr|/2}$ (Fig. 1.1c).

Dimensionality aspects

Finally, let us mention that the solution of the two-atom problem in a harmonic trap is not restricted to dimension $d = 1$. In fact, it had been solved originally for the realistic case $d = 3$ [17] (and later also for an anisotropic trap [66]) by expansion in terms of the free solutions. Rather than indulging in details, let us state that the 1D case connects to the solution in arbitrary d via

$$U(-\epsilon \equiv -[\nu + \tfrac{1}{2}], r) = \frac{1}{2^{\nu/2}} e^{-r^2/4} U\left(-\frac{\nu}{2}, \frac{1}{2}, \frac{1}{2} r^2\right),$$

where $U(a, b, c)$ is the confluent hypergeometric function [65]. This is already the general form of the solution in any d, with the numerical constants in the arguments depending on d. For instance, the 3D s-wave function for the radial coordinate has the form

$$\Psi_\nu(r) = ce^{-r^2/2}\Gamma(-\nu)U\left(-\nu, \frac{3}{2}, r^2\right).$$

This is quite remarkable, since it represents different physics: In 3D, the full wave $\Psi(r) = u(r)/r$ (u being the regular *radial* wave function) exhibits a singularity at points of collision for any $g \neq 0$. This mirrors the behavior of the Green function $G(r) \propto e^{ikr}/r$. A similar solution exists for 2D.

Chapter 2

Many-body methods for ultracold bosons

Technically speaking, the goal of this thesis is of course simply to solve the few-boson Schrödinger equation

$$[i\partial_t - H(t)]\,\Psi(t) = 0 \tag{2.1}$$

subject to the initial condition $\Psi(0)$. Its formal solution reads $\Psi(t) = \mathrm{T}e^{-i\int_0^t H(s)ds}\Psi(0)$, where T denotes time ordering. In the case of time-independent Hamiltonians, this reduces to

$$\Psi(t) = e^{-iHt}\Psi(0) = \sum_m e^{-iE_m t} c_m \Psi_m,$$

in terms of the stationary states[1]

$$(E_m - H)\Psi_m = 0. \tag{2.2}$$

Since, for stationary Hamiltonians, Eq. (2.1) is equivalent to knowing the eigenstates and their corresponding eigenfrequencies, one thus has the choice of tackling it directly as an initial-value problem or via diagonalizing H. Still, this is easier said than done. In fact, there are only very few, rather idealized, borderline cases in which the many-body problem is solved in closed form (see Sec. 1.4). While these may be useful in understanding or even constructing more complicated many-body solutions, one generally has to resort to numerical algorithms, whose essence is to boil down a single unsolvable problem (Eq. 2.1) into (finitely) many feasible ones.

In Sec. 2.1, we attempt to give a coarse overview of some methods widely used in the context of ultracold bosons. One part of this thesis is to develop an *exact diagonalization*, which is presented in Sec. 2.2. However, most results in this thesis have been obtained by a time-dependent method, *Multi-Configuration Time-Dependent Hartree* (MCTDH), a concise description of which is given in Sec. 2.3.

---

[1] We assume a discrete spectrum since we are interested in trapped atoms.

2.1 Overview of some approaches

Even though the method of choice in this thesis is MCTDH (described below in Sec. 2.3), it is worthwhile to review some common approaches in the field. For one thing, it gives an insight into some very general concepts behind many-body methods, and how they relate to one another. More importantly, though, the key ideas underlying these methods already contain a whole lot of physics, which helps us get a new perspective on the system and, conversely, understand what kind of information we discard when we make certain approximations.

Although the numerical schemes may be very different in practice, all methods more or less fall into either of the following categories:

1. Methods that approximate the *solution* numerically. These *ab initio* approaches have the common feature that they make some essentially *exact* representation of the solution which is cut off so as to make the algorithm feasible (i.e., finite). That cutoff may be varied *a posteriori*, giving a handle on the convergence to the exact solution.
2. Methods that approximate the *problem*. In other words, one invests some physical knowledge of the system under consideration and *a priori* replaces the full problem by a simplified one.

To make this distinction clearer, we will now give some examples with a focus on ultracold (*here*: zero-temperature) bosons.

2.1.1 *Ab initio* methods

Exact diagonalization and multi-configurational self-consistent methods The key idea of *exact-diagonalization* approaches lies so much at the heart of quantum mechanics that terming it a “many-body method” of its own seems a bit of a mouthful. In fact, it is certainly the most straightforward scheme, applicable to any stationary problem (2.2): By expanding the exact solution $\Psi \in \mathbb{H}$ in terms of some (known) orthonormal basis,

$$\Psi \sim \sum_{k \leq K} c_k \Phi_k, \quad C \equiv (c_1, , \ldots, c_K)^\top \in \mathbb{C}^K, \tag{2.3}$$

with an arbitrary cutoff K ($K \to \infty$ recovering the exact wave function), the problem readily maps to a matrix problem on $\mathbb{C}^K$:

$$(E\mathbf{1} - H)C = 0, \text{ with } (H)_{kl} = \langle \Phi_k | H | \Phi_l \rangle. \tag{2.4}$$

This is nothing but the well-known isomorphy of any K-dimensional Hilbert space (over $\mathbb{C}$) with $\mathbb{C}^K$, which ensures that $H \equiv (H_{kl}) = H^\dagger$ is also diagonalizable and yields the same spectrum – nothing new so far. The gist is that a matrix problem can be solved numerically using standard routines, provided (H_{kl}) is known and not too large – a succinct statement, which in practice proves highly explosive. In fact, the entire Sec. 2.2 is more or less dedicated to just that little “catch”.

Apparently, the scheme outlined above makes no reference whatsoever to the many-body nature of our problem – in fact, it defines a fairly general *class* of many-body methods. Mostly, when we talk about *exact diagonalization*, the following fine print is understood: The basis vectors are assumed to be number states

$$\Phi_{\boldsymbol{n}} = |\boldsymbol{n}\rangle \equiv \left(\prod_a \frac{1}{\sqrt{n_a!}} (c_a^\dagger)^{n_a} \right) |0\rangle \tag{2.5}$$

in some convenient one-body basis $\{\phi_a\}$. The physical picture is that the true—generally correlated—many-body state is replaced by a superposition of single-particle states $\Phi_{\boldsymbol{a}} = \phi_{a_1} \otimes \cdots \otimes \phi_{a_N}$ or, conforming to the permutation symmetry required for identical particles, symmetrized *configurations* $S_\pm \Phi_{\boldsymbol{a}}$. Of course, nothing stops us from using different basis vectors which already carry explicit correlations [e.g., constructing Φ_k from two-body functions $f(\mathbf{x}_1, \mathbf{x}_2)$], except that it makes life more complicated (cf. Sec. 2.2).

A different version consists in using *self-consistent* one-particle functions ϕ_a to build the basis vectors (2.5). This means that, rather than treating $\{\phi_a\}$ as fixed, the orbitals are *optimized* subject to a variational principle. In the spirit of our laconic remark above, this approach is a trade-off: Optimizing the basis is likely to keep the dimension K small (filtering out the "physically relevant" subspace of $\mathbb{H}$), while it complicates the computation of the Hamilton matrix (H_{kl}). One representative of such multi-configurational *self-consistent* methods is *MCTDH*, which will be explained in detail in Sec. 2.3. It combines variationally optimized basis functions with an inherently time-dependent approach (*wave-packet propagation*).

Density-Matrix Renormalization Group The *density-matrix renormalization group* (DMRG) essentially also pertains to the class of exact-diagonalization methods. While its details are somewhat gory [67] and omitted here, the key idea is worth mentioning, which is to efficiently decimate the Hilbert space to a relevant subspace. The premise is that the Hamiltonian is defined on a real-space 1-D lattice $\mathcal{L} = \{x_s \in \mathbb{R}^1 \mid s = 1, \ldots, S\}$, or can be mapped to one.[2] The procedure now is as follows, here illustrated for the ground state:

1. One picks some site $s < S$ and decomposes the lattice into the union of that site with two sublattices *left* (L_s) and *right* (R_s) of s: $\mathcal{L} = \{x_l\}_{l=1}^{s-1} \cup \{x_s\} \cup \{x_r\}_{r=s+1}^{S}$. For a fixed many-body basis set $\{|\alpha^{(s)}\rangle\}_{\alpha=1}^{K}$ on L_s (and $\{|\beta^{(s)}\rangle\}_{\beta=1}^{K}$ on R_s, respectively), the wave function is expanded in terms of these as

   $$\Psi = \sum_{\alpha,\beta,N_s} C_{\alpha\beta}^{N_s} |\alpha^{(s)}; N_s; \beta^{(s)}\rangle,$$

   where N_s denotes the occupation number of the single-particle state localized on site s.

2. Variationally optimizing this state with respect to $C^{(s)} \equiv (C_{\alpha\beta}^{N_s})$ leads to an effective matrix-eigenvalue problem $(H^{(s)} - \mathbf{1}E)C^{(s)} = 0$. Solving this for the ground state yields the *reduced* density matrix for the subsystem $\mathrm{L}_s \cup \{x_s\}$, $\rho^{(s)} = \mathrm{tr}_{\mathrm{R}_s}(|\Psi\rangle\langle\Psi|)$ by integrating out the right sublattice.

3. A spectral decomposition of $\rho^{(s)} = \sum_\alpha p_\alpha^{(s)} |\Phi_\alpha^{(s)}\rangle\langle\Phi_\alpha^{(s)}|$ reveals the weights $p_\alpha^{(s)}$ of each contributing eigenstate $\Phi_\alpha^{(s)}$ on the reduced lattice. The key step now is to keep only the

---

[2] Of course, this is not a serious restriction, since many methods (like MCTDH in Sec. 2.3) essentially work on a spatial grid. However, in DMRG this is hardwired into the fundamental algorithm and not introduced for technical convenience alone.

most relevant terms $\alpha \leq K$, whereas higher terms are discarded. (This tacitly assumes that the weight distribution falls off sufficiently fast with α.)

4. Substitute the old basis $|\alpha^{(s)}; N_s\rangle$ on $\mathrm{L}_{s+1} = \mathrm{L}_s \cup \{x_s\}$ by a more efficient one, namely the (truncated) eigenstates $\Phi_\alpha^{(s)} =: |\alpha^{(s+1)}\rangle$. Likewise, this can be done for $\mathrm{R}_s = \{x_{s+1}\} \cup \mathrm{R}_{s+1}$. In this sense, the "bookmark" site s has been shifted to the right by one site, and on the updated lattice decomposition $\mathcal{L} = \mathrm{L}_{s+1} \cup \{x_{s+1}\} \cup \mathrm{R}_{s+1}$, the wave function can be written as

   $$\Psi = \sum_{\alpha,\beta,N_{s+1}} C_{\alpha\beta}^{N_{s+1}} |\alpha^{(s+1)}; N_{s+1}; \beta^{(s+1)}\rangle.$$

   Now proceed at step (2.) with $s + 1 \mapsto s$, until the sweep hits the right lattice boundary, i.e., $s = S - 1$ is reached. After that, the whole sweep goes on from right to left, and so on until convergence is achieved.

This defines a procedure to iteratively select a *small* subspace of the full Hilbert space, keeping only the most relevant terms (*here*: for the ground state) – where relevance in each step is defined with respect to the momentary sublattice L_s.

From this angle, it is also plausible that this approach is effectively limited to one dimension: Apart from the technical difficulties in defining an appropriate sublattice—and consistently expanding it—the working hypothesis that the system can be split into different subsystems which are not too strongly entangled is questionable in two or even three spatial dimensions. It goes without saying that the concept sketched above tacitly assumes zero temperature; in fact, this is when DMRG is at its best. Nonetheless, for one-dimensional systems, DMRG has proven quite useful in treating both static and dynamic 1D problems. Its efficiency even for strongly correlated systems with up to $N \sim 100$ particles [45] essentially derives from the fact that it is based on a *spatial* grid and makes no explicit reference to the particle number, as opposed to the basis of *particle configurations* employed in the exact-diagonalization methods, which covers highly redundant regions of the Hilbert space.

It is worth mentioning that the modern viewpoint on DMRG does without the above prescription of extending the left lattice site by site. Rather, it is interpreted as a variational optimization of the wave function within the class of *matrix-product states* – that is, making the ansatz

$$\Psi = \sum_{\boldsymbol{n}} \mathrm{tr}\left(A_1^{(N_1)} \cdots A_S^{(N_S)}\right) |\boldsymbol{n}\rangle,$$

where $\boldsymbol{n} \equiv (N_1, \ldots, N_S)$ $(N_s = 0, \ldots, N_{\max})$ denotes the occupation numbers of each site's orbital, and $A_s^{(N_s)}$ is a $K \times K$ matrix that serves to parametrize the expansion coefficients. Note that this is a restriction: An arbitrary state $\Psi = \sum_{\boldsymbol{n}} c_{\boldsymbol{n}} |\boldsymbol{n}\rangle$ is described by $(N_{\max} + 1)^S$ numbers, whereas for the matrix-product state this scales linearly with the number of sites, $K^2(N_{\max} + 1) \times S$. Now Ψ is variationally optimized with respect to $A_s \equiv \left(A_s^{(N_s)}\right)$ for some fixed site s, which eventually yields an effective matrix-eigenvalue problem of type $(H^{(s)} - \mathbf{1}E)A_s = 0$. Since the Hamiltonian implicitly depends on all $\{A_s\}_{s=1}^S$, this asks for an iterative optimization. This is carried out by sweeping through all s, each time improving on the coefficients $\mathrm{tr}\left(A_1^{1)} \cdots A_S^{(N_S)}\right)$. This procedure is exactly equivalent to the traditional algorithm above, (1.–4.), even though it is not obvious. Likewise, it is far from trivial in what situations the matrix-product expansion is good, apart from the exact-diagonalization limit when $K \to \infty$.

Quantum Monte Carlo While the former approaches in some way still aspire to compute the system's wave function Ψ, *Quantum Monte Carlo* methods (QMC) essentially exploit the Monte Carlo integration technique to calculate many-body observables directly [68]. To illustrate the basic idea, consider some expectation value

$$\langle A \rangle = \int dP(\mathbf{X}) A(\mathbf{X}) \approx \sum_{\mathbf{X}} P(\mathbf{X}) A(\mathbf{X}),$$

where $\mathbf{X} = (x_1, \ldots, x_N)^\top$ denotes a point in configuration space, and $dP(\mathbf{X}) \equiv d\mathbf{X} \varrho(\mathbf{X})$ is a given probability distribution. In the last step, we have discretized the integral into an (ultimately finite) sum over vectors $\{\mathbf{X}\}$. The key idea now is to carry out an *importance sampling* of the configurations $\{\mathbf{X}_k\}_{k=1}^K$, i.e., to pick these such that the relative frequency w_k of an element reflects its physical probability, $w_k \approx P(\mathbf{X}_k)$. In that case, the above sum simply translates into an arithmetic average

$$\langle A \rangle \approx \frac{1}{K} \sum_k A(\mathbf{X}_k),$$

so one is solely left to sum up the local averages of A at certain configurations. In principle, for large enough samples $\{\mathbf{X}\}$, the results become exact up to statistical errors, which may be controlled by doing several simulations.

Of course, the problem has only been "outsourced" to generating such a properly distributed sequence $\{\mathbf{X}_k\}$. However, this mathematical problem is well understood and is tantamount to setting up a *Markov chain* $\mathbf{X} \to \mathbf{X}' \to \cdots$ complying with the following criteria for the transition probabilities:

1. $W(\mathbf{X} \to \mathbf{X}') > 0 \; \forall \mathbf{X}, \mathbf{X}'$
2. $\sum_{\mathbf{X}'} W(\mathbf{X} \to \mathbf{X}') = 1 \; \forall \mathbf{X}$ (completeness)
3. $\sum_{\mathbf{X}} P(\mathbf{X}) W(\mathbf{X} \to \mathbf{X}') = P(\mathbf{X}') \; \forall \mathbf{X}'$ (P is fixed point of W).

A somewhat handier *sufficient* condition often replacing (3.) is that of *detailed balance*, $P(\mathbf{X})/P(\mathbf{X}') = W(\mathbf{X}' \to \mathbf{X})/W(\mathbf{X} \to \mathbf{X}')$. One scheme that respects this criterion and which is widely used to construct such a sequence is the *Metropolis algorithm* [69].

The basic idea sketched above is applicable to all kinds of many-body integrals. Indeed, QMC comes in different flavors. Only to name a few which are of interest for low-temperature properties of bosons:

- *Variational Monte Carlo* computes the ground state Ψ_0 of some Hamiltonian by making an ansatz Φ_α in terms of some parameter set $\alpha = (\alpha_1, \alpha_2, \ldots)$. By the variational principle, $\langle H \rangle_{\Phi_\alpha} \geq E_0$, this gives an upper bound to the true ground-state energy. The bound can be lowered by making an intelligent guess for the ansatz and subsequently varying α so as to minimize the energy $\langle H \rangle_{\Phi_\alpha}$, which is evaluated using Monte Carlo. In principle, this extends to excited states, although that route is rarely pursued in practice. Not only is it cumbersome, but it also crucially depends on an accurate ansatz state.

- *Diffusion Monte Carlo* is tailored to the ground state, using the equivalence of the Schrödinger equation in *imaginary time* $\tau \equiv it$—for which the evolution operator becomes the non-unitary $e^{-H\tau}$— with the diffusion equation. For $\tau \to \infty$, this converges to the true ground state upon renormalization.
- *Path-integral Monte Carlo* takes a somewhat different approach. It makes use of the path-integral representation of the partition function, which allows to extract all observables. Approximating the path integral by a standard, usually high-dimensional, integral, the same machinery as above can be used to sample that integral.

The advantages of QMC are obvious: By doing a random sampling of the configuration space, one has an essentially exact method while permitting a highly flexible form of the wave function. This way, one is not restricted to certain expansions in terms of product states, such as in the previous methods, which permits the treatment of even larger, strongly correlated systems (up to $N \sim 100$) in arbitrary dimensions. This comes at a price: Excitations, and this way quantum dynamics, are not easily accessible since, in principle, all the knowledge about the zeroes of the exact wave function must be built into the scheme *a priori*. The very same issue makes it troublesome to treat fermionic systems or, by extension, mixtures: The antisymmetry imposed by the Pauli principle usually needs to be incorporated in the scheme (the so-called “sign problem”) .

2.1.2 Approximative methods

As might have become transparent in the previous subsection, the distinction between “exact” and “approximative” approaches is really between *controlled* and *uncontrolled* approximations. A priori restricting an essentially exact expansion to only a few modes leaves us with some well-known simplified models, some of which shall be briefly derived below to raise the awareness of their range of validity.

Gross-Pitaevskii The by far simplest “many-body” method is linked to the familiar picture of an *ideal* Bose gas, the historical context of Bose-Einstein condensation [1]. Below a critical temperature near absolute zero, a phase transition occurs which has all (non-interacting) bosons condense into the lowest single-particle eigenstate ϕ_0 of the single-particle Hamiltonian h. The many-body ground state (defined as $T \to 0$) thus reads $\Psi_0 = \phi_0^{\otimes N}$. Equivalently, in the Fock-space language, it is a number state in the single-particle basis $\{\phi_a\}$ of h: $|N_0 = N, N_1 = 0, \dots\rangle$ – actually, this “macroscopic” occupation $\langle \hat{N}_0 \rangle \overset{T\to 0}{\sim} N$ is the textbook signature of Bose condensation.

Needless to say, this is no longer true for interactions $V \neq 0$, simply because the true eigenstate fails to be a (single-particle) eigenstate of $\sum_{i=1}^N h_i$ but contains correlations. Nonetheless, the concept of condensation can be generalized in the following sense: We know from Sec. 1.3 that the concept of occupation-number states $|N_0, N_1, \dots\rangle$ extends to arbitrary states with a one-body density matrix $\rho_1 = \mathrm{tr}_{2,\dots,N}\rho_N$, whose eigenvalues $n_a =: N_a/N$ can be thought of as “occupation numbers” of the corresponding eigenvectors ϕ_a (so-called *natural* orbitals). From this standpoint, an eigenvalue $n_a \sim 1$ has been accepted as a generalized *definition* of Bose-Einstein condensation [70].

Assuming Bose-Einstein condensation, $\Psi = \phi^{\otimes N}$, the matrix Schrödinger equation (2.4) simply boils down to a single equation

$$E = \langle \phi^{\otimes N} | H | \phi^{\otimes N} \rangle = N \langle \phi | h | \phi \rangle + \frac{N(N-1)}{2} \underbrace{\langle \phi^{\otimes 2} | V | \phi^{\otimes 2} \rangle}_{\equiv \int dx_1 \int dx_2 \phi^*(x_1)\phi^*(x_2) V(x_1,x_2) \phi(x_1)\phi(x_2)} .$$

This can be interpreted simply as the energy functional

$$E_{N,g}[\phi^*, \phi] = N \int dx \phi^*(x)(h\phi)(x) + \frac{N(N-1)}{2} \int dx_1 \int dx_2 V(x_1, x_2) \left| \phi(x_1)\phi(x_2) \right|^2 .$$

In view of the variational principle, this gives an upper bound to the exact ground-state energy. That bound can be improved by minimizing it on the unit sphere $\|\phi\| = 1$, which is done by looking for an extremum of $E_{N,g}[\phi^*, \phi] - N\mu(\|\phi\|^2 - 1)$. For the special case $V(x_1, x_2) = g\delta(x_1 - x_2)$, this yields the *Gross-Pitaevskii* equation (GPE)[3]

$$\left(h + (N-1)g \left| \phi \right|^2 \right) \phi = \mu \phi,$$

which automatically guarantees a minimum of $E_{N,g}$. Note that the GPE takes the form of a single-particle Schrödinger equation with a *nonlinear* interaction term governed only by the scaled coupling $\lambda \equiv (N-1)g$ rather than N, g individually. For $\lambda \to 0$, it simply recovers the single-particle case. In the complementary *Thomas-Fermi* limit $\lambda \to \infty$, in turn, the potential terms $U(x) + \lambda \left| \phi(x) \right|^2$ overwhelm the kinetic energy [1], allowing for the trivial solution $\left| \phi(x) \right|^2 = \max\{ [\mu - U(x)] / \lambda ; \, 0 \}$.

The GPE can be shown to become exact in the limit [72]

$$N \to \infty, \; g \to 0 \text{ , with } \lambda \approx Ng = \text{const.}$$

From this point of view, significant deviations are expected for small atom numbers N or strong interactions g.[4] The validity of the GPE may be better understood by taking a *Fock-space* viewpoint. Consider the mode expansion of the field operator (Eq. 1.3) $\psi(x) = \phi_0(x)c_0 + \sum_{a \neq 0} \phi_a(x) c_a$. The “condensate”-mode operator acts on number states as

$$c_0 | N_0, \ldots \rangle = \sqrt{N_0} | N_0 - 1, \ldots \rangle.$$

Assuming condensation and $N_0 \sim N \gg 1$, one can make the heuristic assumption that $c_0 \approx \mathbf{1}\sqrt{N}$, thus ignoring particle annihilation/creation in mode $a = 0$. In that case, the above decomposition reads

$$\psi(x) \approx \sqrt{N} \phi_0(x) + \sum_{a \neq 0} \phi_a(x) c_a =: \langle \psi(x) \rangle + \delta\psi(x).$$

---

[3] The derivation presented here applies to the ground state. However, there also exists a time-dependent version of the GPE, tantamount to replacing the right-hand side by $i\partial_t \phi$. Its proof of validity is far from trivial, though, since during the evolution dynamical excitations might undermine the premise of a condensate [71].

[4] The situation is more difficult in 1D [73], where Bose condensation at $T > 0$ is strictly forbidden in *homogeneous* systems. In traps, however, there still is a *quasi*-condensate with small density but non-negligible phase fluctuations [74].

We have ascribed an expectation value to the field operator, this way introducing a *mean field* $\langle\psi\rangle \equiv \sqrt{N}\phi_0$. The above decomposition implies $\sum_a \hat{N}_a \approx N + \sum_{a\neq 0} \hat{N}_a$, which amounts to allowing for particle-number fluctuations reminiscent of the grand-canonical ensemble. The idea now is to think of this as an *expansion* of the true field operator about its *classical* value (the mean field). Plugging this into the second-quantized Hamiltonian (1.5) yields

$$H = N\int dx\phi_0(x)h\phi_0(x) + \frac{N^2}{2}g\int dx\,|\phi_0(x)|^4 + O(\delta\psi)^2.$$

To zeroth order, and for $N^2 \approx N(N-1)$, this is nothing but the energy functional $E_{N,g}$ encountered in the derivation of the GPE. The procedure of assigning a mean value to a field operator is completely analogous to the modeling of *coherent states* in quantum optics – similarly, the GPE is said to describe coherent or classical states. Including the next order in $\delta\psi$ yields a Hamiltonian that is quadratic in $c_{a\neq 0}$, i.e., describes an effective single-particle Hamiltonian. Its diagonalization leads to the so-called *Bogoliubov equations* [1], which describe small *quantum fluctuations* $\langle\hat{n}(x_1)\hat{n}(x_2)\rangle - n(x_1)n(x_2)$ about the (classical) mean field.

Hartree-Fock vs. Multi-orbital mean field The mean-field methods introduced above assume (almost) complete Bose-Einstein condensation, i.e., one dominant single-particle mode ϕ_0. While this is justified for weak enough interactions in a quasi-homogeneous trap, there are situations when this breaks down. These include, of course, strong interactions, but also having two or more *weakly coupled* condensates such as in a multi-well trap. Similarly, this applies to multi-component condensates like spinors or mixtures.

An obvious way to extend the above mean-field scheme is the following. As pointed out above, the GPE describes the variationally optimal number state $|N_0 = N, \ldots\rangle$ with all bosons in mode ϕ_0. The most straightforward generalization in terms of a single-particle state would be to search the variationally best number state $|\boldsymbol{n} \equiv N_0, \ldots, N_A\rangle$ in the multi-orbital basis $\{\phi_{a\leq A}\}$, with a cutoff $A+1 \leq N$. For $A+1 = N$, i.e., allowing for possibly just as many orbitals as particles, this recovers the (bosonic) *Hartree-Fock* method known from electronic-structure theory. A slight modification is achieved if the number of orbitals included is *a priori* fixed to $A+1 < N$: This implies that the wave function should be searched in the class of functions

$$\Psi = \sqrt{\frac{N!}{\boldsymbol{n}!}}S_+\{\underbrace{\phi_0\otimes\cdots\otimes\phi_0}_{N_0\times}\otimes\cdots\underbrace{\phi_A\otimes\cdots\otimes\phi_A}_{N_A\times}\},$$

where N_a bosons reside in orbital ϕ_a. These orbitals are governed by *multi-component* mean-field equations for $\boldsymbol{\phi} \equiv (\phi_0, \ldots, \phi_A)^\top$, analogous to Hartree-Fock [75]. The difference is that, in addition to the orbitals, also the occupation numbers N_a may be varied so as to minimize $E[\Psi]$. This *multi-orbital mean-field* approach has been applied to a variety of physical situations where interactions make it energetically favorable for bosons to occupy different orbitals rather than a single one (such as modes localized on different sites in a multi-well trap).[5] Note that, just as for the GPE, this readily extends to the time-dependent case.

---

[5] The word *mean field* should be taken with *cum grano salis*. Hartree-Fock and its derivates are *mean-field* methods in the sense that they do not account for physical *inter-particle* interactions. Rather, each particle feels only an effective single-particle "mean-field potential". By contrast, they go far beyond the concept of a "mean field" $\langle\psi\rangle \equiv \sqrt{N}\phi$ as is typically understood in the context of quantum field theory.

2.2 Exact Diagonalization

The basic concept of the *exact diagonalization* scheme, as has been laid out in the previous section, is wrapped up in Eq. (2.4): The time-dependent Schrödinger equation is mapped to a (finite) matrix-eigenvalue problem by expanding Ψ in terms of occupation-number states $|\boldsymbol{n}\rangle$, provided some fixed single-particle basis set $\{\phi_a\}$. The matrix problem is then solved using existing numerical routines. The following technical procedure naturally suggests itself:

1. Choose an appropriate basis (Sec. 2.2.2)
2. Compute the Hamilton-matrix elements (Sec. 2.2.3)
   (a) Break down the many-body matrix elements $\langle \boldsymbol{n}'|H|\boldsymbol{n}\rangle$ into primitive (one- and two-particle) matrix elements $\langle a|h|b\rangle$, $\langle ab|V|cd\rangle$
   (b) Compute $\langle a|h|b\rangle$, $\langle ab|V|cd\rangle$
3. Build up the Hamilton matrix (H_{kl}), i.e., map $|\boldsymbol{n}\rangle$ to a single matrix index k (Sec. 2.2.4) and diagonalize H numerically
4. Analyze the results, that is, compute the reduced densities ρ_n (Sec. 2.2.5)

Here we will concentrate on the fundamental case of a harmonic trap, $U(x) = \frac{1}{2}x^2$. Before going into the details, let us revisit the foundations of the method so as to gain a better understanding of its strengths and limitations.

2.2.1 Preliminary remarks

It is instructive to look at the exact-diagonalization method from a different angle. It is common wisdom that Schrödinger's equation $(E - H)\Psi = 0$ follows from a variational principle, i.e., the minimization of the functional

$$F_E[\Psi^*, \Psi] := \langle\Psi|H|\Psi\rangle - E\langle\Psi|\Psi\rangle,$$

equivalent to seeking the minimum energy on the unit sphere $\{\|\Psi\| = 1\}$. What we do is essentially to look for the *best approximation* of $\Psi \in \mathbb{H}$ on some finite-dimensional subset $S \subset \mathbb{H}$ – where *best* is defined as having the smallest distance from Ψ. Explicitly, we look for $\Upsilon \in S$ fulfilling

$$\|\Upsilon - \Psi\| = \underbrace{\min_{\Phi\in S} \|\Phi - \Psi\|}_{\equiv \mathrm{dist}(S,\Psi)}.$$

A well-known theorem states that, given that $\mathbb{H}$ is a *unitary* vector space (endowed with a scalar-product norm $\|\Psi\|^2 = \langle\Psi|\Psi\rangle$), such a best approximation always exists uniquely. The key is to see that, in this case, minimization of $f(s) := \|(\Upsilon + s\varphi) - \Psi\|^2$ at $s = 0$ (for some $\varphi \in S$) is equivalent to

$$\langle\Upsilon - \Psi|\varphi\rangle \overset{!}{=} 0 \;\forall\varphi \in S.$$

In other words: The difference vector $(\Upsilon - \Psi)$ is orthogonal to S, signifying that the error can only be improved by going out of S.

An explicit construction can be attained by setting $\varphi \equiv \Phi_k$ equal to the (orthonormal) basis vectors spanning S, which yields the intuitive result $\langle \Phi_k | \Upsilon \rangle = \langle \Phi_k | \Psi \rangle$. In our previous notation, this is of course nothing but our initial ansatz $\Upsilon = \sum_k c_k \Phi_k$ leading to the matrix-eigenvalue problem (2.4). This ensures that our approach of directly diagonalizing the Hamilton matrix takes us as close to the true solution as it gets, that is, within the subspace $S = \mathrm{span}\{\Phi_k\}$. Since these vectors are usually number states in some *primitive* basis not related directly to the full Hamiltonian, one may have to take S quite large.

The above standpoint is very abstract; in fact it makes no reference whatsoever to the type of system (i.e., the H). Actually, general statements on the convergence speed of exact diagonalizations are rare. To get an idea of this, let us be more explicit: In our simple yet not uncommon case, we consider a Hamiltonian $H = H_0 + V$ consisting of a single-particle operator H_0 (the easy part) and an interaction V, where our basis set will be constructed as unperturbed eigenstates $(E_k^{(0)} - H_0)\Phi_k = 0$ (see Sec. 2.2.2). Then the full Schrödinger equation can be rewritten in terms of the resolvent $G = (E - H_0)^{-1}$ as a variant of the *Lippmann-Schwinger* equation

$$\Psi = GV\Psi.$$

A straightforward expansion in Φ_k yields the exact, if implicit, expansion (2.3):

$$\Psi = \sum_k \frac{\langle \Phi_k | V | \Psi \rangle}{E - E_k^{(0)}} \Phi_k =: \sum_k c_k \Phi_k. \tag{2.6}$$

For few rare cases where the matrix elements of V can be boiled down to a simple expression, this may actually be employed for an analytic solution (e.g., in [17]). But even in the general case when this does not apply, that relation can provide some insight into the accuracy of our ansatz. Of course, we want the coefficient $c_k \to 0$ to fall off fast enough – ideally, they should vanish for some tolerable cutoff $k > K$. Naively, $|c_k(E)| \ll 1$ should hold when $|E - E_k^{(0)}| \to \infty$, i.e., when the basis states are expected to give small contributions in an energy range far from E. However, there are two qualifications: For one thing, the density of states in the energy range about E should not be too large. On top of that, if V couples Ψ very strongly to many (possibly highly excited) eigenstates Φ_k, $\langle \Phi_k | V | \Psi \rangle$ will become large, which makes for poor convergence. Even though these considerations are limited to a primitive basis set which is not at all adapted to the interactions present in the systems, it casts a light on the general difficulty involved in exact-diagonalization approaches.

2.2.2 Choice of basis

Many-particle basis set

As already insinuated before, we opt to expand the many-body Hamiltonian in a basis of number states

$$|\boldsymbol{n}\rangle = |N_0, \ldots, N_A\rangle, \ |\boldsymbol{n}| = N,$$

based on some single-particle orbitals $\{\phi_a\}_{a=0}^{A}$. This amounts to distributing all N particles over $A + 1$ single-particle states (including multiple occupation for bosons). The number of such combinations determines the dimension of the Hilbert subspace $S \subset \mathbb{H}$:

$$K = \sum_{|\boldsymbol{n}|=N} 1 = \binom{A+N}{N}. \tag{2.7}$$

For large N, this grows like N^A. This exponential growth of the Hamilton matrix makes it practically impossible to treat more than just a few particles ($N < 10$) by brute-force diagonalization, unless one restricts to a very small single-particle space (say, $A = 1$).

One way to handle this would be to use iterative diagonalization techniques (see Sec. 2.2.4). By contrast, a way to reduce the basis-set size would be *not* to take *all* possible combinations (*full Configuration Interaction*), which include unlikely contributions such as $|0, \ldots, N_A = N\rangle$, but only single and double excitations out of a reference state (say, $|N_0 = N\rangle$). A more rigorous procedure, in the spirit of our remarks in Sec. 2.2.1, would be to introduce an energy cutoff $E_{\max}$ such that only basis states with $\langle H\rangle_{\Phi_k} \leq E_{\max}$ are picked (this amounts to setting $c_k(E) \equiv 0$ for states with mean energy above that cutoff). Neither of these schemes has been implemented in the program, however. Yet another remedy often employed is to choose an altogether different basis set – an *explicitly correlated* one $\Phi_{\boldsymbol{\alpha\beta}}(X) = S_+ \left(\prod_{i=1}^N \phi_{\alpha_i}(x_i)\right) \left(\prod_{i<j} f_{\beta_{ij}}(x_i - x_j)\right)$. As this ansatz has the power to include correlations already in a *single* configuration (which otherwise would have to be mimicked by superimposing many number states), it is intelligible that this converges by orders faster in practice (e.g., see [76]). Again, there is no such thing as a free lunch: The numerical costs do not vaporize but rather shift from the basis size (number states) to computing matrix elements (correlated states).

One-particle basis set

After having settled for a number-state basis set $|\boldsymbol{n}\rangle$, we still need to fix the set of orbitals ϕ_a it should be constructed from. In an ideal world, these ought to comply with the following criteria:

1. *Convenience*: The matrix elements should be easy to compute.
2. *Convergence*: For a given number of orbitals K, as few vectors $|\boldsymbol{n}\rangle$ as possible should be necessary to achieve a given accuracy.
3. *Flexibility*: The choice should be adapted to any Hamiltonian, rather than hand-picking a basis set each time the system is changed.

There are different choices for $\{\phi_a\}$ that leap into mind, but obviously each involves a trade-off with respect to the demands above. The by far simplest option would be to take the eigenstates of the one-particle Hamiltonian, $(\epsilon_a - h)\phi_a = 0$. For the prototype case of a harmonic trap, these are known analytically. In this case, all matrix elements can even be computed exactly (although this may not be the most efficient choice). In view of our considerations in Sec. 2.2.1, the fulfilment of (2.) is certainly questionable for stronger interactions. Furthermore, it is not entirely flexible: For pretty much anything but a harmonic trap, $\{\phi_a\}$ is not known in closed form, so h would have to be diagonalized brute force, possibly by expanding it in the oscillator basis.

Despite these drawbacks, the HO basis has been adopted here. Still, it is worth touching on a few alternatives:

- A common way is to take plain (normalized) Gaussians whose widths σ_a and centers x_a are parameters that may be adjusted to the geometry under consideration. This way, typically all primitive matrix elements can be solved analytically. The downside is, clearly, that this basis set is not *ortho*normal. In other words, the positive *overlap* matrix $S = (\langle \phi_a | \phi_b \rangle)$ ceases to be the identity. This needs to be taken into account, either in the computation of the many-body matrix elements or by including a numerical pre-orthogonalization.
- One option would be to take *mean-field* orbitals which already include interaction effects. Rigorously speaking, this amounts to minimizing E not only with respect to the coefficients c_k (leading to the standard matrix-Schrödinger equation), but also varying the single-particle function ϕ_a used to construct the vectors Φ_k (yielding Hartree-Fock-type equations). This is essentially the approach embarked on by MCTDH, as described in Sec. 2.3. This is as good as it gets within an uncorrelated basis set ($|\boldsymbol{n}\rangle$), at the cost of having to solve a set of nonlinear equations on top.
- In an ideal world, it would be preferable to have *two*-particle functions $f_a(x_i, x_j)$. Such a choice would open up the possibility of explicitly accounting for two-body correlations – i.e., to reconstruct the exact behavior near points of collision, $\Psi \propto f(x_i - x_j)$. While this may drastically reduce the basis-set size, it comes at the price of highly involved primitive (few-particle) integrals. This method earns a top ranking in technical sophistication.

2.2.3 Matrix representation

Having settled our basis-set issues, we are left to actually compute the Hamiltonian matrix $\langle \boldsymbol{n}' | H | \boldsymbol{n} \rangle$. To this end, the many-body matrix elements are first broken down to one- and two-particle *primitive* integrals, which in turn can be calculated by combining analytical and numerical techniques.

Matrix elements $\langle \boldsymbol{n}' | H | \boldsymbol{n} \rangle$

Let us now compute the many-body matrix elements $\langle \boldsymbol{n}' | H | \boldsymbol{n} \rangle$. Since we expand the state vector in terms of Fock states constructed from the single-particle basis $\{\phi_a\} \subset \mathbb{H}_1$, it is obvious to do the same for the system Hamiltonian. Pasting our results from Sec. 1.1.2, this reads

$$H = \sum_{a,b} \langle a|h|b \rangle c_a^\dagger c_b + \frac{1}{2} \sum_{ab,cd} \langle ab|V|cd \rangle c_a^\dagger c_b^\dagger c_d c_c. \tag{2.8}$$

Postponing to the next paragraph the numerical evaluation of the primitive one- and two-body integrals

$$\begin{aligned} h_{ab} \equiv \langle a|h|b \rangle &= \int dx \phi_a^*(x)(h\phi_b)(x) \\ V_{abcd} \equiv \langle ab|V|cd \rangle &= \int dx_1 \int dx_2 \phi_a^*(x_1)\phi_b^*(x_2) V(x_1, x_2) \phi_c(x_2) \phi_d(x_2), \end{aligned}$$

which encapsulate the concrete geometry and interaction potential, we are left with the following density-matrix elements: $\langle \boldsymbol{n}'|c_a^\dagger c_b|\boldsymbol{n}\rangle$, $\langle \boldsymbol{n}'|c_a^\dagger c_b^\dagger c_d c_c|\boldsymbol{n}\rangle$. An explicit calculation yields[6]

$$\langle \boldsymbol{n}'|c_a^\dagger c_b|\boldsymbol{n}\rangle = \begin{cases} N_a & (a=b) \qquad \boldsymbol{n}'=\boldsymbol{n} \\ \sqrt{N'_a N_b} & (a\neq b) \quad \boldsymbol{n}'=\boldsymbol{n}+\boldsymbol{e}_a-\boldsymbol{e}_b \end{cases} \tag{2.9}$$

$$\langle \boldsymbol{n}'|c_a^\dagger c_b^\dagger c_d c_c|\boldsymbol{n}\rangle = \begin{cases} \sqrt{N'_a(N'_a-1)N_c(N_c-1)} & (a=b,\, c=d) \qquad \boldsymbol{n}'=\boldsymbol{n}+2\boldsymbol{e}_a-2\boldsymbol{e}_c \\ \sqrt{N'_a(N'_a-1)N_cN_d} & (a=b,\, c\neq d) \quad \boldsymbol{n}'=\boldsymbol{n}+2\boldsymbol{e}_a-\boldsymbol{e}_c-\boldsymbol{e}_d \\ \sqrt{N'_aN'_bN_c(N_c-1)} & (a\neq b,\, c=d) \quad \boldsymbol{n}'=\boldsymbol{n}+\boldsymbol{e}_a+\boldsymbol{e}_b-2\boldsymbol{e}_c \\ \sqrt{N'_aN'_bN_cN_d} & (a\neq b,\, c\neq d) \quad \boldsymbol{n}'=\boldsymbol{n}+\boldsymbol{e}_a+\boldsymbol{e}_b-\boldsymbol{e}_c-\boldsymbol{e}_d \end{cases} .$$

Proof: This follows from the iterative application of the annihilation (creation) operators to $|\boldsymbol{n}\rangle$ ($|\boldsymbol{n}'\rangle$), using the standard rule $c_a|\boldsymbol{n}\rangle = \sqrt{N_a}|\boldsymbol{n}-\boldsymbol{e}_a\rangle$, where $(\boldsymbol{e}_a)_b \equiv \delta_{ab}$ denotes the unit multi-index (cf. Sec. 1.1.2). Note that, for more than one annihilated index, this requires a case distinction whether or not an index, say c, is annihilated twice ($c=d$) or just once ($c\neq d$). Eventually, the matrix elements boil down to overlaps of the type $\langle \boldsymbol{n}'-\boldsymbol{e}_a-\boldsymbol{e}_b|\boldsymbol{n}-\boldsymbol{e}_c-\boldsymbol{e}_d\rangle = \delta_{\boldsymbol{n}',\boldsymbol{n}+\boldsymbol{e}_a+\boldsymbol{e}_b-\boldsymbol{e}_c-\boldsymbol{e}_d}$. Be aware that, so far, case distinctions have been made only *within* the index sets (a,b) and (c,d). □

At this stage, in order to compute $\langle \boldsymbol{n}'|H|\boldsymbol{n}\rangle$, we are left with performing the sum over all indices $ab\,(abcd)$ in Eq. (2.8). To anticipate the result, the Hamilton matrix has the following structure:

$$\langle \boldsymbol{n}'|H|\boldsymbol{n}\rangle =$$

$$\begin{cases} \sum_a \left[h_{aa}N_a + V_{aaaa}\frac{1}{2}N_a(N_a-1)\right] + \sum_{a<b} V_{ab\{ab\}}N_aN_b & \boldsymbol{n}'=\boldsymbol{n} \\ h_{ab}\sqrt{(N_a+1)N_b} + \sum_{k\neq a,b} V_{ka\{kb\}}\sqrt{(N_a+1)N_b}N_k + & \\ +V_{aaab}N_a\sqrt{(N_a+1)N_b} + V_{aaba}\sqrt{(N_a-1)N_b}(N_b-1) & \boldsymbol{n}'=\boldsymbol{n}+\boldsymbol{e}_a-\boldsymbol{e}_b \\ \frac{1}{2}V_{aacc}\sqrt{(N_a+1)(N_a+2)N_c(N_c-1)} & \boldsymbol{n}'=\boldsymbol{n}+2\boldsymbol{e}_a-2\boldsymbol{e}_c \\ V_{aacd}\sqrt{(N_a+1)(N_a+2)N_cN_d} & \boldsymbol{n}'=\boldsymbol{n}+2\boldsymbol{e}_a-\boldsymbol{e}_c-\boldsymbol{e}_d \\ V_{abcc}\sqrt{(N_a+1)(N_b+1)N_c(N_c-1)} & \boldsymbol{n}'=\boldsymbol{n}+\boldsymbol{e}_a+\boldsymbol{e}_b-2\boldsymbol{e}_c \\ V_{ab\{cd\}}\sqrt{(N_a+1)(N_b+1)N_cN_d} & \boldsymbol{n}'=\boldsymbol{n}+\boldsymbol{e}_a+\boldsymbol{e}_b-\boldsymbol{e}_c-\boldsymbol{e}_d \end{cases}$$

with the shorthand $V_{ab\{cd\}} \equiv V_{abcd}+V_{abdc}$. (Any two indices a,b are understood to assume different values here, $a\neq b$.)

Proof: Again, let us focus on the principal procedure. As stated above, all we need to do is to carry out the sums over the density-matrix elements. For the one-particle terms, this reads

$$\begin{aligned} \langle \boldsymbol{n}'|H_1|\boldsymbol{n}\rangle &= \sum_{ab} h_{ab} \times \underbrace{\langle \boldsymbol{n}'|c_a^\dagger c_b|\boldsymbol{n}\rangle}_{=\delta_{\boldsymbol{n}',\boldsymbol{n}}\delta_{ab}N_a+\delta_{\boldsymbol{n}',\boldsymbol{n}+\boldsymbol{e}_a-\boldsymbol{e}_b}(1-\delta_{ab})\sqrt{N'_aN_b}} \\ &= \begin{cases} \sum_a h_{aa}N_a & \boldsymbol{n}'=\boldsymbol{n} \\ h_{ab}\sqrt{N'_aN_b} & \boldsymbol{n}'=\boldsymbol{n}+\boldsymbol{e}_a-\boldsymbol{e}_b \end{cases} , \end{aligned}$$

---

[6] All terms other than those listed vanish. Quite generally, for any n-particle operator A (involving a product of n annihilators and n creators), the matrix element $\langle \boldsymbol{n}'|A|\boldsymbol{n}\rangle$ vanishes if both vectors differ by more than n single-particle occupations, $\sum_a |N_a - N'_a| \le 2n$. This is a physically sensible statement, since an n-particle operator can only couple two states via n-body excitations. This saves us from having to include *all* possible Hamiltonian matrix elements – rather, for $N>2$ particles, our matrix becomes more and more sparse.

where, by construction, $N_a' = N_a + 1$ in the last line. For the two-particle Hamiltonian, the basic strategy is the same, if more tedious. Consider the specific case $\boldsymbol{n}' = \boldsymbol{n} + 2\boldsymbol{e}_a - 2\boldsymbol{e}_c$, so that only $(a = b,\ c = d)$ contribute above: Then we have

$$\begin{aligned}\langle \boldsymbol{n}'|c_a^\dagger c_a^\dagger c_c c_c|\boldsymbol{n}\rangle =& \delta_{\boldsymbol{n}',\boldsymbol{n}}\delta_{ac}N_a(N_a-1)+\\ &\delta_{\boldsymbol{n}',\boldsymbol{n}+2\boldsymbol{e}_a-2\boldsymbol{e}_c}(1-\delta_{ac})\sqrt{N_a'(N_a'-1)N_c(N_c-1)}.\end{aligned}$$

Upon summation, this leaves us with

$$\frac{1}{2}\sum_{a,c} V_{aacc}\langle \boldsymbol{n}'|c_a^\dagger c_a^\dagger c_c c_c|\boldsymbol{n}\rangle = \begin{cases} \sum_a V_{aaaa}\frac{1}{2}N_a(N_a-1) & \boldsymbol{n}' = \boldsymbol{n} \\ \frac{1}{2}V_{aacc}\sqrt{(N_a+1)(N_a+2)N_c(N_c-1)} & \boldsymbol{n}' = \boldsymbol{n} + 2\boldsymbol{e}_a - 2\boldsymbol{e}_c \end{cases}.$$

Analogous case distinctions must be made for all other relations between $\boldsymbol{n}', \boldsymbol{n}$. ☐

Primitive matrix elements h_{ab}, V_{abcd}

After having expressed the matrix elements of our many-body Hamiltonian in terms of *primitive* one- and two-body integrals $\{h_{ab}\}$ and $\{V_{abcd}\}$, we shall now compute these. In general, this necessitates some numerical integration. However, in our case of a harmonic trap, all single-particle orbitals $u_a \in L^2(\mathbb{R})$ are known analytically in terms of the Hermite polynomials H_n (in dimensionless units):

$$u_a(x) = c_a H_a(x) e^{-x^2/2}; \quad c_a = 1/\sqrt{\sqrt{\pi}2^a a!}.$$

This simplifies matters a whole lot. In fact, the one-body integrals are trivial:

$$h_{ab} \equiv \langle \phi_a|h|\phi_b\rangle = \epsilon_a\delta_{ab}, \qquad \epsilon_a = \left(a + \frac{1}{2}\right).$$

The real challenge thus lies in the two-body matrix elements

$$V_{abcd} \equiv \langle ab|V|cd\rangle = \int dx_1 \int dx_2 u_a(x_1)u_b(x_2)V(x_1-x_2)u_c(x_2)u_d(x_2).$$

For one-dimensional systems, we have seen in Sec. 1.2.3 that the effective low-energy interaction is of the form $V(x) = g\delta(x)$. For numerical reasons, we will argue later in Sec. 2.3.3 that it is convenient to mollify the contact potential with a Gaussian of width σ:

$$\delta_\sigma(x) \equiv \frac{1}{\sqrt{2\pi}\sigma}e^{-x^2/2\sigma^2}.$$

Even though this slightly complicates things, it does not restrict the numerical evaluation of the integrals.

Symmetries Before proceeding, let us rewrite the integrals in a technically handier notation,

$$V_{(ac)(bd)} \quad := \quad \int dx \int dx'\,(u_a u_c)(x)(u_b u_d)(x')V(x-x'),$$

and read off a few general *symmetries*:

1. Permutation symmetry $V = P_{12}^{\dagger} V P_{12} \Longrightarrow V_{(ac)(bd)} = V_{(bd)(ac)}$
2. Parity $V = \Pi^{\dagger} V \Pi \Longrightarrow V_{(ac)(bd)} = (-1)^{a+b+c+d} V_{(ac)(bd)}$ ($= 0$ unless $a+b+c+d$ is even)
3. Adjoint symmetry $V = V^{\dagger} \Longrightarrow V_{(ac)(bd)} = V^{*}_{(ca)(db)} = V_{(ca)(db)}$
4. Complex-conjugation symmetry $u_a^* = u_a \Longrightarrow V_{(ac)(bd)} = V_{(ca)(bd)} = V_{(ac)(db)}$

Symmetries (1.–4.) assert that there is a high level of redundancy in the *full* index set $\{a, b, c, d\}$. In fact, it suffices to know $V_{(ac)(bd)}$ in, say, the restricted index set $\{a \geq c,\ b \geq d\}$, which suggests to wrap up each pair (ac) in a *single* index

$$(a, c) := \frac{a(a+1)}{2} + c \qquad [a \geq c]$$

running from $(00) = 0$ up to $(AA) = (A+1)(A+2)/2$. By extension, note that by (1.) even the two pairs (ac) and (bd) are interchangeable as a whole, so we can encode the map $(ac)(bd)$ to the single-index object

$$((a, c), (b, d)) \qquad (a, c) \geq (b, d). \tag{2.10}$$

Analytic solution It should be noted that, for our special case of harmonic-oscillator orbitals and Gaussian interaction, the two-body integrals may be written down in closed form. The key is to rewrite them in center-of-mass and relative coordinates, $x_{1/2} = R \pm r/2$,

$$V_{(ac)(bd)} = \int dR \int dr\, (u_a u_c)_{R+\frac{r}{2}} (u_b u_d)_{R-\frac{r}{2}} \frac{e^{-r^2/2\sigma^2}}{\sqrt{2\pi}\sigma} \qquad (g \equiv 1).$$

This integrand is known as a product of *decentered* oscillator orbitals [77]. Adapting the notation, the final result may be cast as

$$\begin{aligned} V_{(ac)(bd)} = {} & c_a c_c c_b c_d \sum_{p_1=0}^{a+c} \sum_{p_2=0}^{b+d} \sum_{p=0}^{p_1+p_2} \times \\ & \left(\frac{1}{2^{(a+c)/2}} \sum_{i,k|i+k=a+c-p_1} \binom{a}{i} \binom{c}{k} (-1)^k H_{a+c-p_1}(0) \right) \times \\ & \left(\frac{1}{2^{(b+d)/2}} \sum_{j,l|j+l=b+d-p_2} \binom{b}{j} \binom{d}{l} (-1)^l H_{b+d-p_2}(0) \right) \times \\ & \left(\frac{1}{2^{(p_1+p_2)/2}} \sum_{m,n|m+n=p} \binom{p_1}{m} \binom{p_2}{n} (-1)^n \right) \times v_{p_1+p_2-p} w_p, \end{aligned}$$

where

$$v_\alpha \equiv \int dR\, H_\alpha(2R) e^{-(2R)^2/2} = \begin{cases} \sqrt{\frac{\pi}{2}} \frac{\alpha!}{(\alpha/2)!} & \alpha \in 2\mathbb{N}_0 \\ 0 & \text{else} \end{cases}$$

$$w_p \equiv \int dr\, H_p(r) e^{-r^2/2} e^{-r^2/2\sigma^2} = \begin{cases} \sqrt{2\pi}\sigma \frac{p!}{(p/2)!} \frac{(\sigma^2-1)^{p/2}}{(\sigma^2+1)^{(1+p)/2}} & p \in 2\mathbb{N}_0 \\ 0 & \text{else} \end{cases} .$$

The proof exploits an expansion of *products* of decentered oscillator orbitals in terms of *single* oscillator orbitals. To go into the details here would be an exercise in futility, though, since the above formula is a prime example of a closed-form solution that does *not* necessarily imply a simplification when it comes to practical evaluation. The latter would involve a sixfold sum with mostly alternating signs—let alone the myriads of case distinctions and binomial factors—which could hardly be less favorable as far as numerical stability is concerned. In practice, we have resorted to an algorithm which takes advantage of the recursion relations known for harmonic-oscillator functions, as presented now.

Recursion relation The following recursion formula holds for two-body integrals of harmonic-oscillator orbitals:[7]

$$\begin{aligned} V_{(ac)(bd)} &= V_{(a-1,c)(b-1,d)} \frac{1}{2(1+\sigma^2)} \sqrt{\frac{b}{a}} + V_{(a-1,c)(b,d-1)} \frac{1}{2(1+\sigma^2)} \sqrt{\frac{d}{a}} + \\ & \quad V_{(a-1,c-1)(b,d)} \frac{1+2\sigma^2}{2(1+\sigma^2)} \sqrt{\frac{c}{a}} - V_{(a-2,c)(b,d)} \frac{1}{2(1+\sigma^2)} \sqrt{\frac{a-1}{a}}. \end{aligned}$$

Proof: Using the harmonic-oscillator recurrence

$$u_{n+1}(x) = \sqrt{\frac{2}{n+1}} x u_n(x) - \sqrt{\frac{n}{n+1}} u_{n-1}(x) \qquad (n > 0), \tag{2.11}$$

we can split the integral into two parts,

$$V_{(ac)(bd)} = \sqrt{\frac{2}{a}} \int dR \int dr \left(R + \frac{r}{2}\right) (u_{a-1}u_c)_{R+\frac{r}{2}} (u_b u_d)_{R-\frac{r}{2}} \frac{e^{-r^2/2\sigma^2}}{\sqrt{2\pi}\sigma} - \sqrt{\frac{a-1}{a}} V_{(a-2,c)(b,d)}.$$

The second piece we know already from a previous iteration step, while the first integral can be converted via partial integration. To see that, note that the integrand is proportional to

$$(H_{a-1}H_c)_{R+\frac{r}{2}} (H_b H_d)_{R-\frac{r}{2}} e^{-r^2\left(\frac{1}{2}+\frac{1}{2\sigma^2}\right)} e^{-2R^2}.$$

Hence we can substitute the multiplicators R, r by

$$R e^{-2R^2} = -\frac{1}{4} \partial_R e^{-2R^2}; \quad \frac{r}{2} e^{-r^2\left(\frac{1}{2}+\frac{1}{2\sigma^2}\right)} = -\frac{1}{2(1+\sigma^{-2})} \partial_r e^{-r^2\left(\frac{1}{2}+\frac{1}{2\sigma^2}\right)}.$$

Integrating by parts, this allows us to express the first piece above as the derivative of the Hermite-polynomial products. Applying the well-known derivative of Hermite polynomials to our case,

$$\begin{aligned} \partial_R H_n(R \pm \frac{r}{2}) &= 2n H_{n-1}(R \pm \frac{r}{2}) \\ \partial_r H_n(R \pm \frac{r}{2}) &= \pm n H_{n-1}(R \pm \frac{r}{2}), \end{aligned}$$

and picking up the prefactor $c_n = c_{n-1}/\sqrt{2n}$ so as to recast everything in terms of $\{u_n\}$, then the first integral above reduces simply to 2×3 $V_{(\cdot)(\cdot)}$-type integrals. The last step involves

---

[7] A similar relation has been derived for the contact interaction, in which case $\sigma \to 0$ [F. Deuretzbacher, private communication].

simply cleaning up the notation a bit, by combining the different prefactors stemming from the $R\,(r)$ derivative, $1 \pm \frac{1}{1+\sigma^{-2}}$, into a single factor. □

The above formula can be neatly coded: Given the starting value $V_{(00)(00)} = 1/\sqrt{2\pi\sqrt{1+\sigma^2}}$, and trivially setting to zero all integrals involving $a, b, c, d < 0$, one can scan through all of the restricted index set (2.10). The array $V_{((ac)(bd))}$ may be stored in a file and—for not too large cutoffs—read into some array `V[i]`.

2.2.4 Computational Scheme

After having obtained explicit expressions for all matrix elements $\langle \boldsymbol{n}'|H|\boldsymbol{n}\rangle$, we are now all set to diagonalize the Hamiltonian … almost. To build up an actual matrix $(H_{kl}) \in \mathbb{R}^{K\times K}$ —$K = \binom{A+N}{N}$ being the dimension of the Hilbert subspace spanned by $\{|\boldsymbol{n}\rangle\}$—the single index $k \in \mathbb{N}$ has to be mapped to the multi-index

$$\boldsymbol{n} = (N_0, \ldots, N_A) \in \mathbb{N}_0^{A+1}, \text{ with } |\boldsymbol{n}| = N.$$

This is a technical yet salient issue. A straightforward approach would be to simply enumerate the vectors by generating an excitation out of some reference state for each increase of the single index k, such as:

$$|(N)_0\rangle,\ |(N-1)_0, 1_{a_1}\rangle,\ |(N-2)_0, 1_{a_1}, 1_{a_2}\rangle, \ldots, |1_{a_1}, 1_{a_2}, \ldots, 1_{a_N}\rangle,$$

where $\{1, \ldots, A\} \ni a_n \geq a_{n-1}\ \forall n$ so as to avoid double counting. The algorithm implemented here proceeds as follows: One starts with all $a_1 = \cdots = a_N = 0$ (i.e., $N_0 = N$). A given configuration $\boldsymbol{a}$ is then updated in the following way:

1. Count down the auxiliary index $j = N, \ldots, 1$, keeping track of the number of excited particles.
   (a) If $a_j < A$, increase a_j by 1. Break loop at current value of j.
   (b) If $a_j = A$, continue.
2. Set $a_i = a_j$ for $i \geq j$.

This scheme works for the *complete* set $\{|\boldsymbol{n}\rangle\}$. As insinuated above, it ought to be adapted to a more economical, *truncated* basis set, where an additional criterion applies – such as filtering out states that are energetically too far off. Moreover, in a preliminary version, the "black-box" diagonalization routine `dspevx` from the open-access LAPACK library has been used. It essentially performs a *full* diagonalization of the matrix (H_{kl}). For numerically more demanding purposes, more sophisticated *iterative* schemes should be employed.

Finally, let us mention that the symmetries of H can be exploited in a diagonalization: In our case, the total parity $(\Pi\Psi)(X) := \Psi(-X)$ commutes with the Hamiltonian, and thus each eigenstate should have definite parity $\Pi\Psi = \pm\Psi$. In each of these orthogonal subspaces ($\Pi = \pm 1$), the Hamiltonian can be diagonalized separately, employing only basis vectors of appropriate parity $\Pi|\boldsymbol{n}\rangle = (-1)^{\sum_a aN_a}|\boldsymbol{n}\rangle = \pm|\boldsymbol{n}\rangle$. Analogous considerations apply to any symmetry – in particular also to the total particle number N. The latter is trivially conserved, which is ensured by including only basis vectors with equal $\hat{N}|\boldsymbol{n}\rangle = N|\boldsymbol{n}\rangle$.

2.2.5 Analysis aspects

Upon a successful diagonalization, we obtain the eigenpairs E_m and $C^{(m)} \equiv (c_1^{(m)}, , \ldots, c_K^{(m)})^\top$ for specific eigenstates m. As discussed in Sec. 1.3, the reduced density matrices provide a natural way to relate the full wave function to observable quantities. Specifically, let us focus on the two simplest *diagonal* densities:

- the one-body density (or density profile) $\rho(x) = \langle \psi^\dagger(x)\psi(x)\rangle_\Psi / N$
- the two-body density $\rho_2(x_1, x_2) = \langle \psi^\dagger(x_1)\psi^\dagger(x_2)\psi(x_2)\psi(x_1)\rangle_\Psi / N(N-1)$.

One-body density

The density operator $\hat{n} = \psi^\dagger\psi$, being a one-body observable, is relatively straightforward to compute. Expand $\psi(x) = \sum_a u_a(x) c_a$ in terms of the oscillator annihilation operators $\{c_a\}$, and plug in $\Psi = \sum_{\boldsymbol{n}} c_{\boldsymbol{n}} |\boldsymbol{n}\rangle$:

$$\langle \psi^\dagger(x)\psi(x)\rangle_\Psi = \sum_{a,b} u_a(x) u_b(x) \langle c_a^\dagger c_b\rangle_\Psi,$$

where in turn

$$\langle c_a^\dagger c_b\rangle_\Psi = \sum_{\boldsymbol{n},\boldsymbol{n}'} c_{\boldsymbol{n}'} c_{\boldsymbol{n}} \langle \boldsymbol{n}' | c_a^\dagger c_b | \boldsymbol{n}\rangle$$

boils down to the density-matrix elements computed in (2.9), so we obtain

$$\langle c_a^\dagger c_b\rangle_\Psi = \begin{cases} \sum_{\boldsymbol{n}} N_a |c_{\boldsymbol{n}}|^2 & (a = b) \\ \sum_{\boldsymbol{n},\boldsymbol{n}'} c_{\boldsymbol{n}} c_{\boldsymbol{n}'} \sqrt{N_a' N_b}\, \delta_{\boldsymbol{n}', \boldsymbol{n}+\boldsymbol{e}_a-\boldsymbol{e}_b} & (a \neq b) \end{cases}.$$

The procedure is then as follows: First build the matrix $\left(\langle c_a^\dagger c_b\rangle_\Psi\right)$. Then loop over all points x and, for each $a \geq b$, multiply the density-matrix element with the oscillator functions $u_a(x)u_b(x)$. As a technicality, the harmonic-oscillator orbitals are obtained via the recursion relation (2.11) [requiring the input of u_0 and u_1], which is numerically advantageous to a computation directly from their explicit Hermite-polynomial representation.

Two-body density

The calculation here is conceptually similar but technically more challenging. In analogy to above, we obtain

$$\langle \psi^\dagger(x_1)\psi^\dagger(x_2)\psi(x_2)\psi(x_1)\rangle_\Psi = \sum_{a,b,c,d} (u_a u_c)(x_1)(u_b u_d)(x_2) \langle c_a^\dagger c_b^\dagger c_d c_c\rangle_\Psi,$$

where $\langle c_a^\dagger c_b^\dagger c_d c_c\rangle_\Psi = \sum_{\boldsymbol{n},\boldsymbol{n}'} c_{\boldsymbol{n}'} c_{\boldsymbol{n}} \langle \boldsymbol{n}' | c_a^\dagger c_b^\dagger c_d c_c | \boldsymbol{n}\rangle$ again reduces to the matrix elements derived in Eqs. (2.9). Even though symmetry considerations go some way to reducing the quadruple sum over $\{abcd\}$, this is by far the most time-consuming analysis step.

2.3 Multi-Configuration Time-Dependent Hartree

In the previous section, we have pursued the approach of diagonalizing the Hamiltonian in some basis set of *uncorrelated* states constructed from single-particle functions. From this time-independent perspective, the essential difference of the *multi-configurational time-dependent Hartree* method (MCTDH) is simply to take *variationally optimal*, i.e., self-consistent single-particle functions rather than primitive orbitals as before. Despite this close analogy, the MCTDH approach in its original form is explicitly *time dependent*, and we shall see below that the computation of stationary states is more or less a by-product. Moreover, it is designed for the treatment of distinguishable particles, even though in recent years derivates have been put forward that are inherently adapted to identical quantum particles (aptly termed MCTDHF [78] and MCTDHB [79] for fermions and bosons, respectively). Here we will give a brief introduction to the general theory of MCTDH (Sec. 2.3.1) as well as its implementation (Sec. 2.3.2). This is complemented by a discussion of how MCTDH can be applied to treat ultracold few-boson systems.

2.3.1 Principal idea

The underlying idea of MCTDH [80] is to solve the time-dependent Schrödinger equation (2.1) directly as an initial-value problem by expanding $\Psi(t)$ in terms of direct (or Hartree) products $\Phi_J \equiv \varphi_{j_1}^{(1)} \otimes \cdots \otimes \varphi_{j_N}^{(N)}$:

$$\Psi(X,t) = \sum_{J\in\mathcal{J}} A_J(t)\Phi_J(X,t). \tag{2.12}$$

Here N denotes the number of degrees of freedom, and the multi-index $J \equiv (j_1,\dots,j_N)$ runs over the set $\mathcal{J} = \{(j_1,\dots,j_N) \mid j_\kappa \le n_\kappa\}$. Note that, in this truncated expansion, both the coefficients A_J and the basis vectors Φ_J are time dependent.[8] In the spirit of Sec. 2.2.1, this is again an approximation problem on the (implicit) subset $\mathrm{span}\{\Phi_J\} \subset \mathbb{H}_N$. The best approximate solution Ψ can be found by requiring variations $\delta\Psi$ to be orthogonal to the "error" $[i\partial_t - H(t)]\Psi(t)$,

$$\langle\delta\Psi|[i\partial_t - H(t)]\Psi(t)\rangle = 0,$$

known as the *Dirac-Frenkel variational principle* [81]. This leads to the following equations of motion:

$$\begin{aligned} i\dot{A}_J &= \sum_L \langle\Phi_J|H|\Phi_L\rangle A_L, & (2.13)\\ i\dot{\boldsymbol{\varphi}}^{(\kappa)} &= \left(1 - P^{(\kappa)}\right)\left(\boldsymbol{\rho}^{(\kappa)}\right)^{-1}\langle\mathbf{H}\rangle^{(\kappa)}\boldsymbol{\varphi}^{(\kappa)}. & (2.14)\end{aligned}$$

---

[8] Needless to say, this is ambiguous: For each term J, any factor can be absorbed either in A_J or in Φ_J. This can be made unique by demanding that

$$\langle\varphi_j^{(\kappa)}(t)|\varphi_l^{(\kappa)}(t)\rangle = \delta_{jl}\ \forall t.$$

Upon time differentiation, this is equivalent to $\langle\varphi_j^{(\kappa)}(t)|\dot{\varphi}_l^{(\kappa)}(t)\rangle = \langle\dot{\varphi}_j^{(\kappa)}(t)|\varphi_l^{(\kappa)}(t)\rangle$. A clearly sufficient condition is to require $i\dot{\varphi}_l^{(\kappa)}(t) = g^{(\kappa)}\varphi_l^{(\kappa)}(t)$ on $\mathrm{span}\{\varphi_j^{(\kappa)}\}_{j=1}^{n_\kappa}$ for some arbitrary, hermitian operator $g^{(\kappa)}$. It is this constraint that is implemented in MCTDH so as to make the problem well defined .

This needs some explanation: The coefficient vectors A_J fulfill the standard *matrix* Schrödinger equation, as they would in the time-dependent formulation of (2.4). What is new is that the single-particle functions $\varphi_{j_\kappa}^{(\kappa)}$ —here collected in a convenient multi-orbital vector $\boldsymbol{\varphi}^{(\kappa)} = \left(\varphi_1^{(\kappa)}, \dots, \varphi_{n_\kappa}^{(\kappa)}\right)^\top$—are *not* fixed but obey an effective Schrödinger equation governed by the *mean-field Hamiltonian* $\langle \mathbf{H} \rangle^{(\kappa)}$

$$\langle H \rangle_{jl}^{(\kappa)} \quad = \quad \langle \Psi_j^{(\kappa)} | H | \Psi_l^{(\kappa)} \rangle, \tag{2.15}$$

defined in terms of the *hole functions* $\Psi_l^{(\kappa)} := \langle \varphi_l^{(\kappa)} | \Psi \rangle \in \bigotimes_{\kappa' \neq \kappa} \mathbb{H}_1^{(\kappa')}$ (the notation indicating that the κ-th degree of freedom is integrated out). These mean fields are effective one-particle operators acting solely on the one-particle space $\mathbb{H}_1^{(\kappa)}$ and are analogues of the well-known mean fields in *Hartree(-Fock)* theory. Likewise, the mean-field equations (2.14) are nonlinear Schrödinger-type equations and must be solved self-consistently. Moreover, the right-hand side is multiplied by the inverse of the reduced one-body density matrix in the basis of the single-particle functions,

$$\rho_{jl}^{(\kappa)} \quad := \quad \langle \Psi_j^{(\kappa)} | \Psi_l^{(\kappa)} \rangle = \langle \varphi_l^{(\kappa)} | \hat{\rho}_1^{(\kappa)} | \varphi_j^{(\kappa)} \rangle, \tag{2.16}$$

as well as the projector on the orthogonal complement of the single-particle space, with

$$P^{(\kappa)} = \sum_{j=1}^{n_\kappa} |\varphi_j^{(\kappa)}\rangle\langle\varphi_j^{(\kappa)}|.$$

Equations (2.13-2.14) constitute a differential-equation system that can be integrated iteratively starting from the initial condition $\Psi(0) \equiv \sum_J A_J(0)\Phi_J(\cdot, 0)$, this way giving us access to $\Psi(t)$ via (2.12). Its efficient numerical integration is technically nontrivial and beyond the scope of this thesis; for further reading see [80].

Remarks

- As implied above, the single-particle basis functions $\varphi_j^{(\kappa)}(t)$ are variationally optimal at each time step t. In the light of our remarks in the previous section, they incorporate interaction effects already on a single-particle mean-field level. Thus our basis set $\{\Phi_J(t)\}$ is the *best* possible direct-product basis, which is important numerically as it allows us to keep the basis size—given by n_κ—small. Needless to say, this cannot account for real *two-body* correlations of type $f(x_i - x_j)$, for which it is necessary to superimpose different one-body configurations Φ_J.
- A word on the numerical scaling is in order: Assume $n_\kappa = n \; \forall \kappa$ (as is the case for identical particles, see Sec. 2.3.3). Then the number of configurations that need to be included is $\sum_J 1 = \prod_\kappa n_\kappa = n^N$. For small particle numbers, this is similar to that of identical bosons (Eq. 2.7, with $A \equiv n + 1$).[9] In fact, for larger $N \gg 1$, this blows up exponentially, a prohibitive feature shared by both approaches. However, since the single-particle basis can be kept small due to variational optimization, the base n is typ-

---

[9] One should stress that MCTDH double-counts configurations which are permutationally equivalent, $\Phi_J \leftrightarrow \Phi_{P(J)}$, see Sec. 2.3.3. For larger particle numbers $N \sim 10$, this redundancy becomes more and more inefficient.

ically by an order smaller than in primitive approaches, which alleviates the exponential scaling.

- It may be instructive to apply Eqs. (2.13-2.14) to the case of a single orbital $\varphi_{j_\kappa}^{(\kappa)} \equiv \varphi$ ($n_\kappa = 1\ \forall\kappa$). In that case, $\Psi(t) = 1 \times \varphi(t)^{\otimes N}$ and the equations of motion reduce to the time-dependent version the Gross-Pitaevskii equation encountered in Sec. 2.1.2, $i\partial_t\varphi = [h + \langle\varphi|V|\varphi\rangle]\,\varphi$. Here the mean-field Hamiltonian $\langle H\rangle_{00}^{(\kappa)} = h + \langle\varphi|V|\varphi\rangle$ (for all κ) consists of the single-particle Hamiltonian plus an implicit potential $\langle\varphi|V|\varphi\rangle \to g\,|\varphi|^2$.

2.3.2 Implementation

Although the general theory of MCTDH has been set up now, there are some core aspects concerning its numerical implementation which are vital when dealing with the method (cf. [80, 82] for details).

Discrete variable representation The equations of motion for the single-particle functions (2.14) constitute a system of partial differential equations. To solve these, the orbitals have to be represented numerically. MCTDH handles this by expanding them in terms of a time-independent (*primitive*) set of functions

$$\varphi_{j_\kappa}^{(\kappa)}(\cdot,t) = \sum_{i=1}^{N_\kappa} c_{i,j_\kappa}^{(\kappa)}(t)\,u_i^{(\kappa)}. \tag{2.17}$$

Typically, these primitive functions u_i are weighted polynomials such as harmonic-oscillator functions or Legendre polynomials. To simplify the evaluation of matrix elements, one goes one step further by introducing a so-called *discrete variable representation* (DVR). Here one picks a *localized* basis set obtained by diagonalizing the position operator $\hat{x}$ in the basis $\{u_i\}$:

$$(Q - \mathbf{1}q_k)\chi_k = 0, \qquad (Q)_{ij} \equiv \langle u_i^{(\kappa)}|\hat{x}|u_j^{(\kappa)}\rangle.$$

The χ_k are *discrete* analogues of position eigenstates $\chi_{x'}(x) = \delta(x - x')$; their domain is the grid $\{q_k\}_{k=1}^{N_\kappa}$ determined by the primitive basis set. In fact, DVR may be thought of as an *interpolation* or Gaussian quadrature, where a function f is replaced by its grid values $\{f(q_k)\}$ [80].

Product representation of the potential Solving the MCTDH equations provides the knowledge of the MCTDH wave function, which is the key to the system's time evolution. However, their exact solution is complicated by the fact that it requires the matrix elements of the Hamiltonian, $\langle\Phi_J(t)|H|\Phi_L(t)\rangle$, and the mean fields at each time step. These N- or $(N-1)$-dimensional numerical integrals have to be avoided. The way MCTDH manages that is, in essence, to boil these integrals down to one-dimensional ones via the requirement

$$H^{(s)} = \sum_{r=1}^{s} c_r H_r, \quad \text{with } H_r \equiv \bigotimes_{\kappa=1}^{N} h_r^{(\kappa)}\,,$$

enforcing that the Hamiltonian be written as the sum of s products of one-particle operators (direct-product form). The remaining integrals are much more accessible for numerical integration. This is of course a drastic assumption for the *true* Hamilton operator, since we know that interaction terms like $V(x_i - x_j)$ generally are not separable. However, just as in the wave-function expansion (2.12), this ought to be regarded as a *fit* to the exact Hamiltonian H, such that $\left\| H - H^{(s)} \right\|$ becomes minimal in an appropriate operator norm [80, 83, 84].[10]

Relaxation method: Stationary states The general MCTDH theory as laid out above is inherently time dependent, thus circumventing the detour over the time-independent formalism for energy-conserving problems. Still, it is sometimes desirable to compute stationary states, be it to obtain general insights into the system (e.g., its ground state) or to better understand the dynamics. The conceptually simplest way to implement this in the MCTDH framework is by reformulating the eigenvalue problem for the *stationary* states, $(E - H)\Psi = 0$, in terms of the asymptotic limit of a *propagation* in imaginary time, $\tau = it$ – i.e., using the non-unitary evolution operator $e^{-H\tau}$. For an initial state $\Psi(0) = \sum_m c_m \Psi_m$ with nonzero overlap with the *true* ground state Ψ_0, this damps out exponentially all contributions but that stemming from the exact ground state,

$$e^{-H\tau}\Psi(0) \overset{\tau \to \infty}{=} c_0 e^{-E_0\tau}\Psi_0 \left[1 + O(e^{-(E_m - E_0)\tau}) \right],$$

where renormalization to unity ensures the *relaxation* to the ground state, Ψ_0.

By extension, if the initial state is kept orthogonal to any underlying eigenstates, i.e., $c_m = 0 \, \forall m < n$, this converges to an excited state Ψ_n. However, this is not the most stable algorithm. In practice, one relies on a more sophisticated scheme termed *improved relaxation* [85, 86], which is much more viable especially (but not only) for excitations. Here again one starts from the conventional, time-independent variational principle, where $E[\Psi] = \langle \Psi | H | \Psi \rangle$ is minimized with respect to both the coefficients A_J and the orbitals φ_j. This leads to

1. a standard eigenvalue problem $(E - H)A = 0$ for

   $$(H)_{JK} \equiv \langle \Phi_J | H | \Phi_K \rangle,$$

   which yields $A \equiv (A_J)$ as eigenvectors
2. a mean-field (self-consistent) "eigenvalue problem" for the orbitals $\varphi_j^{(\kappa)}$,

   $$0 = \sum_{l=1}^{n_\kappa} \left(\langle H \rangle_{jl}^{(\kappa)} - \epsilon_{jl}^{(\kappa)} \right) \varphi_l^{(\kappa)} = \left(1 - P^{(\kappa)} \right) \sum_{l=1}^{n_\kappa} \langle H \rangle_{jl}^{(\kappa)} \varphi_l^{(\kappa)}.$$

   Up to the inverse of $\boldsymbol{\rho}^{(\kappa)}$, this *eigenvalue problem* defines the stationary points of the *imaginary-time evolution* of the orbitals under (2.14), $\dot{\varphi}_l^{(\kappa)} = 0$.

The procedure is then as follows: For an initial state $\Psi(0) \equiv \sum_J A_J(0)\Phi_J(0)$, one first diagonalizes (H_{JK}) for (A_J) with fixed orbitals. Then one "optimizes" $\{\varphi_j^{(\kappa)}\}$ by propagating them in imaginary time over a short period. That cycle will then be repeated.

---

[10] Using the code documented in [82], this is done ahead of a computation for each non-separable term of the Hamiltonian using the program POTFIT, and the fitted potentials are included in an MCTDH run.

2.3.3 Application of the method

Up until now, we have outlined the MCTDH method in all generality. However, there are two peculiarities that set this problem apart from those typically tackled via MCTDH. For one thing, this is the requirement of bosonic permutation symmetry – i.e., demanding that the true wave function reside in the symmetry-restricted Hilbert space $\mathbb{H}_+ = \{\Psi \in \mathbb{H}_1^{\otimes N} \mid S_+\Psi = \Psi\}$, where S_+ denotes the symmetrization operator over all permutations. The second issue is that the effective interaction potential $V(x) = g\delta(x)$ introduced in Sec. 1.2.3 does not vary smoothly but rather has distribution character. Here we shall comment on how MCTDH can be applied to the problem of ultracold bosons.

Permutation symmetry The fact that MCTDH is designed for distinguishable particles reflects in the MCTDH ansatz (2.12) for the wave function,

$$\Psi(\cdot,t) = \sum_J A_J(t)\Phi_J(\cdot,t), \qquad \Phi_J \equiv \varphi_{j_1} \otimes \cdots \otimes \varphi_{j_N}.$$

Note that permutation symmetry of H clearly requires the set of single-particle functions $\{\varphi_j\}_{j=1}^n$ to be *identical* for each particle. Even so, the basis vectors Φ_J are generally not symmetric, as would be an obvious demand when dealing with bosons.[11] This is not a conceptual problem, though, since one may just as well keep the coefficients symmetric, $A_J = A_{P(J)}$. While this is highly redundant for $N \gg 1$, it works reasonably well for small systems. In practice, it is rarely necessary to explicitly project onto $\mathbb{H}_+$, the reason being that a symmetric initial state will not lose its symmetry under (real or imaginary) time evolution.

However, this comes with a catch: When numerical instabilities come into play, the permutation symmetry may indeed be lost, as can be checked by projecting onto $\mathbb{H}_+$. However, this has been encountered only when not enough basis functions were included. To give a plastic example: As $g \to \infty$, in which case bosonic and *fermionic* states become degenerate by the Bose-Fermi map, only a small numerical perturbation suffices to drive the *improved relaxation* algorithm into a fermionic eigenstate $|1,\ldots,1\rangle_- \propto S_-\{\varphi_1 \otimes \cdots \otimes \varphi_N\}$ if only $n \sim N$ orbitals are included.

Modeling the interaction The second issue does not impose a serious restriction. In fact, while the point interaction $g\delta(x)$ is convenient as an analytic tool and for perturbative approaches, it is only one specific effective potential. At low enough energies, any model potential may be chosen so long as the low-energy scattering parameters are reproduced. Actually, for exact many-body calculations, the δ function is not an overly practical choice as it imposes discontinuities on the derivative of Ψ, which is an unphysical consequence of the zero-range limit. We opt to mollify the delta function by a more realistic Gaussian

$$\delta_\sigma(x) = \frac{1}{\sqrt{2\pi}\sigma} e^{-x^2/2\sigma^2},$$

---

[11] Indeed, one might employ the symmetrized version $S_+\Phi_J$, viz., number states $|n_1, n_2, \ldots\rangle_+$ in the single-particle basis, as we did in the exact diagonalization.

which converges to $\delta(x)$ in the distribution sense for ranges $\sigma \ll 2\hbar^2/M\,|g|$ smaller than the 1D scattering length. However, only the weaker constraint of being short-ranged compared to the average inter-particle distance is vital, $\sigma \ll L/N$ (L being the system's spatial extension). On the other hand, the range ought to be at least on the order of the grid spacing Δ_g, so that the details of V are sampled sufficiently. Concordantly, the number of grid points $N_\mathrm{g} \sim L/\Delta_\mathrm{g}$ must be high enough – in our case, typically $N_\mathrm{g} \sim 150$. This corresponds to a harmonic-oscillator DVR $\{\chi_k\}_{k=1}^{N_\mathrm{g}}$ spanning a grid of length $L \sim 2 \times 4$ (i.e., $|x| \leq 4$ typically). Thus the grid is sufficiently fine for an interaction of width $\sigma = 0.05a_\|$ (in terms of the 1D oscillator length). In addition to the high number of single-particle functions φ_j needed to describe very strong correlations correctly (for our purposes, $n \sim 15$ typically suffices), this naturally limits the application of MCTDH to as few as five atoms.

Technical aspects: Excited states and propagation Whereas the convergence to the ground state via *improved relaxation* is practically bulletproof, matters are known to get trickier for excited states (see [86]). This should come as no surprise, granted that one cannot just seek the energetically lowest state but should remain orthogonal to any neighboring vectors Ψ_m. That is why, at bottom, the convergence turns out to be highly sensitive to the basis size—that is, to n—even for small correlations: The lower states simply must be represented accurately enough. For practical purposes, the most solid procedure has proven to be the following. In the non-interacting case, $g = 0$, we construct the eigenstates as number states $|\boldsymbol{n}\rangle \equiv |N_0, N_1, \ldots\rangle$ in the single-particle basis $\{\phi_a\}$. Starting from a given $|\boldsymbol{n}\rangle$, the eigenstate Ψ_m for $g \neq 0$ is found by an improved relaxation while sieving out the eigenvector *closest* to its initial state $|\boldsymbol{n}\rangle$.[12] The resulting eigenstate will then in turn serve as a starting point for an even larger g value, and so on.

Let us mention here two empirical observations concerning MCTDH. In some cases, it may become extremely difficult to converge to quasi-degenerate eigenstates in a conventional improved relaxation, unless the basis is enlarged substantially. In these cases, a simultaneous *block relaxation* of a whole set of these eigenstates may help bypass this divergence. A related problem concerns the time evolution if the initial state $\Psi(0)$ is close to a superposition of two quasi-degenerate states. It often occurs that MCTDH artificially "equilibrates" in the sense that, from some time step on, MCTDH deviates from the exact time evolution and rather seems to get locked in some spurious state unless a huge basis is included (in some cases as large as $n \sim 50$). Quite generally, MCTDH tends to violate energy conservation during a propagation involving sufficiently strong short-range interactions. This is due to the fact that, in that case, the interaction energy becomes very sensitive to very narrow intersections $\{x_i = x_j\}$ in configuration space. To sample this area accurately, a very small error tolerance needs to chosen for the integration, typically $\varepsilon \leq 10^{-8}$.

---

[12] Technically, this is ensured via the keyword `relaxation = lock` [82].

Chapter 3

Ground state: Mechanism of the fermionization crossover

The general aim of this thesis is to study the interacting 1D Bose gas from a few-body perspective. We have seen that, for infinitely repulsive point interactions, the bosons can be mapped to an ideal Fermi gas. While this fermionization limit is a mathematical borderline case, we would like to explore the mechanism of the *crossover* from noninteracting bosons to the strongly correlated fermionization limit. In this chapter, we will focus on the *ground state* of such trapped bosons. In Sec. 3.2, we will first analyze the nature of that transition in the prototype case of a harmonic trap, mainly from the perspective of *local* densities. A key aspect will be the interplay between interatomic and trapping forces, which is illuminated by comparing to the fermionization crossover in a double-well trap. In Sec. 3.3, we go one step further and study how this depends on the interaction potential. Specifically, we consider a setup where the interaction is *inhomogeneous*, i.e., the inter-particle forces depend on the position of a collision, too. Section 3.4 rounds off the investigation of the ground state by looking into the role played by *nonlocal* properties throughout the fermionization crossover, specifically the (off-diagonal) one-body density matrix and, closely related, the system's momentum distribution.

3.1 Model and scales

In this thesis, we investigate a system of few interacting bosons in a quasi-1D trap. As we have seen, this system can be descibed by the effective 1D Hamiltonian

$$H = \sum_{i=1}^{N} h(p_i, x_i) + \sum_{i<j} V(x_i - x_j),$$

where the one-body Hamiltonian $h(p,x) = \frac{1}{2M}p^2 + U(x)$ entails kinetic plus trapping energy (to be specified below), while the effective interaction may be written as a contact interaction $V(x) = g_{1\mathrm{D}}\delta(x)$. For the case of transverse harmonic confinement with length $a_\perp \equiv \sqrt{\hbar/M\omega_\perp}$, this can be related explicitly to the system parameters [21]:

$$g_{1\mathrm{D}} = \frac{2\hbar^2 a_0}{M a_\perp^2}\left(1 - \mathcal{C}\frac{a_0}{a_\perp}\right)^{-1}, \qquad \mathcal{C} = \frac{|\zeta\left(\frac{1}{2}\right)|}{\sqrt{2}} = 1.0326\ldots$$

$\omega_\parallel/2\pi$ Hz	$a_0'(\mathrm{Na})$	$g_{1\mathrm{D}}'$	$a_0'(\mathrm{Rb})$	$g_{1\mathrm{D}}'$
10^2	$1.9\cdot10^{-3}$	0.39	$5\cdot10^{-3}$	1.1
10^3	$6\cdot10^{-3}$	1.3	$1.6\cdot10^{-2}$	4.1
10^4	$1.9\cdot10^{-2}$	5.2	$5\cdot10^{-2}$	38
10^5	$6\cdot10^{-2}$	95	$1.6\cdot10^{-1}$	-24

Table 3.1: Values of the scaled coupling strength $g_{1\mathrm{D}}'$ for Sodium and Rubidium for different trap frequencies $\omega_\parallel/2\pi$ and $a_\perp' = .1$.

For technical reasons already detailed in Sec. 2.3.3, we mollify the contact interaction by a Gaussian of width σ small compared to the inter-particle distance , $V(x) = g_{1\mathrm{D}}\delta_\sigma(x)$. Throughout this thesis, we focus on repulsive forces, $g \equiv g_{1\mathrm{D}} \geq 0$.

3.1.1 Scaling

For reasons of universality as well as computational aspects, we will work with a Hamiltonian rescaled to the length scale of the 1D-longitudinal system, $a_\parallel$. More specifically, we carry out a global coordinate transform $X' := X/a_\parallel$, with $X \equiv (x_1, \ldots, x_N)^T$, which leads to

$$\underbrace{H(X)/\hbar\omega_\parallel}_{=:H'(X')} = \sum_i \left(-\frac{1}{2}\partial_i'^2 + U'(x_i')\right) + \sum_{i<j} V'(x_i' - x_j').$$

Here $\omega_\parallel \equiv \hbar/Ma_\parallel^2$ defines the energy scale, and $U'(x') := U(x = x'a_\parallel)/\hbar\omega_\parallel$ etc. denotes the rescaled potential deprived of any dimensionful parameters. H' naturally lends itself as a convenient working Hamiltonian, and we will skip all primes from here on.

As an illustration, for a harmonic trap $U(x) = \frac{1}{2}M\omega_\parallel^2 x^2$, setting $a_\parallel \equiv \sqrt{\hbar/M\omega_\parallel}$, we are simply left with $U'(x') = \frac{1}{2}x'^2$. The 1D point interaction in turn reduces to

$$V'(x') = g_{1\mathrm{D}}'\delta(x'), \quad g_{1\mathrm{D}}' := g_{1\mathrm{D}}\sqrt{\frac{M}{\hbar^3\omega_\parallel}} = \frac{2a_0'}{a_\perp'^2}\left(1 - \mathcal{C}\frac{a_0'}{a_\perp'}\right)^{-1}. \tag{3.1}$$

The only relevant parameter is thus the scaled interaction strength, which in turn requires only the knowledge of the (scaled) scattering length $a_0' = a_0/a_\parallel$ and the transverse confinement $a_\perp' = a_\perp/a_\parallel$.

3.1.2 Parameter regimes

As mentioned above, two parameters enter our Hamiltonian: $a_0' = a_0/a_\parallel$ and $a_\perp' = a_\perp/a_\parallel$. Both of course depend on

- the 1D length scale $a_\parallel = \sqrt{\hbar/M\omega_\parallel}$ (due to scaling)
- the scattering length $a_0 < a_\parallel$ of the atomic species considered (of order 100 a.u. for alkalis; only positive values are considered here).
- the transversal length scale $a_\perp \ll a_\parallel$. Of course $a_\perp > a_0$ is required unless the validity of the 'bare' pseudopotential is put into question.

According to (3.1), $g_{1\mathrm{D}}$ does not depend linearly on a_0, but rather tends to $+\infty$ as $a_0 \to a_\perp/\mathcal{C}$ from below. In other words, the system becomes strongly correlated when the scattering length

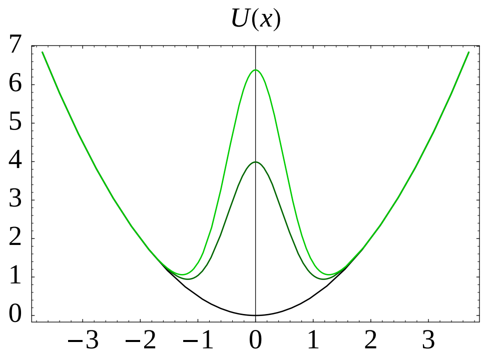

Figure 3.1: Sketch of the model potential $U(x) = \frac{1}{2}x^2 + h\delta_w(x)$, consisting of a harmonic trap plus a normalized Gaussian of width $w = 0.5$ and barrier strengths $h = 0, 5, 8$.

approaches the transverse-confinement scale, no matter if the 3D system was strongly interacting to begin with. Table 3.1 illustrates the range of values of a'_0 for different (longitudinal) trap frequencies $\omega_{\|}$, and what $g'_{1\mathrm{D}}$ they correspond to for Na/Rb (at fixed $a'_{\perp} = 0.1$).

3.2 Basic mechanism

In this as well as in the following two sections, we consider the ground-state properties of bosons in a double-well trap modeled by

$$U(x) = \frac{1}{2}x^2 + h\delta_w(x).$$

This potential is a superposition of a harmonic oscillator (HO), which it equals asymptotically, and a central barrier splitting the trap into two fragments (Fig. 3.1). The barrier is shaped as a normalized Gaussian δ_w of width w and 'barrier strength' h. As $w \to 0$, the effect of the barrier reduces to that of a mere boundary condition (since $\delta_w \to \delta$), and the corresponding *one-particle* problem can be solved analytically (see Appendix A, which also reviews some basics on double-well potentials). Although this soluble borderline case presents a neat calibration, the exact width w does not play a decisive role, as long as it is larger than the grid spacing and $w < 1$ so as to confine the barrier's effect to the central region. We choose $w = 0.5$ as a trade-off.

For $h = 0$, the case of interacting bosons in a harmonic trap is reproduced. In Sec. 3.2.1, we witness the transition from a simple, weakly interacting "condensate" ($g \to 0$) to the *Tonks-Girardeau* limit ($g \to \infty$). As $h \to \infty$, the energy barrier will greatly exceed the energy available to the atoms, and we end up with two *isolated wells*. Higher g then affect only the fragmentation *within* each of these wells. In between, there is an interesting interplay between the barrier forces (h) and the inter-particle forces (g). We study this intermediate regime on the example of $h = 5$ in Sec. 3.2.2.

3.2.1 Harmonic trap

Density profiles To get a feeling for what happens when we go from the noninteracting case ($g = 0$) to the strongly correlated fermionization limit $g \to \infty$, let us first look at the one-body

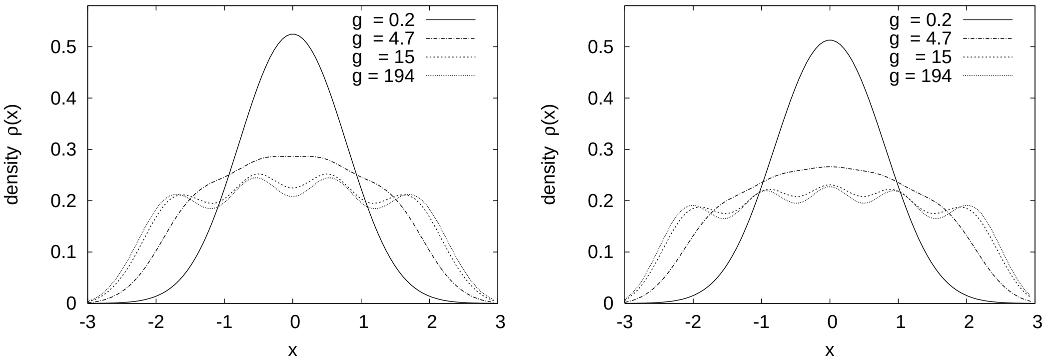

Figure 3.2: Fermionization of bosons in a harmonic trap: One-body density $\rho(x)$ for $N = 4$ (*left*), $N = 5$ (*right*) for different interactions g. Note how the profile changes from a weakly interacting one ($g = 0.2$) to a flattened one due to fragmentation, and finally to a fermionized profile featuring N humps ($g \geq 15$).

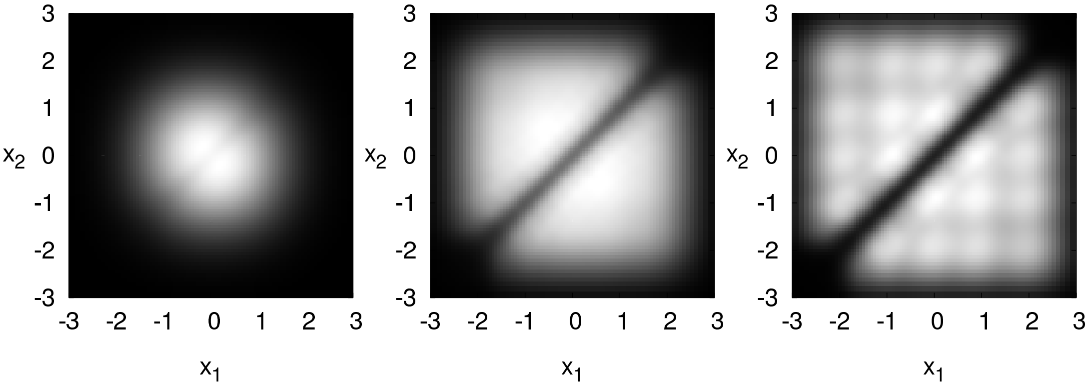

Figure 3.3: Two-body density $\rho_2(x_1, x_2)$ for $N = 5$ bosons in a harmonic trap. Shown are the interaction strengths $g = 0.4,\ 4.7,\ 15$ from left to right.

density profile $\rho(x)$, giving the probability density to find one particle at position x. Figure 3.2 visualizes the crossover for $N = 4, 5$ atoms: Near $g = 0$, all bosons reside in the single-particle ground state of the harmonic oscillator, $\Psi = \phi_0^{\otimes N}$, which is broadened due to repulsion. For stronger interactions ($g = 4.7$), however, the profile already deviates visibly from the Gaussian shape [40,43,44]. For very large $g = 15$, in turn, a structure of N peaks in the profile emerges. Physically, this means that, if we were to measure the position of a boson, it would be likely to find it at N discrete spots, and not so likely to detect it anywhere in between. This *localization* effect has a simple intuitive explanation: If the bosons repel each other very strongly, $g \to \infty$, they try to isolate each other so as to pay less interaction energy. However, they cannot do that indefinitely as they are confined in a trap. As a consequence, they tend to be pinpointed to more or less discrete positions. Note that this is the same profile one obtains for an ideal fermion gas, in which the ground state $|N_0 = 1, \ldots, N_{N-1} = 1\rangle_-$ is given by filling up the one-particle levels up to the Fermi edge, so that the fermionized density is simply $\rho = \sum_{a=0}^{N-1} |\phi_a|^2$. There, the seeming localization comes about because of the exclusion principle, which prevents the fermions from occupying the same point in space. By contrast, the effect here is caused by the ultrastrong repulsion. Note that this "localization" shared with noninteracting fermions is a true few-body feature; for $N \gg 1$ the peaks become ever tinier modulations on the envelope density, which for a harmonic trap can be computed as $\bar{\rho}(x) = \sqrt{2N - x^2}/N\pi$ [87].

Two-body correlations To better understand the underlying mechanism, let us revisit the fermionization from the perspective of the two-body correlations. Figure 3.3 depicts the evo-

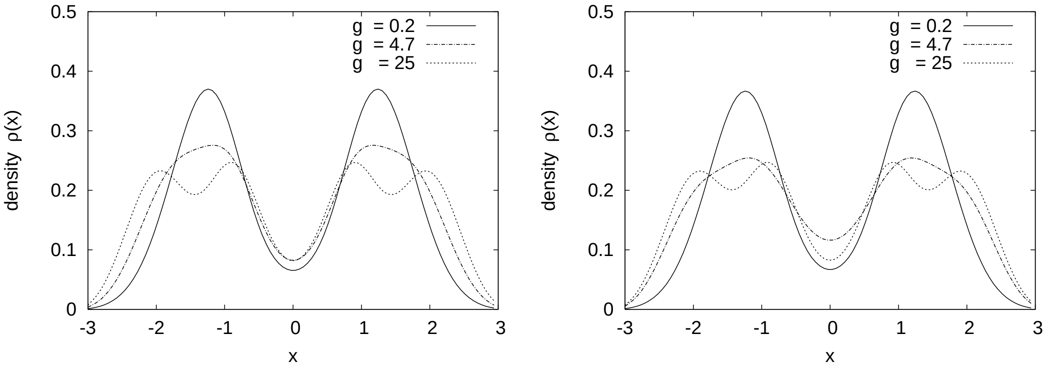

Figure 3.4: Fermionization of bosons in a double-well trap ($h = 5$): One-body density $\rho(x)$ for $N = 4$ (*left*), $N = 5$ (*right*) for different interactions g.

lution of the two-body density $\rho_2(x_1, x_2)$, which tells us the probability density of measuring one particle as position x_1 and any second at x_2. In the absence of correlations, at $g = 0$, $\rho_2 = \rho_1 \otimes \rho_1$ factorizes. This leads to the symmetric Gaussian density still visible for smaller interactions $g = 0.4$ (Fig. 3.3). To be sure, minor imperfections of the Gaussian shape are already anticipated here – these become even clearer when we go to higher values of $g = 4.7$. Apart from a significant broadening due to repulsion, what we see here is a *correlation hole* on the diagonal $\{x_1 = x_2\}$, signifying a depression of the two-body density. This is fairly intuitive: If the particles repel each other, it will cost a lot of energy for any two atoms to sit on top of one another, so such a configuration is avoided. This is also clear from the interaction energy $\mathrm{tr}(V\rho_2) \overset{\sigma\to 0}{\sim} g \int dx \rho_2(x, x)$. Note that this correlation hole is an inherent two-body picture; in the one-body density $\rho = \int dx_2 \rho_2(\cdot, x_2)$ it is smoothed out and only reflects in a smeared-out profile.

When this is taken to extremes, yet another effect emerges: For $g = 15$, Fig. 3.3 reveals the formation of a checkerboard pattern, which is already fairly close to the fermionization limit [26]

$$\rho_2(x_1, x_2) = \frac{1}{N(N-1)} \sum_{0 \le a < b < N} \left[\phi_a(x_1)\phi_b(x_2) - \phi_b(x_1)\phi_a(x_2)\right].$$

This corresponds to the density wiggles seen in the one-body picture near fermionization. Here it has the following interpretation: Suppose we measure a first particle at, say, $x_1 \approx 2$. Then, of course, the probability to find any second one at $x_2 \approx x_1$ is zero, while the remaining $N - 1$ particles can be found at $N - 1$ more or less “discrete” spots x_2. Note that this feature cannot be understood from the two-body picture alone, but rather is a manifestation of the hard-core boundary conditions $\Psi|_{x_i = x_j} = 0$.

3.2.2 Double well

We now introduce a central barrier of height $h = 5$, this way turning the harmonic trap into a double well. In this case there is a competition between the tendency to distribute the particles over the two wells so as to save potential energy, and to reduce the interaction energy by trying to isolate the particles as $g \to \infty$.

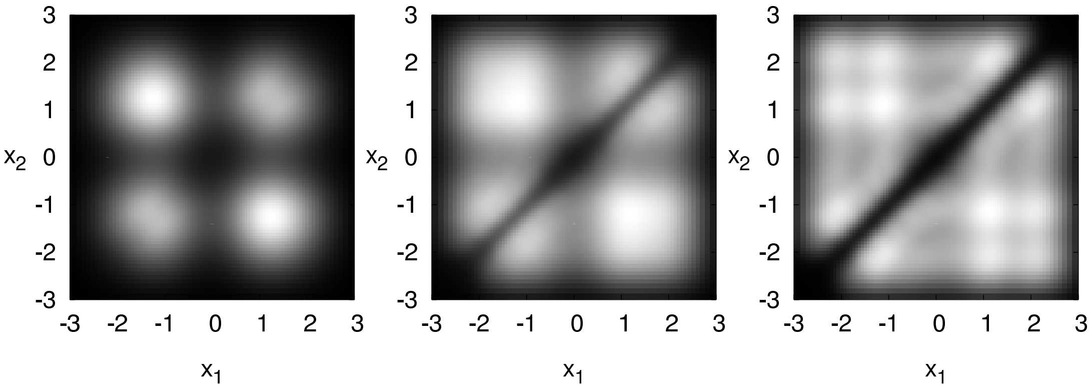

Figure 3.5: Two-body density $\rho_2(x_1, x_2)$ for $N = 5$ bosons in a double-well trap $(h = 5)$. Shown are the interaction strengths $g = 0.4,\ 4.7,\ 15$ from left to right.

Density profiles Figure 3.4 depicts the evolution of the density profile $\rho(x)$ as g is increased throughout the fermionization crossover. For *even* atom numbers, $N = 4$, the general picture looks fairly similar to the single-well case. Near $g = 0$, all atoms are in the single-particle ground state ϕ_0, which now is delocalized over the two wells. As we switch on g, the atoms repel each other, leading to a broadened density in each well (cf. $g = 4.7$). Toward the fermionization limit, the bosons again arrange in N more or less discrete positions, given by density maxima, although of course with a strongly reduced likelihood at $x = 0$.

The situation differs for *odd* numbers, see $N = 5$. For very large $g = 25$, we see only $N - 1 = 4$ wiggles, which makes it tempting to say that the extra, fifth particle is now delocalized over the two wells rather than pinned down as in the harmonic trap. This is fairly intuitive because if an odd number of bosons are distributed discretely over the trap, by symmetry, one boson should reside at $x = 0$. However, this is strongly suppressed energetically due to the central barrier; so as a trade-off, the extra atom is smeared out about the barrier region.

Thought of as an ideal Fermi gas, the ground state for even N is one with all N lowest bands (i.e., doublets) filled: $|1_0^{(0)}, 1_1^{(0)}; \ldots; 1_0^{(N/2-1)}, 1_1^{(N/2-1)}\rangle_-$ (where $1_{a_\beta}^{(\beta)}$ denotes occupation of the symmetric ($a_\beta = 0$) or antisymmetric ($a_\beta = 1$) orbital in band β; cf. Sec. A.1). These filled bands correspond exactly to the situation above with all N fermions pinpointed to N maxima. If we now add another particle # $N + 1$, this will *delocalize* over the next upper, previously empty band $\beta = N/2$. In this light, the even-vs.-odd distinction ought to persist for all N, tacitly assuming that the energetically highest atom is still below the barrier energy and not in the classical region. Of course, as before the density oscillations will shrink to tiny modulations on the envelope as $N \to \infty$.

Two-body correlations As in the reference case of the harmonic trap, the two-body correlations ρ_2 reveal some of the underlying fermionization mechanism in the double well. Figure 3.5 shows that, at small $g = 0.4$, the $N = 5$ atoms are coherently distributed over the two wells. Thus it makes little difference as to whether two particles are in the same well (the diagonal peaks $x_1 \approx x_2$) or in opposite ones ($x_1 \approx -x_2$). For stronger repulsion, $g = 4.7$, the familiar correlation hole builds up. Moreover, the density peaks are visibly smeared out and distorted due to on-site repulsion. As we approach the fermionization limit ($g = 15$), again a characteristic checkerboard pattern emerges. However, compared to the simple harmonic case displayed in Fig. 3.3, it strikes that now, upon measuring the first particle, there are not $N - 1 = 4$

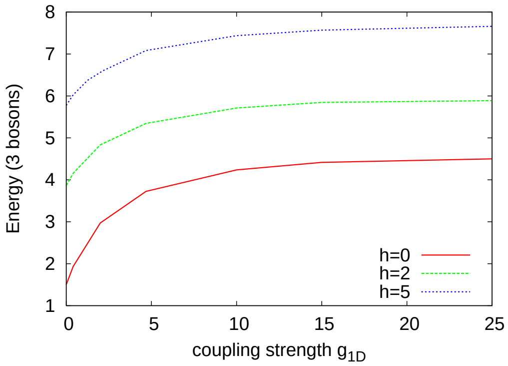

Figure 3.6: Energy $E(g)$ for the case $N = 3$. Note the slightly different effect of the interaction, measured by the slope at $g = 0$, for different barrier strengths $h = 0$ (harmonic trap) and $h = 2, 5$. The saturation as $g \to \infty$ corresponds about to a fermionized state.

maxima for finding the four remaining particles. Rather, the missing peak expected at $x = 0$ is smeared out over the central-barrier region, which is but the two-body perspective on the interpretation given above.

3.2.3 Ground-state energy

Our previous analyses are in a way wrapped up in Fig. 3.6, which depicts the ground-state energies $E(g)$ as a function of the coupling strength. Invoking the Bose-Fermi map, the ground-state energy may be interpreted as connecting the free bosonic value, $E(g = 0) = N\epsilon_0$, and the free fermionic value, corresponding to the saturation $E(g \to \infty) = \sum_{a=0}^{N-1} \epsilon_a$ (in terms of the respective single-particle levels $\{\epsilon_a\}$).

The effect of the interaction at $g = 0$ can be measured by the slope

$$\frac{dE}{dg}(0) = \frac{N(N-1)}{2} \langle 00|\delta_\sigma(x_1 - x_2)|00\rangle \overset{\sigma\to 0}{\sim} \frac{N(N-1)}{2} \int |\phi_0(x)|^4 dx,$$

given by the density overlap of two atoms in the non-interacting ground state. The centered harmonic-oscillator orbital ϕ_{HO} by construction has a low curvature (i.e., kinetic energy), thus producing a rather high density overlap. It is thus more susceptible to the onset of interactions. By contrast, the presence of a central potential-energy barrier ($h \to \infty$) evokes an orbital ϕ_{DW} delocalized in both wells. Its density overlap in turn will be smaller, which can be seen schematically by assuming for a moment that $\phi_{\mathrm{DW}}(x) \sim \frac{1}{\sqrt{2L}} \left[\phi_{\mathrm{HO}}\left(\frac{x-x_0}{L}\right) + \phi_{\mathrm{HO}}\left(\frac{x+x_0}{L}\right)\right]$ is built from a HO orbital centered in both minima $\pm x_0$, and rescaled by the well width L. Neglecting the density overlap between the right- and left-hand contributions, $\int |\phi_{\mathrm{DW}}|^4 \simeq \frac{1}{2L} \int |\phi_{\mathrm{HO}}|^4$, suggesting that in a double well with not-too-large squeezing, the atoms will feel a slightly lesser effect when interactions are turned on. This can be seen in Fig. 3.6.

The above formula also tells us something about the dependence on the particle number N. The relative increase at $g = 0^+$ will scale with the number of pairs $N(N-1)/2$ as opposed to the single-particle energy, thus the perturbative impact is expected to rise with larger N. Note that the harmonic-trap fermionization energy $E = \sum_{a<N}(a + \frac{1}{2}) = N^2/2$ exceeds the ground-state energy at $g = 0$ by a factor of N, which is also indicative of the growing influence of the particle number. A little more information may be gained by comparing to the thermodynamic limit solution given in Sec. 1.4.2, $E = Nn^2 e(\gamma \equiv g/n)$, where the number

density $n(x) = N\rho(x)$ now becomes position dependent. From that standpoint, the regime of strong (and likewise weak) interactions is universally given by $\gamma \gg 1$ or $g \gg n(x)$. Given that, in the harmonic case, the fermionized density is $n(0) = \sqrt{2N}/\pi$ (cf. Sec. 3.2.1), this asserts that convergence to the fermionization limit should be slowed down by a factor of $\sqrt{N}$ for larger particle numbers, an effect which is hard to see for small atom numbers.

3.3 Inhomogeneous interactions

Up to now, we have analyzed the fermionization crossover with a focus on the interplay between inter-particle forces with different external forces and the role of the atom number. In this section, we would like to indicate how this depends on the interaction potential itself. So far, we have assumed point interactions which are fully defined by the coupling constant g. One way to go beyond this would be to regard different *shapes* of V. However, we have argued in Sec. 1.2.2 that, in the low-energy limit, the physics of short-range interactions should become shape independent. (The field of long-range forces relevant, e.g., in dipolar systems [88, 89] is beyond the scope of this thesis.)

Still, one can think of this in yet another way. We have so far relied on the assumption of *homogeneous* two-particle forces. These are invariant under global translations and thus depend on $x_i - x_j$ alone. While this premise is most natural from a fundamental point of view, we should keep in mind that our description is not a *fully* microscopic one, even if we ignore the internal structure of the underlying atoms. Rather, it is an effective model stripped not only of the transverse degrees of freedom, but of course also of the electromagnetic fields that manipulate both external and inter-particle forces. With this in mind, it appears legitimate to conceive situations where the strength of the interaction depends in addition on the *absolute position* where the collision takes place, as was done in a mean-field framework in Ref. [90] (see also citations therein). This may be induced by means of a Feshbach resonance, tuning $a_0(\mathbf{B})$ by adding a spatial dependence to the magnetic field. In our one-dimensional setting, it seems even more convenient to exploit the parametric dependence on the transverse subsystem, and modify $a_\perp$ locally so as to imprint a spatial dependence on g.

Without reference to the specific experimental realization, we now perform a case study where g takes on different values on both sides of the trap. This model will be presented in Sec. 3.3.1. The interplay of that dynamical inhomogeneity with the external forces will be studied for a harmonic (Sec. 3.3.2) and a double-well trap (Sec. 3.3.3).

3.3.1 Model interaction

Whereas modeling a position-dependent interaction in a mean-field description (as in [90]) is straightforward, since one only has an effective one-particle problem, one faces a conceptual problem when using a many-body framework. In general, the coupling would depend on both participants x_i, x_j, which is technically possible if somewhat awkward. For it to make sense intuitively, we require that its modulation length scale be much larger than the 'radius' of collision, σ.

With this is mind, it is natural to model our interaction in terms of the respective relative coordinate $r := x_i - x_j$ (for fixed i, j) and—in order to keep V formally symmetric— the

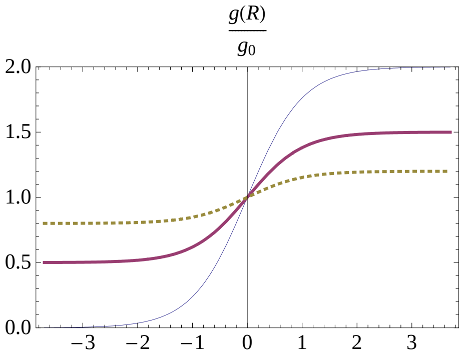

Figure 3.7: Our model of the position-dependent coupling $g(R)/g_0 = 1 + \alpha \tanh\left(\frac{R}{L}\right)$. The relative modulation, here $\alpha \in \{0.2, 0.5, 1\}$, determines the asymptotic difference from the average value g_0, while the modulation length $L = 1$ shall remain fixed.

center of mass $2R := x_i + x_j$:

$$V(r, R) = g(R)\delta_\sigma(r).$$

There are various possibilities just what scenario should be examined, be it some kind of collision-enhanced tunneling or dynamical self-trapping [90]. We concentrate on a specific model where g is essentially imbalanced between the right- and left-hand sides of the trap (Fig. 3.7):

$$g(R) = g_0 \left[1 + \alpha \tanh\left(\frac{R}{L}\right)\right].$$

This signifies that for $|R| \gg L$, the coupling takes on the asymptotic values

$$g_\pm \equiv \lim_{R\to\pm\infty} g(R) = g_0(1 \pm \alpha),$$

while it changes on a scale of L near the trap's center about g_0. The parameter α regulates both the relative difference between the asymptotic strengths and their ratio:

$$\begin{aligned} \Delta g &\equiv |g_\pm - g_0| = g_0\alpha, \\ \frac{g_+}{g_-} &= \frac{1+\alpha}{1-\alpha}. \end{aligned}$$

The above criterion that g vary slowly can be met if $L \gg \sigma\alpha$, which is effortlessly fulfilled if we choose $L = 1$ for convenience.

3.3.2 Harmonic trap

Assuming that we start with a weakly interacting ensemble, the ground state of atoms immersed in a harmonic trap will be centered at the trap's bottom. Hence the modulation of the coupling strength $g(x)$ beyond $x = 0$ will pass them largely unnoticed. It is only for strong enough repulsive interaction that the density profile will start to spread and shift partly outward, thus experiencing an asymmetry.

This picture is supported by our calculations, as demonstrated in Figure 3.8 for $N = 5$ atoms. For low enough average interaction strengths, $g_0 = 0.4$, the harmonic profile is barely altered from the homogeneous case $\alpha = 0$. An imbalance is noticed for medium $g_0 = 4.7$: The atoms are now able to sample the modulation of the coupling strength and find it cheaper

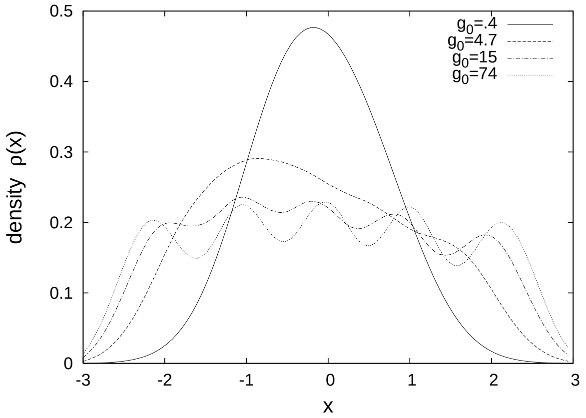

Figure 3.8: One-particle densities $\rho(x)$ for a harmonic trap ($N = 5$) in the case of inhomogeneous interactions, here $\alpha = .5$. The profile features an imbalance for smaller interactions g_0, where the wave packet is centered too much to sample the modulation of $g(R)$. When fragmentation sets in, the profile splits and the asymmetry becomes more distinct. In the fermionization limit, the energy costs of an imbalance become too large to keep it up.

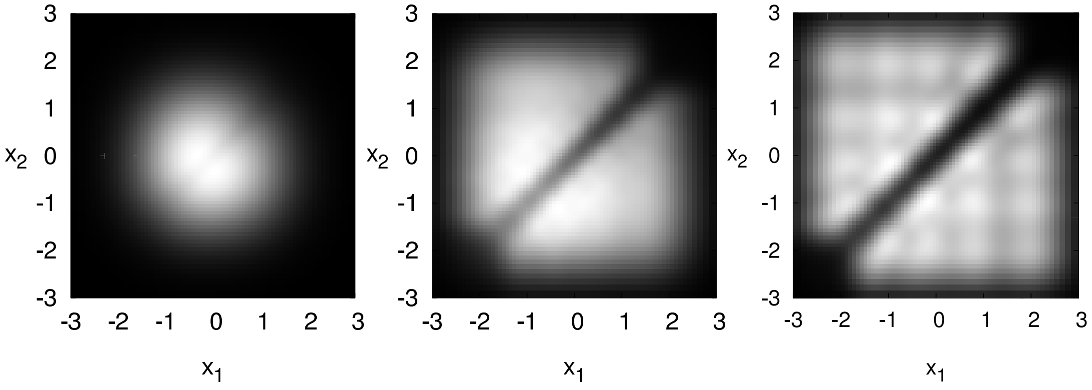

(a) (b) (c)

Figure 3.9: Two-particle density for a harmonic trap in the presence of inhomogeneous interactions ($N = 5$). (a) For $g_0 = 0.4$, the packet is localized about the center, thus widely ignoring the modulation. (b) For $g_0 = 4.7$, it starts to delocalize and consequently shifts to $R < 0$. (c) Toward fermionization, $g_0 = 15$, the imbalance is destroyed.

to locate in the less repulsive zone $\{x < 0\}$ (governed by g_-). However, this effect ceases as the repulsion becomes larger ($g_0 \geq 15$). This may be interpreted as follows: the energetical costs for concentrating several particles near one spot are soaring, and this *in total* eventually outweighs the *relative* energy savings reached by an imbalance.

A look into the two-body correlations $\rho_2(x_1, x_2)$ in Fig. 3.9 helps us clarify what happens. For the inhomogeneity to become effective, clearly the density must be spread out enough on the diagonal $\{x_1 = x_2\}$ in order to sample the spatial modulation $g(R)$. This is not the case for small interactions. Indeed, for $g_0 = 0.4$, the packet is localized about the center, thus widely ignoring the modulation. Yet for medium $g_0 = 4.7$ (Fig. 3.9b), the repulsion-driven broadening has become distinct enough for the ground states to exhibit some left-right asymmetry. Near the fermionization limit, the correlation diagonal in turn is fully depleted ($g_0 = 15$), so obviously the atoms can no longer realize the modulation and thus are no longer displaced. It should be emphasized that, in the ultimate limit $g(R) \to +\infty$, the hard-core boundary conditions (1.17) apply, and thus the mapping to ideal fermions from Sec. 1.4.1 becomes exact, irrespective of the actual modulation $g(R)$.

The above findings are nicely wrapped up in Fig. 3.10, showing graphs of $\langle x \rangle = \mathrm{tr}(\rho_1 x)$

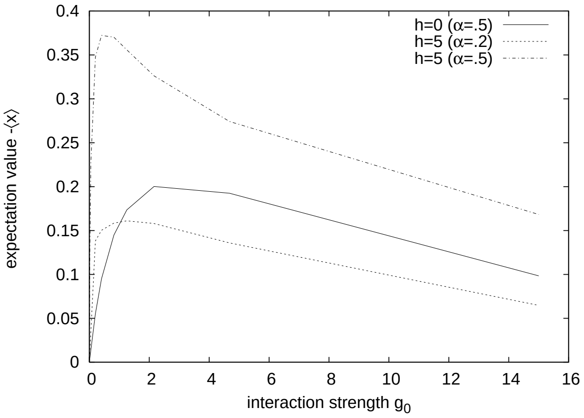

Figure 3.10: The ground-state displacement $-\langle x\rangle$ as a function of the average interaction g_0 $(N=5)$. Its universal behavior is an increase up to a maximum value followed by a slow decay. The increase at $g_0 = 0$ is strongly enhanced in the presence of a barrier $h > 0$, while for the purely harmonic trap ($h = 0$), it is rather slow. Of course the maximum itself is much more pronounced for higher modulations α, while being absent in the homogeneous case $\alpha = 0$.

as a function of g_0 for $N = 5$. For $\alpha = 0$, and of course for $g_0 = 0$, no modulation exists and, by symmetry, $\langle x\rangle = 0$. Notably, the same goes for $g_0 \to \infty$, when the correlation hole is pronounced as delineated above, even though the displacement will vanish only very slowly. There is a trade-off in between for which $\langle x\rangle$ becomes extremal. The value where this occurs, $g_0^\star(\alpha)$, depends only weakly on the relative modulation α—despite the fact that the maximum ground-state displacement $-\langle x\rangle^\star$ will of course increase monotonically with α.

3.3.3 Double well

In the presence of a sufficiently strong barrier, the situation is a different one. To begin with ($g_0 = 0$), the atoms are not centered as before but rather coherently distributed over the two wells. Hence, upon switching on the inhomogeneous interaction, they can immediately feel the full impact of its modulation on both sides. For finite barrier strength h, they can then re-distribute so as to find a compromise between minimum repulsion and potential energy.

The above process is illustrated in Fig. 3.11, which evidences an immediate shift from the right well to the left one, where the repulsion is weaker. This still corresponds to the Gross-Pitaevskii regime of a single dominant orbital: There is no correlation hole; in fact the probability density of finding both particles in the left well, $\rho_2(-x_0, -x_0)$, may even be larger than that for separation, $\rho_2(\pm x_0, \mp x_0)$. As the interaction passes a critical strength, fragmentation sets in, somewhat more pronounced on the right-hand side (Fig. 3.11b). Note how the diagonal $\{x_1 = x_2\}$ is being emptied, signifying the incipient destruction of the imbalance.

This reflects in the one-particle density displayed in Fig. 3.12. The density is almost 'instantaneously' shuffled from the right to the left. In the curve for $g_0 = 4.7$, it becomes apparent that the fragmentation essentially kicks in separately for both wells, where only the right well exhibits the typical repulsion-induced split-up. As asserted already for the harmonic case ($h = 0$), the modulation becomes marginal in the fermionization limit. At least for an even number $N = 4$ (Fig. 3.12a), this may also be discerned here. By contrast, Fig. 3.12(b) conveys an impression how slow the convergence to the fermionization limit is for odd $N = 5$. Even

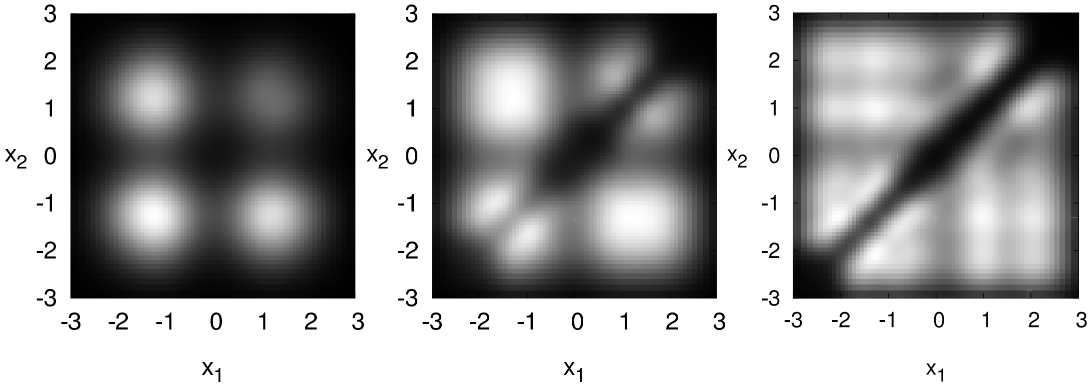

(a) (b) (c)

Figure 3.11: 2-particle density for $N = 5$ bosons in a double-well trap ($h = 5$) and with inhomogeneous interactions ($\alpha = 0.5$). (a) Already for $g_0 = 0.2$, the probability of finding any two atoms in the left well is significantly enhanced. (b) At $g_0 = 4.7$, the diagonal $\{x_1 = x_2\}$ is starting to deplete, which is even more pronounced for $g_0 = 15$ (c).

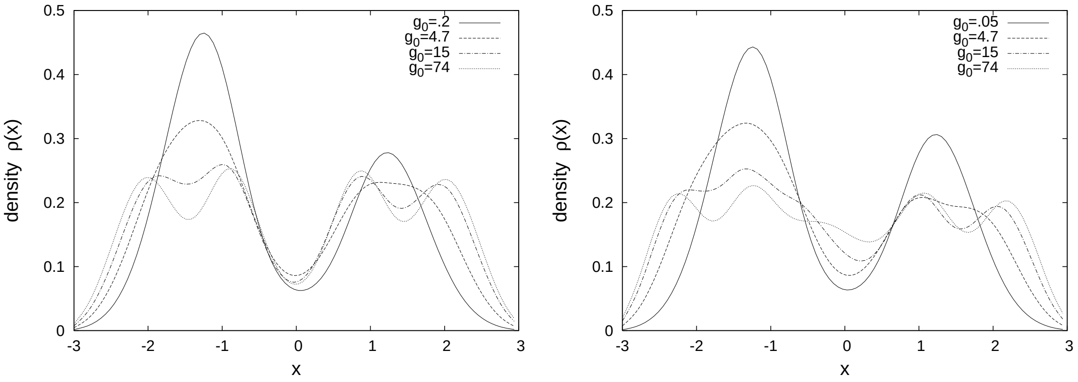

(a) (b)

Figure 3.12: One-particle density for a double well ($h = 5$) and modulated coupling strength ($\alpha = 0.5$): Even atom numbers $N = 4$ (a) versus odd numbers $N = 5$ (b).

for utterly large $g_0 = 74$, the “spare” particle is still practically accommodated in the left well rather than delocalized over both wells, as expected for $g_0 \to \infty$.

The nature of the ground-state displacement is again summarized in the graph of $-\langle x\rangle$ (Fig. 3.10). While the harmonic system turned out to be rather irresponsive to g_0, the displacement now exhibits a dramatic increase with raising g_0, as laid out above. It finds a maximum, which corresponds to the trade-off between localizing in the left well and maximum spreading. As before, the modulation α does not so much alter the critical $g_0^\star(\alpha)$, but of course makes for a stronger maximum displacement $\langle -x\rangle^\star$. The displacement decreases again slowly beyond that point. A notable side effect is that the displacement in the presence of a central barrier may in fact drop *below* the one without it, although of course this can only happen if the modulation α was smaller to begin with. That is simply because the double well, favoring the delocalization of the atoms, not only supports the modulation’s effect, but also accelerates fragmentation and hence—eventually—destruction of the asymmetry.

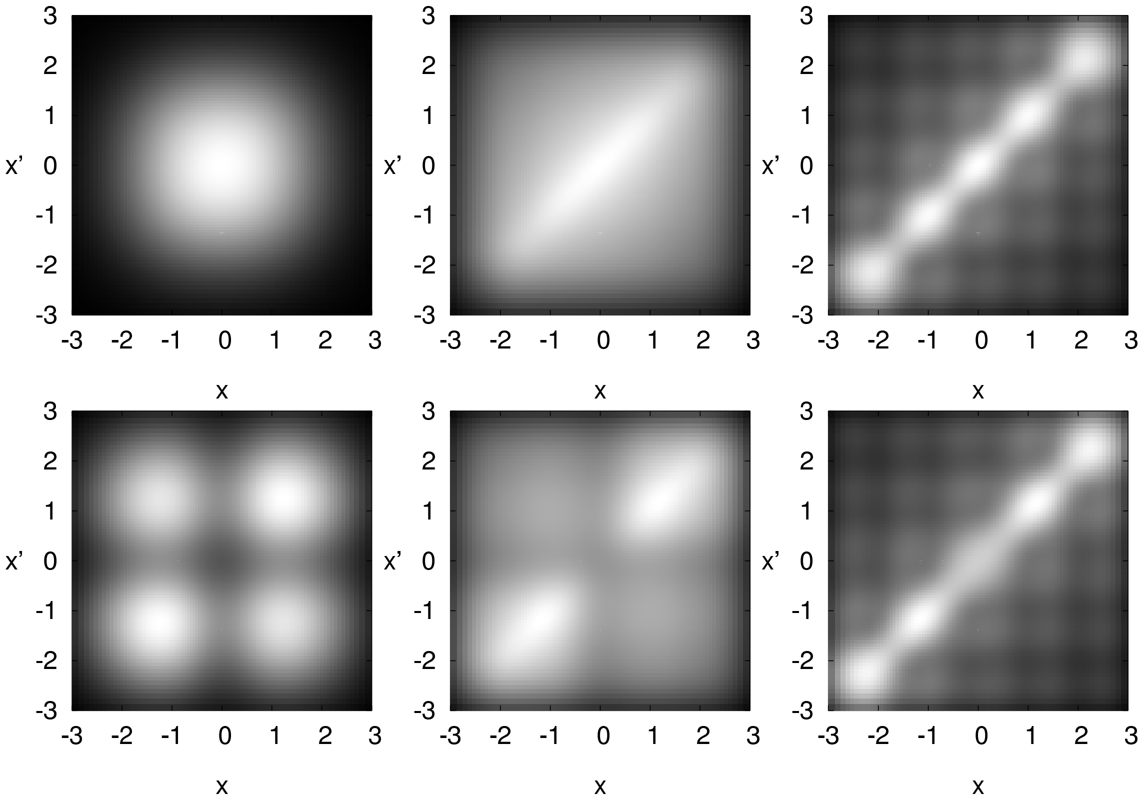

Figure 3.13: One-particle density matrix $\rho_1(x,x')$ for $N=5$ bosons. *Top row*: harmonic trap, *bottom row*: double well (barrier height $h=5$). Results are shown for the interaction strengths $g=0.4,\ 4.7,\ 194$ from left to right.

3.4 One-particle correlations

In the previous sections, we have explored the fermionization crossover from the perspective of *local* quantities derived from $|\Psi(X)|^2 = \langle X|\rho_N|X\rangle$, such as the reduced densities. From what we have seen thus far, one might jump to the conclusion that, in the course of fermionization, the system actually becomes *fermionic*. This is of course not true: The atoms still keep their bosonic permutation symmetry, which reflects in *nonlocal* properties. The simplest case where this can be seen is on the one-body level, which is completely described by the one-body density matrix ρ_1 (cf. Sec. 1.3). In this section, we seek to revisit the fermionization crossover from the perspective of nonlocal one-body correlations, thus gaining a complementary viewpoint on its mechanism. We focus on different angles, whose connection will become clear soon:

- In Sec. 3.4.1, we study the off-diagonal density matrix $\rho_1(x,x') \equiv \langle x|\rho_1|x'\rangle$, which relates to the question of off-diagonal long-range order.

- Section 3.4.2 studies the spectral decomposition of $\rho_1 = \sum_a n_a|\phi_a\rangle\langle\phi_a|$ in terms of natural orbitals and their occupations, which is often used to characterize the interacting system through effective single-particle states.

- Section 3.4.3 makes the link to the experimentally relevant momentum distribution $\tilde{\rho}(k) = 2\pi\langle k|\rho_1|k\rangle$.

3.4.1 One-particle density matrix and long-range order

The one-body density matrix ρ_1 contains all the information about the single-particle aspects of the system, and it serves as a good measure for the degree of coherence. In this subsection, we will analyze it from the most immediate perspective, i.e., we investigate its integral kernel $\rho_1(x,x') \equiv \langle x|\rho_1|x'\rangle = \rho_1(x',x)^*$. Since any density matrix is non-negative, so is the one-body density $\rho(x) \equiv \rho_1(x,x)$. As opposed to that, the off-diagonal part will even be complex in general (although, in this paper, a real representation is employed). It is therefore certainly not an observable in its own right, although it is indirectly accessible via interferometry experiments [2]. Nonetheless, it gives us access to all single-particle quantities, in particular nonlocal ones such as the momentum distribution

$$\tilde{\rho}(k) = 2\pi\langle k|\rho_1|k\rangle = \int dx \int dx' e^{-ik(x-x')}\rho_1(x,x').$$

It is reflection symmetric if ρ_1 is real symmetric. Moreover, it can be understood as the Fourier transform of the integrated 'off-diagonal' correlation function [2]

$$\tilde{\rho}(k) = \int dr e^{-ikr}\bar{\rho}_1(r),$$

with $\bar{\rho}_1(r) := \int dR\rho_1(R+\frac{r}{2}, R-\frac{r}{2})$. Note that $\bar{\rho}_1$ is again generally complex and reflection symmetric, and it is normalized to $\bar{\rho}_1(0) = 1$. From this, it becomes clear that the off-diagonal behavior of ρ_1 (encoded in $\bar{\rho}_1$) has a 1-1 correspondence to the momentum distribution.

More specifically, the short-distance behavior determines the high-k asymptotics, which for a point interaction $V(x) = g\delta(x)$ in the limit $g \to \infty$ has been shown to display the universal decay $\tilde{\rho}(k) = O(k^{-4})$ [91]. Conversely, the off-diagonal asymptotics $r \to \infty$ relates to the low-k regime. This, however, depends on the nature of the external potential. For a homogeneous system (as in Sec. 1.4.2), it has been argued that Bose condensation were equivalent to *off-diagonal long-range order*, i.e. $\bar{\rho}_1(r) = O(1)$ [92]. By contrast, in the limit $g \to \infty$, it has in turn been shown that $\bar{\rho}_1(r) = O(r^{-1/2})$, which implies an infrared momentum divergence $\tilde{\rho}(k) \sim c/\sqrt{k}$ as $k \to 0$ [93].

In Figure 3.13, the fermionization transition as reflected in $\rho_1(x,x')$ is visualized for $N = 5$ bosons in a harmonic trap ($h = 0$, top row) and a double well of barrier strength $h = 5$ (bottom). In the harmonic case, the system starts at $g = 0$ with a direct-product state $\Psi = \phi_0^{\otimes N}$, i.e., with a density matrix $\rho_1(x,x') = \phi_0(x)\phi_0^*(x') \propto e^{-R^2}e^{-r^2/4}$ in terms of $r = x - x'$ and $2R = x + x'$. From this point of view, the system does not exhibit genuine off-diagonal long-range order, which is simply rooted in the fact that it is spatially bounded. Of course, it is nonetheless in a coherent state and thus features *weak* long-range order in that $\rho_1(x,-x) \sim \sqrt{\rho(x)\rho(-x)}$ as $x \to \infty$. This property persists so long as the correlations induced by the interactions are weak enough for the system to remain in such a single-particle state (the Gross-Pitaevskii regime), such as for $g = 0.4$. To make this point even clearer, Fig. 3.14 plots the one-body coherence (or correlation) function as defined in Eq. (1.16)

$$g_1(x,0) = \frac{\rho_1(x,0)}{\sqrt{\rho(x)\rho(0)}},$$

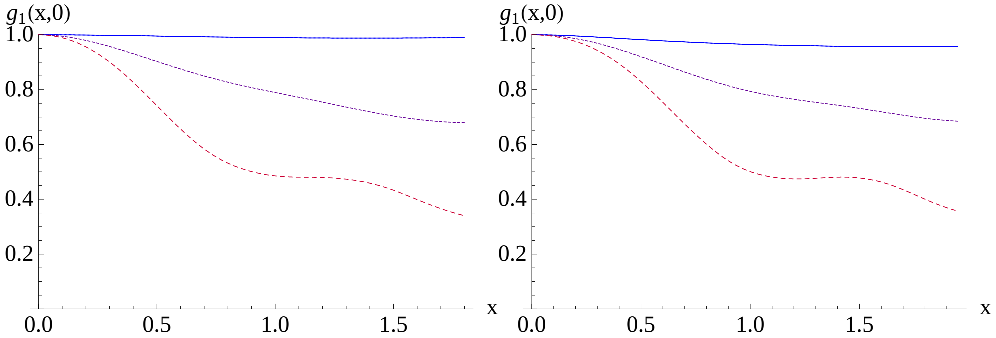

Figure 3.14: One-particle coherence function $g_1(x,0) = \rho_1(x,0)/\sqrt{\rho(x)\rho(0)}$ for $N = 5$ bosons. *Left*: harmonic trap, *right*: double well. Results are shown for the interaction strengths $g = 0.4$ (—), $g = 4.7$ $(\cdots)$, and $g = 194$ $(- - -)$.

which in a way filters out the effect of the trapping potential. Note that, for $g = 0.4$, $g_1(x,0)$ does not drop below unity. For $g = 4.7$, however, the symmetry in R and r breaks up. The density profile $\rho(x) \equiv \rho_1(x,x)$ flattens, and one can see that the off-diagonal range is somewhat extended, too. However, as g is increased further, the support of $\rho_1(x,x')$ will concentrate more and more in the diagonal region $\{x = x'\}$, where the typical fermionized profile is recovered (cf. $g = 194$). By contrast, the off-diagonal contributions will be washed out, indicating the reduced coherence of the system. Still it is noteworthy that even in this limit, a rest of coherence is preserved in a faint checkerboard pattern.

For the double well ($h = 5$; bottom row in Fig. 3.13), the situation is slightly different. As before, the system exhibits coherence at $g = 0.4$, only that the orbital is now delocalized in both minima $\pm x_0$ and may be written as $\phi_0(x) = \frac{1}{\sqrt{2}}[w(x-x_0)+w(x+x_0)]$. Unlike the harmonic case, the off-diagonal range is not initially increased but directly destroyed upon switching on g. While for $g = 4.7$ the density matrix $\rho_1(x,x')$ may still be thought of as pertaining to two separate subsystems, it eventually reaches the Tonks-Girardeau limit ($g = 194$), where the only obvious difference toward $h = 0$ consists in the density suppression at $x, x' = 0$.

3.4.2 Natural orbitals and their populations

While, in principle, the *full* density matrix $\rho_1(x,x')$ as studied in the previous section contains all the information at the one-particle level, it is somewhat less amenable to intuition. A handier criterion is offered by its spectral decomposition

$$\rho_1 \equiv \sum_a n_a |\phi_a\rangle\langle\phi_a|, \tag{3.2}$$

where $n_a \in [0,1]$ is said to be the population of the *natural orbital* ϕ_a. If all $N_a \equiv n_a N \in \mathbb{N}$ ($\sum_a N_a = N$), then the density may be mapped to the (uncorrelated) number state $|N_0, N_1, \dots\rangle$ based on the one-particle basis $\{\phi_a\}$; for non-integer values it extends that concept. In particular, the highest such occupation, n_0, may serve as a measure of *non*-fragmentation, a criterion put forward by Penrose and Onsager [70]. For $n_0 = 1$, a simple condensate is recovered. This is the well-known borderline case of the Gross-Pitaevskii equation: As $g \to 0$, $\rho_1 \to |\phi_0\rangle\langle\phi_0|$ [73] and $\rho_2 = \rho_1 \otimes \rho_1$, so that the interaction above can be replaced by a mean field $\bar{V} = \mathrm{tr}(\rho_1 V)$. In this sense, the natural orbitals and their populations tell us how close the system is to a pure one-orbital state.

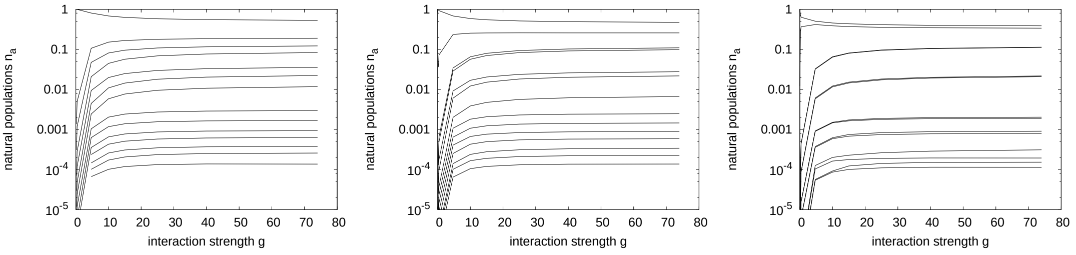

(a) (b) (c)

Figure 3.15: Natural populations $n_a(g)$ $(a \leq 13)$ for $N = 4$ bosons in a harmonic trap (a) and in a double well with barrier height $h = 5$ (b) , $h = 10$ (c).

Natural populations as a measure of fragmentation

Figures 3.15(a-c) show typical plots of the natural populations as the interaction is increased, $\{n_a(g)\}$, for four bosons and $h \in \{0, 5, 10\}$. Starting from $n_0 = 1$ for the non-interacting case, the lower lines rise steeply until they end up saturating in a fermionized state at $g \to \infty$. Note that this pattern is roughly detached from the specific shape of the trap, i.e, from what the underlying *orbitals* look like. This indicates why the set $\{n_a\}$ lends itself as a criterion for fragmentation. The details of the system are essentially encoded in (i) the exact sequence of n_a in the Tonks-Girardeau limit, and (ii) in the transition between the two extreme regimes $g = 0$ and $g \to \infty$.

For the harmonic oscillator ($h = 0$), the plot reveals a relatively simple hierarchy. The value of n_0 decreases smoothly to its Tonks-Girardeau limit $n_0 \sim 1/\sqrt{N}$ [26, 27]. All the remaining populations increase dramatically up until $g \sim 10$, and accumulate in a more or less equidistant spacing (on a log scale). But even the next-to-dominant weight n_1 is nowhere near the ‘condensate’ fraction n_0; the obvious gap between these two reflects the difficulty to observe fragmentation in the harmonic oscillator as compared to $h > 0$. Note that the group of lines $\{n_0, \ldots, n_{N-1}\}$ reveals a faint yet discernible separation from the lines below. The accumulation of points $n_a(g)$—in other words, the slow decay of n_a as $a \to \infty$—makes for an utterly slow numerical convergence for large g.

For a barrier height $h = 5$, a little more structure can be identified in the line sequence $n_a(g)$. The accumulation persists, but at least the more populated orbitals $\#a$ seem to come in groups of two. This will become clearer when looking into the natural orbitals. Even more striking is the behavior of the second orbital’s population, n_1. It increases with g much more rapidly than all the others, and it becomes comparable with n_0 already for modest $g \sim 5$. This scale separation between the pair $n_{0/1}$ and the rest is in sharp contrast to the HO case. It gives a qualitative justification of the two-mode approximation widely used in double-well systems, which assumes that the system can be described in terms of two localized orbitals $w_{\mathrm{L,R}}$ ([94], see also Sec. A.2). To make this more evident, we have plotted the results for a much higher barrier, $h = 10$. Here n_1 ‘jumps’ to a value of order $\frac{1}{2}$ almost instantaneously (for $g \ll 1$), whereas the remaining occupations only catch up only much later (for $g \sim 5$). It is in that regime that the two-mode model works brilliantly.

The reason why fragmentation is facilitated when the central barrier is raised is intuitively clear. The particles’ tendency to separate due to repulsion is usually obstructed by the higher costs of kinetic and potential energy. The potential-energy barrier creates an additional incen-

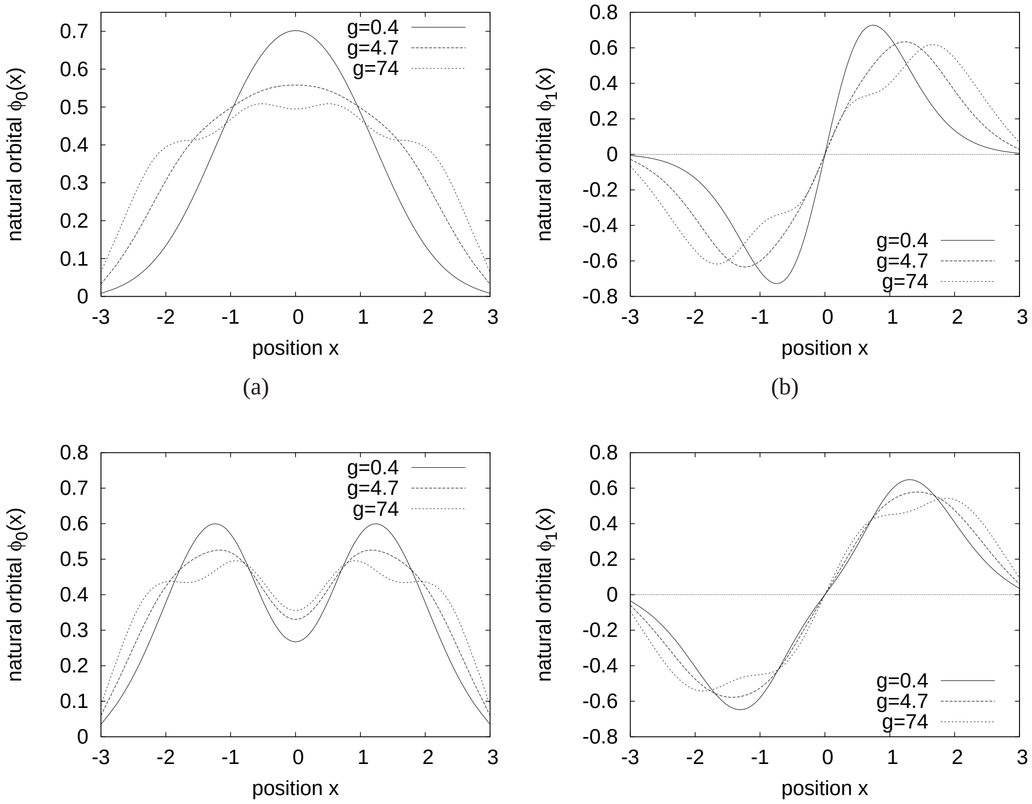

(a) (b)

(c) (d)

Figure 3.16: Natural orbitals ϕ_a for different interaction strengths g ($N = 4$ atoms). *Top row*: Harmonic-trap orbitals ϕ_0 (a) and ϕ_1 (b) . *Bottom*: Double-well orbitals ϕ_0 (c) and ϕ_1 (d).

tive for the bosons to fragment. This has also been argued on more quantitative grounds (see, e.g., [95]). In a naive single-particle picture, the energy gap Δ_h in a double well between anti- and symmetric state, $\phi_{\pm}(x) = \frac{1}{\sqrt{2}}[w(x - x_0) \pm w(x + x_0)]$, vanishes as $h \to \infty$. It is thus far easier for the interaction to bridge that gap for larger barriers, in particular compared to the gap for the harmonic trap, $\Delta_{h=0} = 1$.

Natural orbitals

Even though the natural orbitals (ϕ_a) are not of direct physical importance, they are a valuable tool to gain some insight into the process of fragmentation, as they determine both the spatial density matrix $\rho_1(x, x')$ as well as the momentum density $\tilde{\rho}$, to be discussed in the following subsection. In the uncorrelated case $g = 0$, the system is in a number state $|N, 0, \dots\rangle$ and thus the natural orbitals coincide with the single-particle eigenstates. Since V is a continuous perturbation, the orbitals ϕ_a will be continuously distorted in the course of increasing g. For small enough g—i.e., in the Gross-Pitaevskii regime—that modified ϕ_0 will suffice for an accurate description. Conversely, if correlations are sufficiently influential, many orbitals will contribute to ρ_1, and studying their interplay will illuminate our results on the density matrix and the momentum distribution.

Harmonic trap For the harmonic trap (Figs. 3.16a,b), the initial HO function ϕ_0 is only slightly flattened in the Gross-Pitaevskii regime (cf. $g = 0.4$). The onset of fragmentation not only smears out the lowest orbital, but also admixes an antisymmetric HO-type orbital ϕ_1. In the fermionization limit, it is astonishing that already ϕ_0 exhibits all the features of the fermionized density profile $\rho(x)$, that is, N wiggles mirroring the spatial isolation of the atoms. This is intelligible given that ϕ_0 still has a *dominant* weight, which ought to be contrasted with the philosophy of multi-orbital mean-field schemes [42], where that pattern is produced by N spatially localized orbitals of *equal* population $N_{a<N} = 1$.

Interesting as the orbitals may be in their own right, they also prove helpful in clarifying the diminished coherence found in Sec. 3.4.1. The onset of fragmentation, as for $g = 4.7$, leads to a broadened diagonal profile $\rho_1(x, x)$, but not equally so for the off-diagonal part. That is simply because the ϕ_a have alternate parity $(-1)^a$, and thus the admixture of another orbital leads to $\rho_1(x, -x) = \sum_a (-1)^a n_a |\phi_a(x)|^2$. Hence the fragmentation into different orbitals tends to deplete the off-diagonal as compared to the diagonal density. For $g = 4.7$, this effect is still tiny as $n_1 \sim 0.1$ only, and therefore outweighed by the altogether extended support of ϕ_0. However, as more and more orbitals are mixed, as is the case in the fermionization limit (see $g = 74$), this reduction of coherence attains its full impact. We remark that the faint checkerboard pattern (Fig. 3.13) is still rooted in the dominance of the lowest orbital, $n_0 \sim 1/\sqrt{N}$.

Double well In the case of a central barrier ($h = 5$; see Figs. 3.16c,d), the natural orbitals in the non-interacting limit will again be the single-particle eigenstates, approximately the (anti-)symmetric linear combinations above. For high enough barriers, any of these two should be quasi-degenerate, which shines a light on why their weights n_a tended to come in doublets (Fig. 3.15). In the Gross-Pitaevskii regime ($g = 0.4$), the lowest orbital is only marginally flattened due to interactions. However, the minor admixture of the antisymmetric ϕ_1 leads to a slight reduction of the off-diagonal peaks $\rho_1(x_0, -x_0)$ observed in Fig. 3.13. For $g = 4.7$, fragmentation has set in, not only smearing out the orbitals $\phi_{0/1}$ —and thus the (diagonal) density—but along the way washing out much of the off-diagonal long-range order. As emphasized before, the fermionization pattern tends to be generic for different h, which reflects both in the density matrix as well as in the natural orbitals.

3.4.3 Momentum distribution

The discussion so far focused on rather abstract aspects of the one-body correlations. Yet it can help us cast a light on an experimentally more amenable quantity, the momentum density $\tilde{\rho}(k) = 2\pi\langle k|\rho_1|k\rangle = \sum_a n_a |\tilde{\phi}_a(k)|^2$.

Harmonic trap For this case, the momentum distribution has recently been computed ([44]; see also Ref. [37]). We plot it in Figure 3.17 for comparison. It evolves from a Gaussian $\tilde{\rho}(k)/2\pi = \pi^{-1/2} e^{-k^2}$ at $g = 0$ (with a maximum at $\tilde{\rho}(0) = .35\ldots$) to a slightly sharper peak, here depicted for $g = 0.4$. This squares with the broadened natural orbital ϕ_0 in that regime, as found in Sec. 3.4.2. By virtue of $(\Delta p)^2 = \langle p^2 \rangle$, the narrower momentum distribution leads to a *decrease* of kinetic energy, which has been shown to be a signature of the mean-field regime [44].

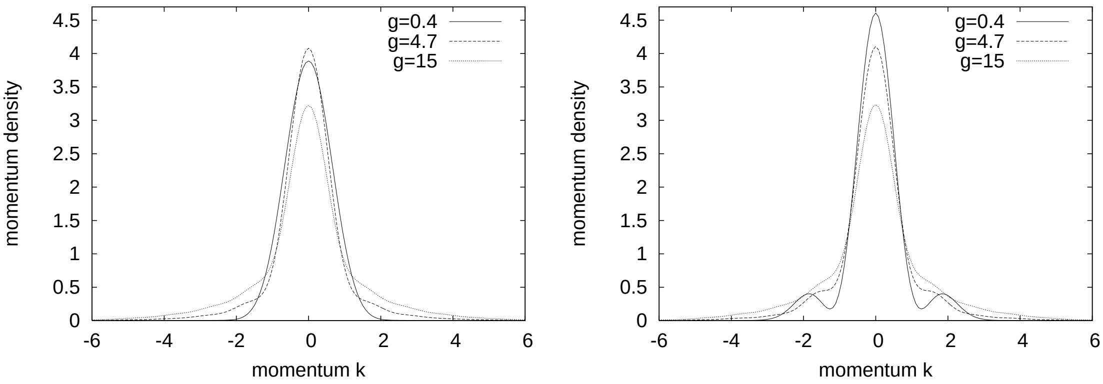

Figure 3.17: Momentum distribution $\tilde{\rho}(k)$ for $N = 5$ bosons in a double-well trap of barrier height h. *Left*: $h = 0$, *right*: $h = 5$. Shown are the interaction strengths $g = 0.4,\ 4.7,\ 15$.

For $g = 4.7$, in the intermediate regime between "condensation" and fermionization, the peak at $k = 0$ is even more pronounced, while $\tilde{\rho}(k)$ has also developed a long-range tail. Both observations are easily accounted for. The $k = 0$ behavior, for one thing, was argued to correspond to the off-diagonal long-range behavior of $\rho_1(x, x')$ in Sec. 3.4.1. This fits in with our observation that the off-diagonal range was indeed extended in that g-regime, as seen in Fig. 3.13. The asymptotics $k \to \infty$ is in turn determined solely by the short-range interaction, which is known to culminate in the k^{-4} tail in the fermionization limit [91].

This latter consequence is in fact confirmed here (see $g = 15$). Moreover, notice that the $k = 0$ peak is bound to diminish. In other words, the momentum spectrum is redistributed toward higher k, in accordance with the reduction of off-diagonal long-range order. This fact stands in marked contrast to the homogeneous system, which in the Tonks-Girardeau limit had an infrared divergence $\tilde{\rho}(k) = O(k^{-1/2})$ [93]. The seeming contradiction is owed to the fact that we deal with a bounded system, which cannot display true long-range order.

Double well The momentum spectrum for a double well ($h = 5$) looks quite different from the start ($g = 0.4$): It exhibits two sidelobes. This can be explained by the symmetric orbital $\phi_0(x) = \frac{1}{\sqrt{2}}[w(x - x_0) + w(x + x_0)]$, which leads to a cosine-type modulation of $\tilde{\rho}$ due to $\tilde{\phi}_0(k) = \sqrt{2}\cos(kx_0)\tilde{\varphi}(k)$. These sidelobes are most distinct for $g = 0$ and tightly localized w.

With increasing repulsion ($g = 4.7$), there are two competing effects. On the one hand, the orbitals are flattened a little, which should result in a slightly sharper momentum distribution. It turns out, though, that the effect of fragmentation outperforms the former one even for tiny interactions: Admixing an anti-symmetric orbital ϕ_1 adds a $\sin(kx_0)$-type modulation, thus washing out the sidelobes as well as the central peak. In other words, the signature of the Gross-Pitaevskii regime in the harmonic trap—the initial sharpening of the $k = 0$ peak—is lost in the case of a sufficiently pronounced double well.

Along the lines of the remarks in the previous paragraph, we mention that the behavior for large interactions g is again universal as far as the k^{-4} tail for $k \to \infty$ is concerned. It also has a reduced peak for zero momentum, in accordance with the reduction of long-range order found in Sec. 3.4.1.

Chapter 4

Excitations

By now, we have obtained a thorough understanding of the ground-state mechanism of the crossover from weak to strongly repulsive interactions. In this chapter, we seek to extend that study to the (low-lying) excited states of trapped few-boson systems. An understanding of these is interesting not only from a fundamental perspective, given the richness of the ground-state crossover. It is also vital for the control of few-boson systems, since in principle the knowledge of the system's excitations both gives access to finite-temperature effects and also builds a bridge to the quantum dynamics studied in Ch. 5.

In Sec. 4.1 we will look into the low-lying spectrum $\sigma(H) = \{E_m\}$, whose corresponding eigenstates Ψ_m will be analyzed in detail (Sec. 4.2). As the spectral properties in the cases of a single and a double well will turn out to be quite different, the question as to how they connect naturally arises. That crossover will be the subject of 4.3.

4.1 Spectrum

In this section, we study the evolution of the lowest eigen-energies $E_m(g)$ as g passes from the non-interacting to the fermionization limit. Figures 4.1,4.3 convey an impression of this transition for $N = 3, 4, 5$ bosons in a harmonic trap ($h = 0$) and in a double well ($h = 5$), respectively. Before dwelling on the details, let us first capture some general features of the spectra.

In the uncorrelated limit, $g \to 0$, the energies are simply given by distributing the atoms over the single-particle levels ϵ_a, starting from $N_{a=0} = N$ (the Bose 'condensate'):

$$E = N \,\mathrm{tr}\,(\rho_1 h) = \sum_a N_a \epsilon_a. \tag{4.1}$$

In particular, $E_0 = N\epsilon_0$; hence the 'chemical potential' $\mu_N \equiv E_0^{(N+1)} - E_0^{(N)} = \epsilon_0$, as usual. Note that Eq. (4.1) implies degeneracy if two single-particle energies are commensurate, i.e., $\sum_a (N_a - \tilde{N}_a)\epsilon_a = 0$ for two $\boldsymbol{n} \neq \tilde{\boldsymbol{n}}$.

In the Tonks-Girardeau limit, on the other hand, the spectrum becomes that of a free fermionic system. Thus one can find some (auxiliary) $\boldsymbol{n}$ with $N_a \in \{0, 1\}$ such that

$$\lim_{g\to\infty} E(g) = \sum_a N_a \epsilon_a. \tag{4.2}$$

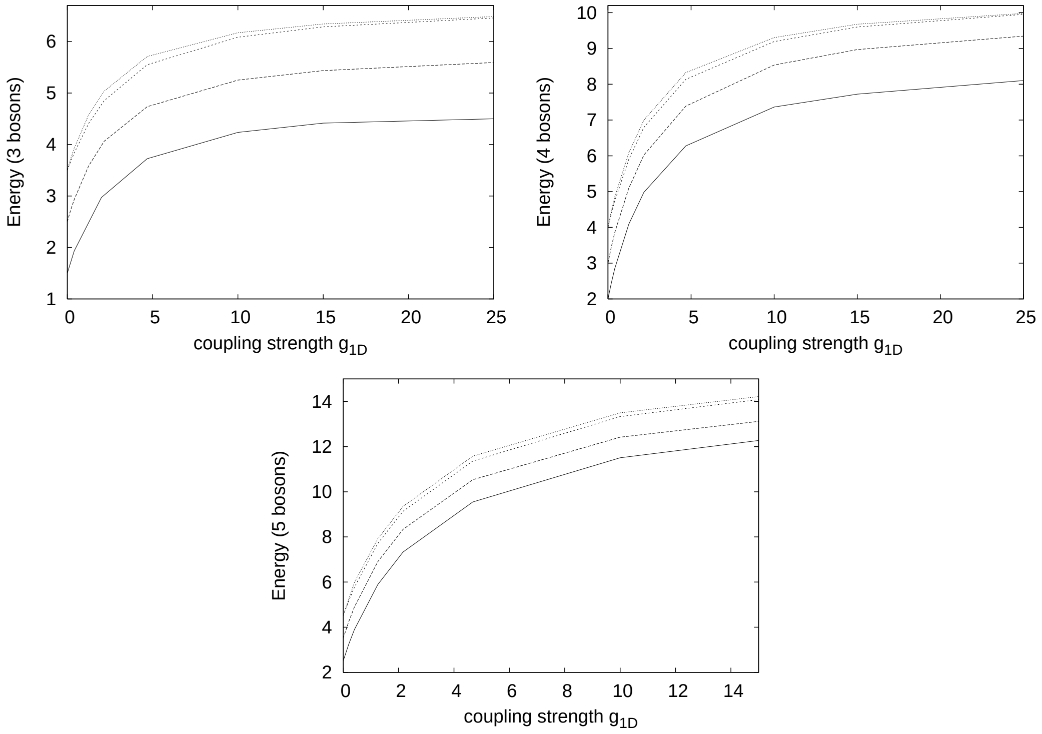

Figure 4.1: Lowest energies E_m in a harmonic trap ($h = 0$) for $N = 3, 4, 5$ bosons. (The lines connect the data points to guide the eye.)

In the ground state, the particles can therefore be thought of as filling the energy ladder up to the Fermi edge, $\epsilon_a < \epsilon_N = \mu_N$. For a harmonic confinement, the chemical potential will thus be $\propto N$, so $E^{(N)} = O(N^2)$.

It should be pointed out that, in the spirit of the Bose-Fermi map, the borderline cases of no and infinite repulsion may be perceived as one and the same (non-interacting) system, their sole difference being the ‘exchange symmetry’ emulating the effect of interactions. Therefore the same type of energy spacings and (quasi-)degeneracies should appear at both ends of the spectrum.

4.1.1 Harmonic trap

For a single well, the one-particle spectrum $\{\epsilon_a = a + \frac{1}{2}\}$ is known analytically, which readily equips us with the full spectrum for both the non-interacting and the fermionization limit. First consider the case $g = 0$. Then $E_0 = N/2$, while all other levels follow with an equal spacing of $\Delta_0 = 1$. Owing to that equidistance, the degree of degeneracy goes up with each step, measured by the average occupation $N\bar{a} \equiv \sum_a N_a a$. Explicitly, while both $\Psi_{m=0,1}$ are non-degenerate, the eigenspace pertaining to $E_2 = E_3 = N/2+2$ is two-dimensional (see Fig. 4.1), etc.

To understand this degeneracy and how it is lifted, let us recall that, in a harmonic trap with homogeneous interactions $V(x_i - x_j)$, the center of mass (CM) $R := \sum_{i=1}^{N} x_i/N$ is separable from the relative motion. Hence one can decompose the Hilbert space $\mathbb{H} = \mathbb{H}_{\mathrm{CM}} \otimes \mathbb{H}_{\mathrm{rel}}$ so as to write

$$\Psi = \phi_{\mathcal{N}} \otimes \psi_{\mathrm{rel}}; \quad E(g) = (\mathcal{N} + \tfrac{1}{2}) + \epsilon_{\mathrm{rel}}(g).$$

This signifies that for every level for the *relative* motion, $\epsilon_{\mathrm{rel}}(g)$, there is a countable set of

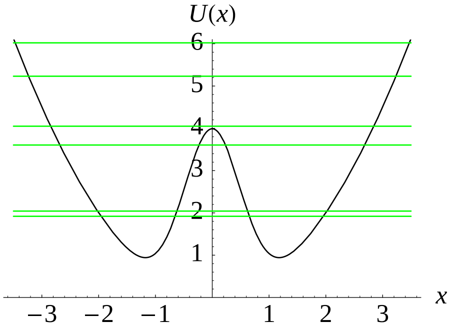

Figure 4.2: Single-particle spectrum $\{\epsilon_a\}$ in a double well with barrier height $h = 5$.

copies shifted upward by $\mathcal{N} = 1, 2, \ldots$. For $g = 0$, ψ_{rel} is a harmonic eigenstate as well, so $\epsilon_{\mathrm{rel}}^{(\nu)}(0) = \nu + \frac{N-1}{2}$ for some ν, and several different combinations of $(\mathcal{N}, \nu)$ may coincide. Switching on $g > 0$, however, breaks that symmetry, leaving $\mathcal{N}$ untouched while pushing each level $\epsilon_{\mathrm{rel}}^{(\nu)}$ upward—which materializes in different slopes

$$\left.\frac{dE}{dg}\right|_0 = \left.\frac{d}{dg}\epsilon_{\mathrm{rel}}\right|_0 .$$

This fact is nicely illustrated on the example of $N = 2$ atoms (Sec. 1.4.3), where

$$\left.\frac{d}{dg}\epsilon_{\mathrm{rel}}^{(\nu)}\right|_0 = \langle\psi_\nu|\delta(r)|\psi_\nu\rangle = |\psi_\nu(0)|^2 .$$

Since $|\psi_\nu(0)|^2$ decreases monotonically with ν, higher excited relative states 'feel' the interaction less. This fits in with our findings in Fig. 4.1: The two states $m = 2, 3$ break up, the lower curve— in light of the reasoning above—pertaining to higher internal excitation.

Apart from that, the spectral pattern does not give an air of being overly intricate but follows the general theme known from the two-atom case. All levels first rise quickly in the linear perturbative regime, but start saturating once they enter the strongly interacting domain ($g \sim 10$). As insinuated, the fermionization limit is known exactly, which endows us with a helpful calibration. Since the limits $g \to 0(\infty)$ can be regarded simply as bosonic (fermionic) counterparts of the same non-interacting system, the two share exactly the same energy scales, $\Delta_0 = 1$. Indeed, building on the ground-state energy $E_0 = \sum_{a<N} \epsilon_a = N^2/2$, all levels again follow in equal steps Δ_0. This fact, effortless as it may come out of the theory, is a strong statement, for it implies that the very interaction that drives some degenerate lines apart at $g = 0$ is also responsible for gluing them together again if it gets sufficiently repulsive. An indication of this effect may actually be observed in Fig. 4.1.

4.1.2 Double well

As opposed to the purely harmonic trap, the (low-lying) *single-particle* spectrum of the double well (Fig. 4.2) is not that simple but rather has a doublet structure (cf. Appendix A). These doublets or *bands* $\beta = 0, 1, \ldots$ correspond to (anti-)symmetric orbitals of the type $\phi_{a_\beta=0,1}^{(\beta)}(x) = \frac{1}{\sqrt{2}}\left[w^{(\beta)}(x + x_0) \pm w^{(\beta)}(x - x_0)\right]$, where $w^{(\beta)}$ is some localized functions, and which are separated in energy only by the tunnel splitting $\epsilon_1^{(\beta)} - \epsilon_0^{(\beta)} = \Delta^{(\beta)} \ll \Delta\epsilon^{(\beta)}$ small compared to the gap to the next band. The non-interacting *many-body* spectrum $\{E_{\boldsymbol{n}} = \sum_a N_a \epsilon_a\}$ will

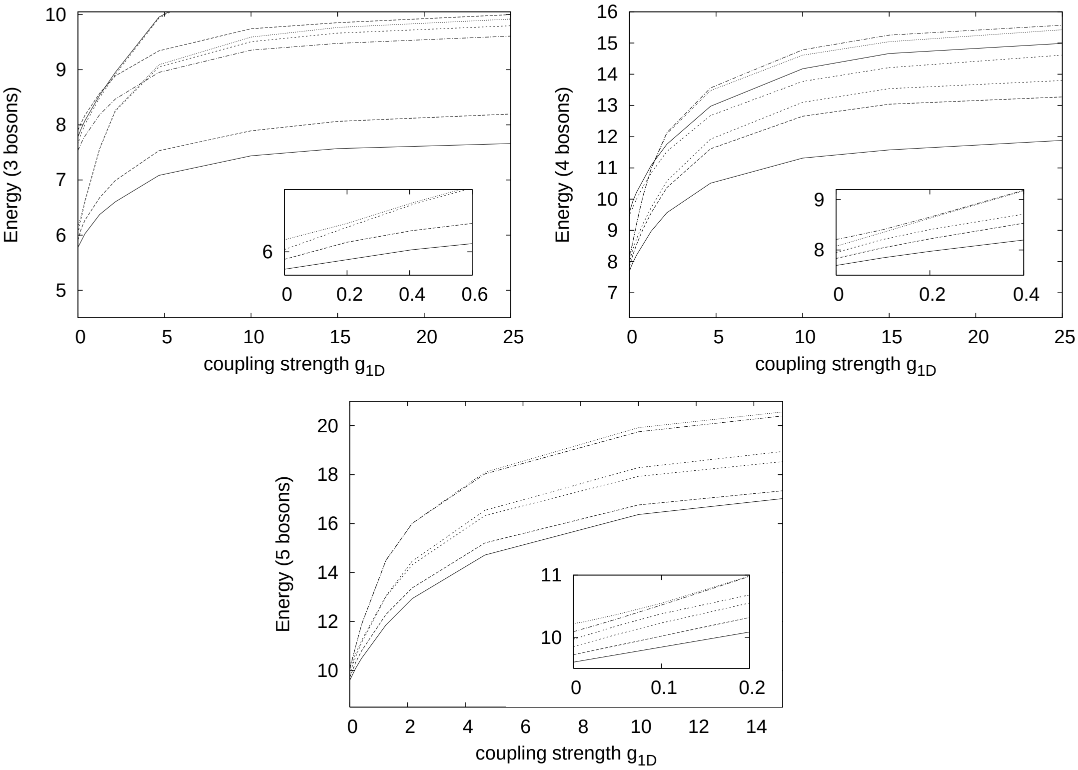

Figure 4.3: Lowest energies E_m in a double well ($h = 5$) for $N = 3, 4, 5$ bosons. *Inset:* Level adhesion for the states $m = N - 1, N$ (counted from below at $g = 0$).

then be composed of a lowest *cluster* of states within the $(N + 1)$-dimensional subspace

$$\mathrm{span}\{|N_0^{(0)}, N_1^{(0)}\rangle \equiv |N - m, m\rangle\}_{m=0,\ldots,N}, \text{ with } E_m = E_0 + m\Delta^{(0)}.$$

The next group—obtained by removing one particle from the lowest levels $\epsilon_{a_0}^{(0)}$—is then shifted upward by $\Delta\epsilon^{(0)}$.

The situation gets slightly more involved in the fermionization limit $g \to \infty$. Here the spectrum is generated by (fictitious) fermionic states $|\boldsymbol{n}\rangle_-$ with $N_{a_\beta}^{(\beta)} \in \{0, 1\}$, so $E_{\boldsymbol{n}} = \sum_{\beta,a_\beta} N_{a_\beta}^{(\beta)}\epsilon_{a_\beta}^{(\beta)}$. Clearly, the ground state is given by filling up the Fermi energy ladder up to the Fermi edge $\epsilon_N = \mu_N$, with the lowest excitations obtained by removing particles from right below the Fermi edge to the next higher band. For *even* N, this yields the following ground state $m = 0$, followed by exactly four single-particle excitations:

State $\lvert\boldsymbol{n}\rangle_-$	m
$\lvert 1_0^{(0)}1_1^{(0)};\ldots;\mathbf{1}_0^{(N/2-1)}\mathbf{1}_1^{(N/2-1)};0_0^{(N/2)}0_1^{(N/2)}\rangle$	0
$\lvert 1_0^{(0)}1_1^{(0)};\ldots;\mathbf{1}_0^{(N/2-1)}0_1^{(N/2-1)};\mathbf{1}_0^{(N/2)}0_1^{(N/2)}\rangle$	1
$\lvert 1_0^{(0)}1_1^{(0)};\ldots;0_0^{(N/2-1)}\mathbf{1}_1^{(N/2-1)};\mathbf{1}_0^{(N/2)}0_1^{(N/2)}\rangle$	2
$\lvert 1_0^{(0)}1_1^{(0)};\ldots;\mathbf{1}_0^{(N/2-1)}0_1^{(N/2-1)};0_0^{(N/2)}\mathbf{1}_1^{(N/2)}\rangle$	3
$\lvert 1_0^{(0)}1_1^{(0)};\ldots;0_0^{(N/2-1)}\mathbf{1}_1^{(N/2-1)};0_0^{(N/2)}\mathbf{1}_1^{(N/2)}\rangle$	4

In Fig. 4.3, this basic structure is visible for $N = 4$, if somewhat blurred by the occurrence of two other, only slightly higher, lines. These are not well separated in energy since, for the higher-band orbitals involved in these excitations, the strict doublet structure gets lost.

For *odd* numbers, there is only one major qualification, which had already been implied in

Sec. 3.2.2: If we now add another particle # $N+1$, this will now go to the previously empty band $\beta = N/2$ above. This way, that band is only half filled, and an *intra-band* excitation will only cost a small energy $\Delta^{(N/2)}$. This explains why the ground state for odd $N = 3, 5$ in Fig. 4.3 is always accompanied by another, very close level.

The two ends of the spectrum in Fig. 4.3 connect in a highly nontrivial way. As can be seen in the insets, the reordering of the spectrum already kicks in for fairly small $g < 1$, when the $N+1$ lowest-band states are still well separated from the next upper cluster, so we can focus on these for the moment. What happens is that the *highest excited* levels virtually glue to one another so as to form doublets, which —even on the zoomed scale of the insets—are practically impossible to resolve. A qualitative explanation for this level adhesion can be obtained by resorting to the lowest-band two-mode model [94] (or Bose-Hubbard model, cf. Appendix A): If the on-site repulsion energy $U^{(0)}$ dominates the tunnel coupling $\Delta^{(0)}$, then the number states $|N_{\mathrm{L}} = \nu, N_{\mathrm{R}} = N - \nu\rangle$ in the left/right-*localized* orbitals $w^{(0)}_{\mathrm{L(R)}} = \frac{1}{\sqrt{2}}\left(\phi^{(0)}_0 \mp \phi^{(0)}_1\right)$ become eigenstates of H, at least to zeroth order in $\Delta^{(0)}$. Of course, the eigenstates should obey parity symmetry, so we really have linear combinations of the type $|\nu, N-\nu\rangle \pm |N-\nu, \nu\rangle$. The on-site repulsion is particularly dominant for the highest excitations, $|N, 0\rangle \pm |0, N\rangle$, which correspond to the sharp doublets observed in the insets. By contrast, the ground state will have minimum on-site interaction (e.g., of the type $|N/2, N/2\rangle$ for even N) and thus will have a non-negligible share of kinetic energy.[1]

This lowest-band picture ceases to be qualitatively correct as soon as crossings with states emerging from the next cluster come into play, as, e.g., for $N = 3$ at $g \approx 3$. As a consequence, not only are the quasi-degenerate doublets broken up, but also a dramatic rearrangement of the level structure toward the fermionization limit takes place.

4.2 Excited states

As yet, we have looked into the spectrum and its evolution from the weakly to the strongly interacting regime. We now aspire to get a deeper insight into the underlying states $\Psi_{m\geq 1}$, which may be also beneficial for studying the dynamics in future applications.

Generally speaking, the non-interacting limit is described in terms of number states $|\boldsymbol{n}\rangle$ in the respective one-particle basis. Owing to the asymptotically harmonic confinement, we thus have an overall Gaussian profile $\rho(x) \propto \exp\left(-x^2\right)$, which is modulated by the central barrier as well as the degree of excitation. At least for the low-lying states, the length scale is therefore about that of the harmonic confinement, $a_{\|} = 1$. Being single-particle states, they are essentially devoid of two-body correlations, reflected in $\rho_2 = \frac{1}{2}(1 + P_{12})\rho_1 \otimes \rho_1$ (with the permutation operator P_{12}).

When interactions are added, some extra interaction energy $\frac{N(N-1)}{2}\mathrm{tr}\,(V\rho_2)$ must be paid. Hence, the system will respond by depleting the correlation diagonal $\rho_2(x_1, x_2 = x_1)$, roughly speaking. As $g \to \infty$, this culminates in the system's fermionization. In particular, the density profile $\rho = \sum_a |\phi_a|^2$ becomes broader, with a length scale of order $\sqrt{2N}$ [87], while the strongly correlated nature is captured in the fermionic two-body density $\rho_2(x_1, x_2) = \left(\rho(x_1)\rho(x_2) - |\rho_1(x_1, x_2)|^2\right)/2$, which vanishes at points of collision.

---

[1] For an extension of this mechanism to a two-band picture, see [96].

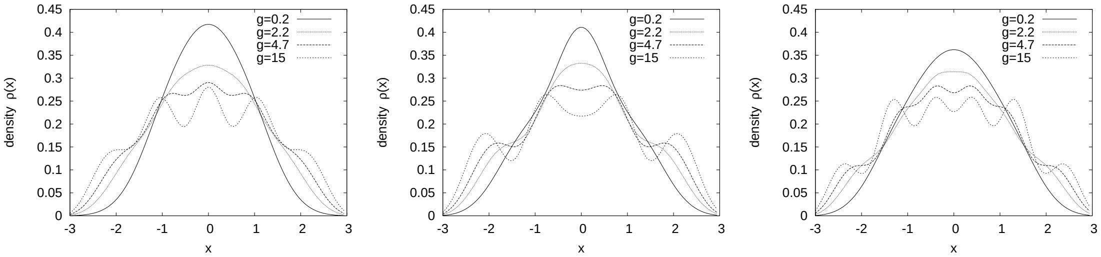

Figure 4.4: Density profiles of $N = 4$ bosons in a harmonic trap ($h = 0$) for the excited states $m = 1, 2, 3$ (from left to right).

4.2.1 Harmonic trap

A look at the one-body density $\rho(x)$, shown in Fig. 4.4 for different states $m = 1, \ldots, 3$, suggests that essentially the same mechanisms as for the ground state are at work. The noninteracting density profiles have a Gaussian envelope. This may be seen in the plot for $g = 0.2$, the somewhat peculiar shape for the states $m = 2, 3$ stemming from the fact that, at $g = 0$, the affiliated number states $|N - 1, 0, 1\rangle$ and $|N - 2, 2, 0\rangle$ are degenerate, which is why the perturbation $H_\mathrm{I} = \sum_{i<j} V(x_i - x_j)$ selects linear combinations that are CM and relative-motion eigenstates. This is also illustrated in the two-body density ρ_2 (Fig. 4.5).

Upon increasing g, the density is being flattened, reflecting the atoms' repelling one another. Eventually, a fermionized state is reached, featuring characteristic humps in the density. As in the ground-state case, these signify *localization* in the sense that it is more likely to find one atom at discrete spots x_i. However, here the fermionization pattern eludes an obvious interpretation, since these are excited rather than equilibrium states. In particular, now the number of humps need not equal N, as can be seen for $m = 1$.

A look behind the scene is offered by the two-body density ρ_2 displayed in Fig. 4.5, which recovers the density profile $\rho = \int dx_2 \rho_2(\cdot, x_2)$ by averaging over the second atom. It illustrates nicely how the interaction imprints a correlation hole at $\{x_1 = x_2\}$ at mediate $g = 2.2$, which relates to the washed-out profile in Fig. 4.4. A complex fragmentation of the (x_1, x_2) plane can be witnessed as we go to larger g, which is different from the very obvious checkerboard pattern of the ground state encountered in Sec. 3.2. The latter one provided a simple interpretation, namely that the atoms are evenly distributed at discrete positions over the trap (up to a Gaussian density modulation), but with zero probability of finding two atoms at the same spot. Here the atoms are apparently more localized in the center. On top of that, if one atom is fixed at some x_1, one cannot unconditionally ascribe definite positions for the $N - 1$ remaining particles as before.

4.2.2 Double well

Figure 4.6 summarizes the evolution of the lowest excited states' densities for $N = 4$. For large but finite barrier heights, the lowest excitations at $g = 0$ will be formed by the two-mode vectors $|N_0^{(0)}, N - N_0^{(0)}\rangle$. All of these will exhibit similar density profiles since $\rho(x)$ only differs significantly near the trap's center; specifically $\rho(0) = n_0 \left|\phi_0(0)\right|^2$. This quasi-noninteracting behavior can be verified for $g = 0.05$. As the interaction is turned on, $g = 0.2$, we argued in Sec. 4.1.2 that the higher states (here: $m = 3, 4$) tend to form doublets of left-right localized states as a consequence of on-site repulsion. While this barely affects the density

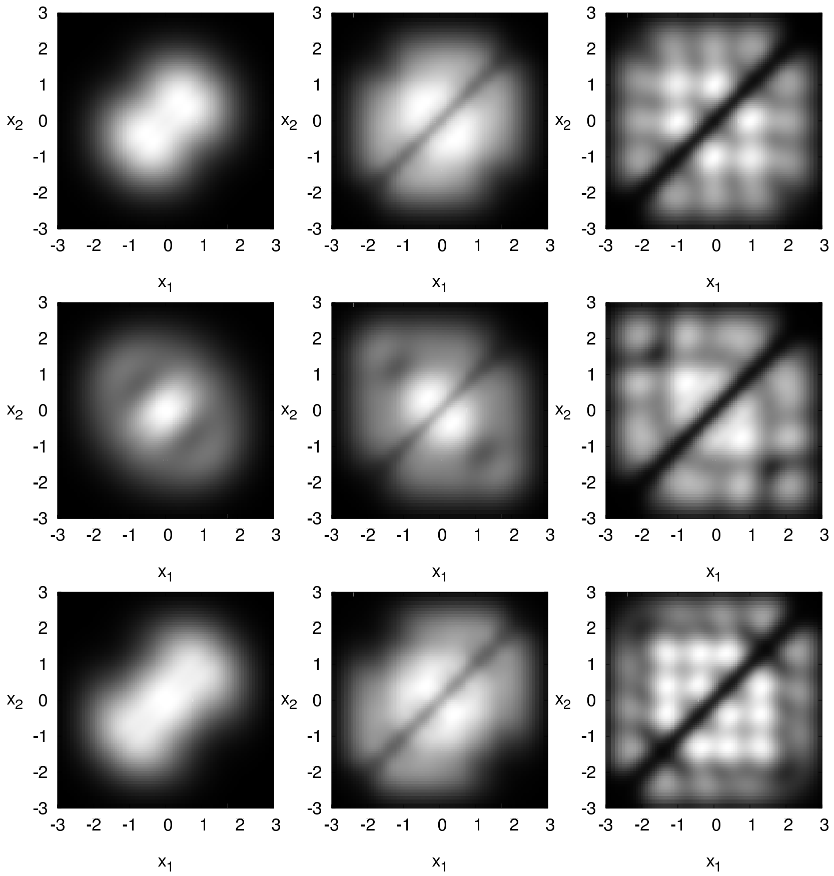

Figure 4.5: Two-particle density $\rho_2(x_1, x_2)$ for $N = 4$ bosons in a harmonic trap. *From top to bottom*: excited state $m = 1, \ldots, 3$; shown are the interaction strengths $g = 0.2,\ 2.2,\ 15$ from left to right.

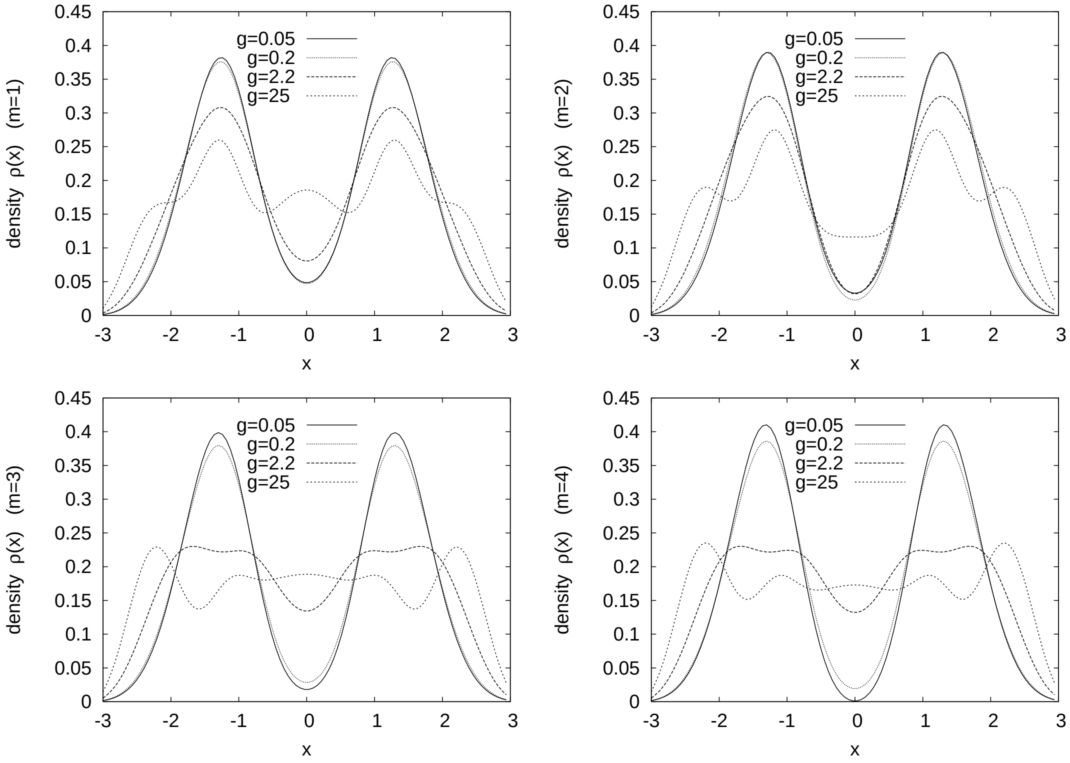

Figure 4.6: Density profiles of $N = 4$ bosons in a double well ($h = 5$) for the lowest excited states $m = 1, \ldots, 4$.

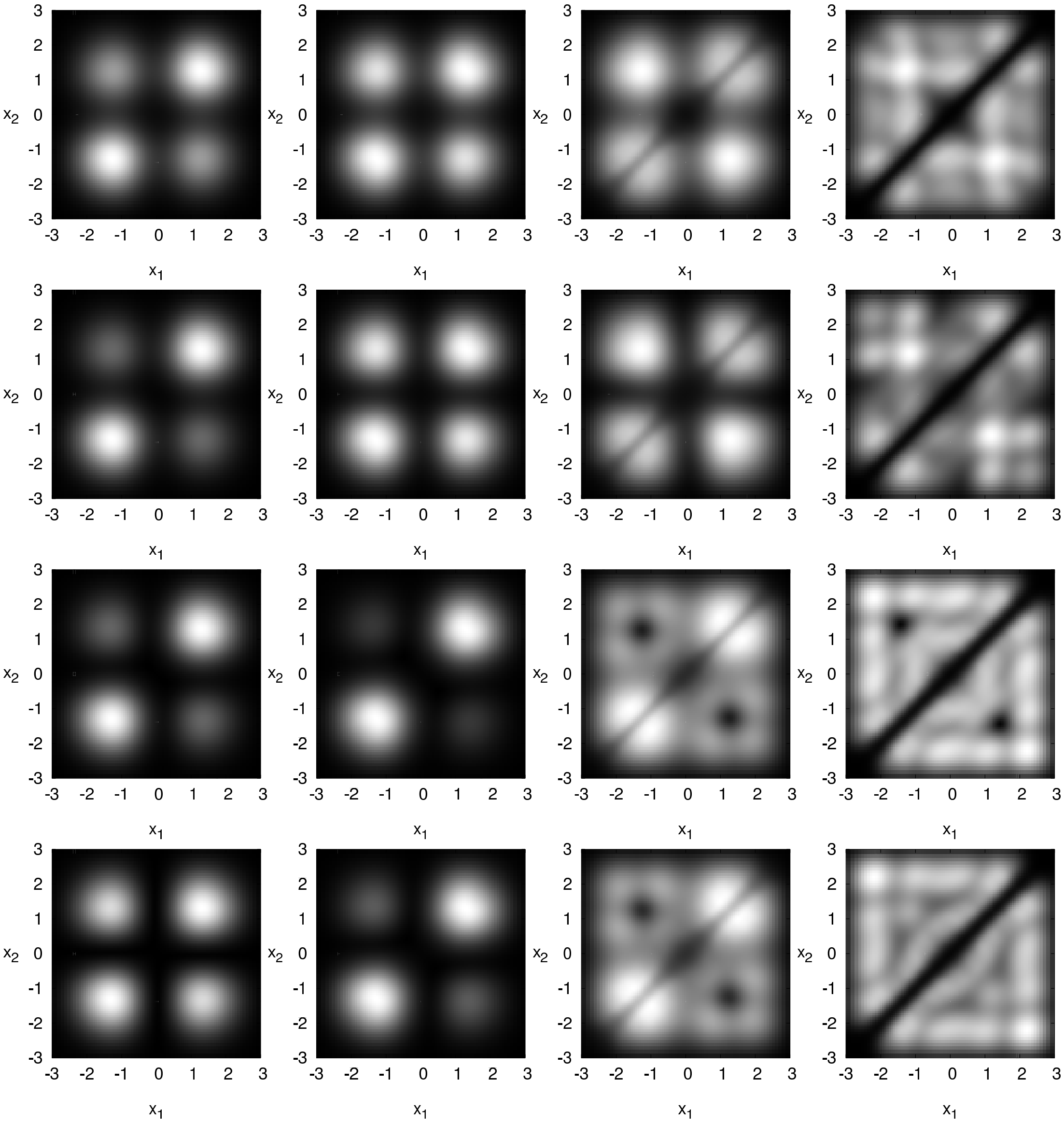

Figure 4.7: Two-particle density $\rho_2(x_1, x_2)$ for $N = 4$ bosons in a double-well trap $(h = 5)$. *From top to bottom*: excited state $m = 1, \ldots$,4; shown are the interaction strengths $g = 0.05,\ 0.2,\ 2.2,\ 25$ from left to right.

profiles in Fig. 4.6, the change in the two-body density $\rho_2(x_1, x_2)$ is hard to ignore (Fig. 4.7): The states $m = 3, 4$ become virtually indistinguishable and have strong *diagonal* peaks at $x_1 = x_2$, supporting our hypothesis that these could be thought of as superpositions of *localized* states $|4_{\rm L}, 0_{\rm R}\rangle \pm |0_{\rm L}, 4_{\rm R}\rangle$. This effect is less pronounced for the lower-lying states $m = 1, 2$.

For stronger repulsion, $g = 2.2$, Fig. 4.7 nicely illustrates the characteristic correlation hole imprinted in ρ_2, signaling the crossover to fermionization. On the one-body level (Fig. 4.6), this is accompanied by a broadening of the density profiles, which even acquire some wiggly structure. This saturates as the fermionization limit is approached ($g = 25$), where again a trademark checkerboard pattern can be witnessed. In that regime, the diagonal $\rho_2(x_1, x_2 = x_1)$ is fully depleted, which comes along with the break-up of the quasi-degenerate level pairs observed for weaker repulsion.

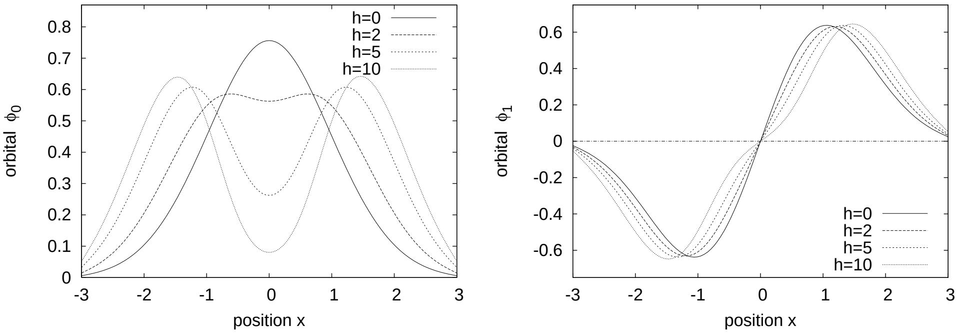

Figure 4.8: Evolution of the natural orbitals ϕ_a as $h \to \infty$ for the case $N = 3$ ($g = 0.2$). *Top*: The first symmetric orbital ϕ_0 is notched at $x = 0$. *Bottom*: The antisymmetric one (ϕ_1) is barely altered.

4.3 Crossover from single to double well

We have come a long way studying in depth the spectral properties of a single and a double well. As opposed to the ground-state case, the link between the two is far from obvious. In the harmonic trap, the fermionization transition was fairly tame, while in the presence of a fixed barrier $h = 5$, there not only seemed to be a strikingly different level structure to begin with, but also the onset of a zoo of crossings and quasi-degeneracies. On that score, it would be desirable to get an understanding of the crossover from a single to a double well. To this end, we will again borrow some inspiration from the simple model of a point-split trap $h\delta(x)$ (see [33] and Appendix A.1).

First consider the borderline case $g = 0$. Then the one-particle occupations $\boldsymbol{n}$ are conserved for any parameter h, so we can assume number states $|\boldsymbol{n}\rangle$ as eigenstates (up to degeneracies). Let us start with the harmonic trap ($h = 0$), where the spectrum is arranged in steps of $\Delta_{h=0} = 1$ according to $E_{\boldsymbol{n}} = \sum_a N_a(a + \frac{1}{2})$ and the particles are distributed over the oscillator orbitals ϕ_a. Now let us switch on a central barrier $h > 0$ peaked at $x = 0$. Then each even orbital $a \in 2\mathbb{N}_0$ will be notched at $x = 0$, until its density $|\phi_a|^2$ will equal that of the next, odd orbital ϕ_{a+1}. Figure 4.8 gives an illustration of this by displaying the natural orbitals $\phi_{0/1}$ at $g = 0.2$. Along that line, the energies will evolve continuously from ϵ_a to $\epsilon_{a+1} = \epsilon_a + 1$. On the other hand, granted that the barrier is supported exclusively at $x = 0$, the odd orbitals themselves will remain completely untouched. Hence, in the limit $h \to \infty$, we would end up with a doubly degenerate *single-particle* spectrum (or, more realistically, a level gap $\Delta_h \ll 1$), which readily translates to a shift of $\Delta E_{\boldsymbol{n}} = \sum_{a \in 2\mathbb{N}} N_a \times 1 =: N_{\text{even}}$ with respect to $h = 0$, depending on how many even orbitals were populated to begin with. Altogether, as the barrier h is run up, the spectrum $\{N/2, N/2 + 1, \dots\}$ at $h = 0$ is expected to transform into one with a lowest cluster of $1 + N$ (quasi-)degenerate levels pertaining to $\{|N_0, N - N_0\rangle\}$ at energies $E \sim 3N/2$, followed by another one at $E \sim 3N/2 + 2$.

A realistic reasoning should take into account the finite barrier width ($w = 0.5$), but the above toy model provides us with a rough picture to understand the crossover computed for $g = 0.2$ in Fig. 4.9(a). Note that the sketched metamorphosis inevitably brings about crossings between different levels as $h \to \infty$ since, for instance, $|0, N\rangle$ is barely altered while $|N_0, 0, N - N_0\rangle$ is shifted by about $\Delta E \sim N$.

The above approach may be readily extended to the fermionization limit. All we need to do is construct auxiliary fermion states $\{|\boldsymbol{n}\rangle_- \mid N_a = 0, 1\}$ and apply the same machinery.

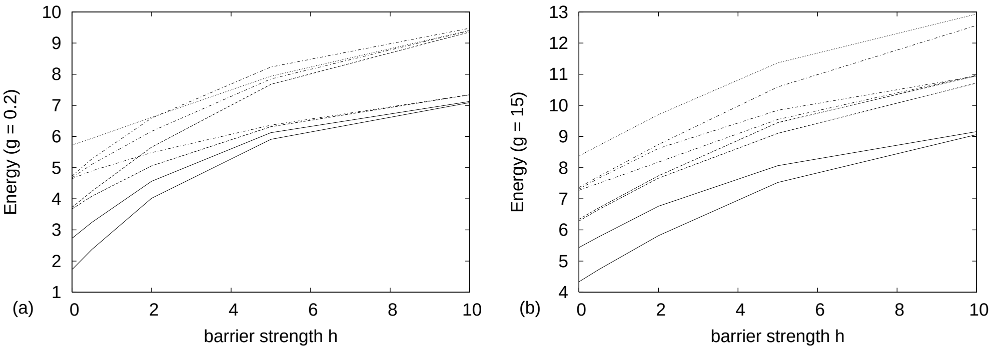

Figure 4.9: Crossover of the lowest energies $E_m(h)$ with varying barrier strength h for $N = 3$ bosons at interaction strengths $g = 0.2$ (a); $g = 15$ (b). (The line styles are assigned so as to distinguish the different level groups at $h = 0$.)

However, a look at Fig. 4.9(b) ($g = 15$) makes clear that the rearrangement of the levels is not as wild as as in the non-interacting case. That is simply because the 'fermions' can only occupy a level once; hence at $h \to \infty$ the lowest group is made up of one or two states only (for even/odd numbers, respectively), followed by a cluster of four levels regardless of the atom number. [2]

For intermediate values of g, in turn, one cannot use the same line of argument since there is no simple single-particle description, and $\boldsymbol{n}$ is no longer a good set of quantum numbers. Still, the knowledge of the limiting cases highlighted above gives a guideline for the crossover. Generally speaking, changing h for any g will affect the energy via

$$\frac{d}{dh}E = N\mathrm{tr}\left[\rho_1\delta_w(x)\right] = N\bar{\rho}(0),$$

i.e, the coarse-grained density $\bar{\rho} \equiv \rho * \delta_w$ about the center will be reduced so as to minimize the energy costs. This will determine the fate of each state when changing over from a single to a double well, thus completing our picture of the lowest excitations in double-well traps.

---

[2] You might notice that the second band emerging as $h \to \infty$ is not perfectly bunched at $E(h = 10) \simeq 11$, but really has a runaway at $E(h = 10) \simeq 10.7$. This can be traced back to the inclusion of a higher orbital ϕ_4 in the fermionic state: in such higher regions, the spectrum ceases to be perfectly doublet-like, foiling our previous considerations.

Chapter 5

Tunneling dynamics

Thus far, we have gained an understanding of the fermionization crossover for the stationary states. It is natural to ask how this affects the quantum dynamics of few-boson systems. Specifically, the double-well potential we have focused on so far is a paradigm model for one of the most fundamental quantum effects – tunneling. Using ultracold bosonic atoms, it has become possible to study this system at an unprecedented level of precision and control. This has led, e.g., to the observation of *Josephson oscillations* of Bose-Einstein condensates [94, 97, 98] and the complementary *nonlinear self-trapping* effect [97, 99, 100]. In the case of Josephson oscillations, the atoms—initially prepared mostly in one well—simply tunnel back and forth between two potential wells in analogy to a current in a Josephson junction. However, above a critical interaction strength, the atoms essentially remain trapped in that well for the experimental lifetime even though they repel each other. While these effects have been observed for macroscopic coherent matter waves, the recently observed stability of repulsively bound atom pairs moving in a lattice [101], whose first- and second-order tunneling dynamics have later been evidenced directly [102], indicates that akin situations also exist on the *few-body* level.

All of these effects are confined to the regime of relatively weak interactions, where the dynamics can be understood qualitatively by means of a very simple two-mode model. Here we want to investigate the case where a few atoms are loaded into one well and explore how the tunneling dynamics changes as we vary the interaction strength from zero up to the fermionization limit. This is done for a symmetric double well in Sec. 5.1, first for the case of two atoms (Secs. 5.1.1–5.1.3), where the extension to higher atom numbers is discussed in Sec. 5.1.4. In Sec. 5.2, we illuminate the effect of tilting the double well, which makes it possible to tune specific tunnel resonances.

5.1 Symmetric double well

In this section, we investigate the tunneling dynamics in a symmetric well as we pass from uncorrelated tunneling ($g = 0$) to tunneling in the presence of correlations and finally to the fermionization limit ($g \to \infty$). The preparation of the initial state $\Psi(0)$ with a population imbalance—in our case, such that almost all atoms reside in the *right* well only—is sketched in Fig. 5.1. We make that site energetically favorable by adding a linear external potential, $U(x) - d \cdot x$, (with sufficiently large $d \sim 0.1 - 1$, depending on N and g) and let the system relax to its

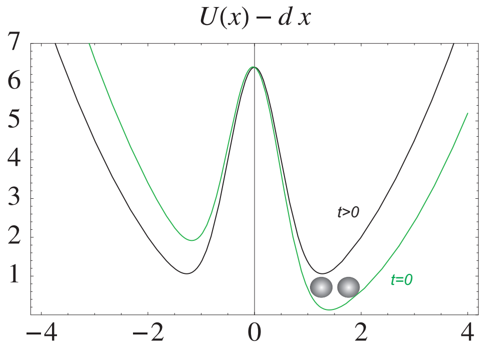

Figure 5.1: Sketch of the setup: At $t = 0$, atoms are prepared in the ground state of the double well $U(x) - d \cdot x$ tilted to the right (green). The asymmetry is then ramped down nonadiabatically, $d(t) \to 0$, thus triggering the tunnel dynamics in the symmetric double well.

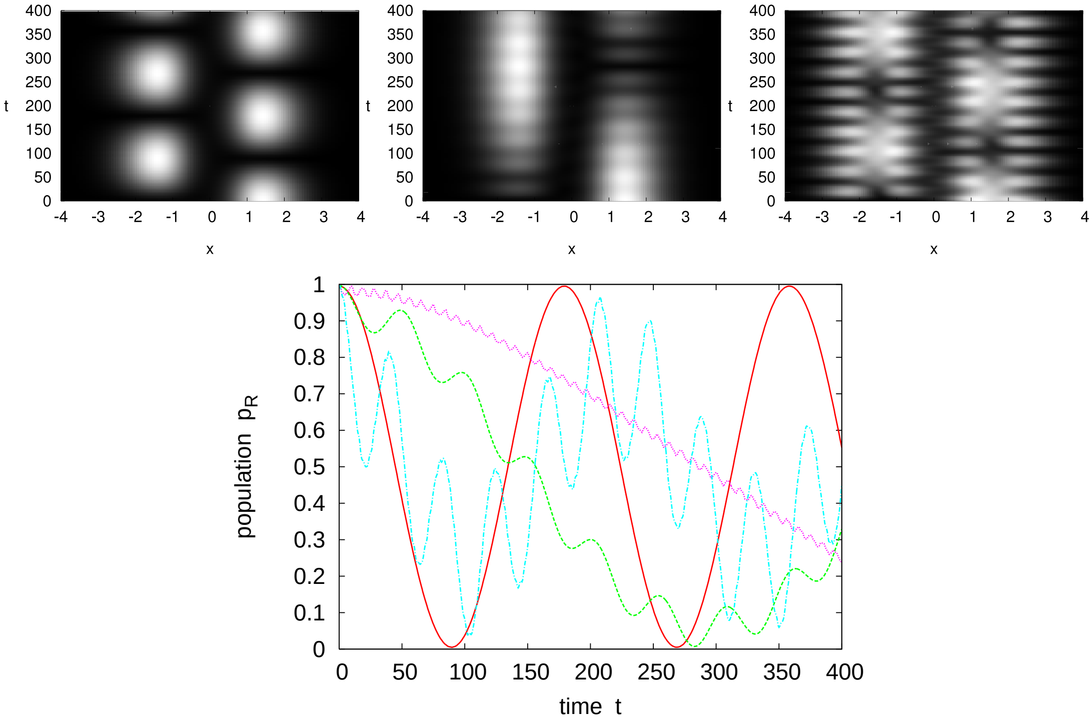

Figure 5.2: Two-atom dynamics in a double well.
Top: Density evolution $\rho(x;t)$ for $g = 0$, 0.2, and $g = 25$ (*from left to right*)
Bottom: Population of the right-hand well over time, $p_{\mathrm{R}}(t)$, for $g = 0$ (—), $g = 0.2$ (- - -), $g = 4.7$ (· · ·), and $g = 25$ (— · —).

ground state $\Psi_0^{(d>0)}$. The asymmetry d will be ramped down to $d(t) \to 0$ nonadiabatically (we typically choose a ramp time $\tau \sim 1$). By extension, it is possible to take any final asymmetry $\lim_{t\to\infty} d(t) \neq 0$, which allows us to look at the case where one well is energetically offset (Sec. 5.2). It is natural to first look at the conceptually clearest situation where $N = 2$ atoms initially reside in the right-hand well (Sec. 5.1.1), with an eye toward the link between tunneling times and the few-body spectrum (Sec. 5.1.2) as well as the role of two-body correlations (Sec. 5.1.3). With this insight, we tackle the more complicated dynamics of $N = 3, 4, \ldots$ atoms in Sec. 5.1.4.

5.1.1 From uncorrelated to pair tunneling

At $g = 0$, the atoms simply *Rabi*-oscillate back and forth between both wells (Fig. 5.2, top). This can be monitored by counting the percentage of atoms in the right well,

$$p_{\mathrm{R}}(t) = \langle \Theta(x) \rangle_{\Psi(t)} = \int_0^\infty \rho(x;t)dx \tag{5.1}$$

(ρ being the one-body density) or, correspondingly, the population imbalance $\delta = p_{\mathrm{R}} - p_{\mathrm{L}} = 2p_{\mathrm{R}} - 1$. Figure 5.2 (*bottom*) confirms that p_{R} harmonically oscillates between 1 and 0.

If we switch on repulsive interactions, cf. $g = 0.2$, one might naively expect the tunneling to be enhanced. By contrast, Fig. 5.2 reveals that, for short times, there is just a minute oscillation, while complete population transfer occurs on a much longer time scale ($T/2 \sim 300$). A look at the population dynamics confirms that the tunneling oscillations have become a two-mode process: There is a fast (small-amplitude) oscillation which modulates a much slower one in which the atoms eventually tunnel completely ($p_{\mathrm{R}} \approx 0$). In case g is increased further to $g = 1.3$ (not displayed here), we have found that the tunneling period becomes as large as 2×10^3. What remains is a very fast oscillation with only a minute amplitude – this may be understood as the few-body analog of quantum self-trapping, as will be discussed in Sec. 5.1.2. As we go over to much stronger couplings (see $g = 4.7$), we find that the time evolution becomes more complex, even though this is barely captured in the reduced quantity p_{R} (Fig. 5.2, *bottom*).

Remarkably, near the fermionization limit (see $g = 25$) again a simple picture emerges: The tunneling, whose period roughly equals that of the Rabi oscillations, is superimposed by a faster, large-amplitude motion. This states that the strongly repulsive atoms coherently tunnel back and forth as a *fragmented pair* almost like a single particle.

5.1.2 Spectral analysis

To gain a better understanding of the very different time scales involved throughout the crossover, let us analyze the evolution of the few-body spectrum $\{E_m(g)\}$ as g is varied (Fig. 5.3a). The discussion will lean upon that in Ch. 4; however, we will keep it self-contained.

In the noninteracting case, the low-lying spectrum of $N = 2$ atoms is given by distributing all atoms over the symmetric and antisymmetric single-particle orbital of the lowest doublet $\epsilon_{0/1}^{(0)}$ (illustrated in Fig. 5.3b). This yields the $N + 1$ energies

$$\{E_m = E_0 + m\Delta^{(0)} \mid m = 0, \ldots, N\},$$

where $\Delta^{(0)} = \epsilon_1^{(0)} - \epsilon_0^{(0)}$ is the energy gap between these two orbitals or, in other words, the width of the lowest *band*. Assuming that for sufficiently small g still only $N + 1 = 3$ levels are populated in $\Psi(t) = \sum_m e^{-iE_m t} c_m \Psi_m$, then the imbalance $\delta(t) \equiv \langle \Theta(x) - \Theta(-x) \rangle_{\Psi(t)}$ (and likewise p_{R}) can easily be computed to be

$$\delta(t) = \delta^{(01)} \cos(\omega_{01} t) + \delta^{(12)} \cos(\omega_{12} t), \tag{5.2}$$

where $\omega_{mn} = E_m - E_n$ and $\delta^{(mn)} = 4\langle \Psi_m | \Theta(x) | \Psi_n \rangle c_m c_n$ is determined by the participating

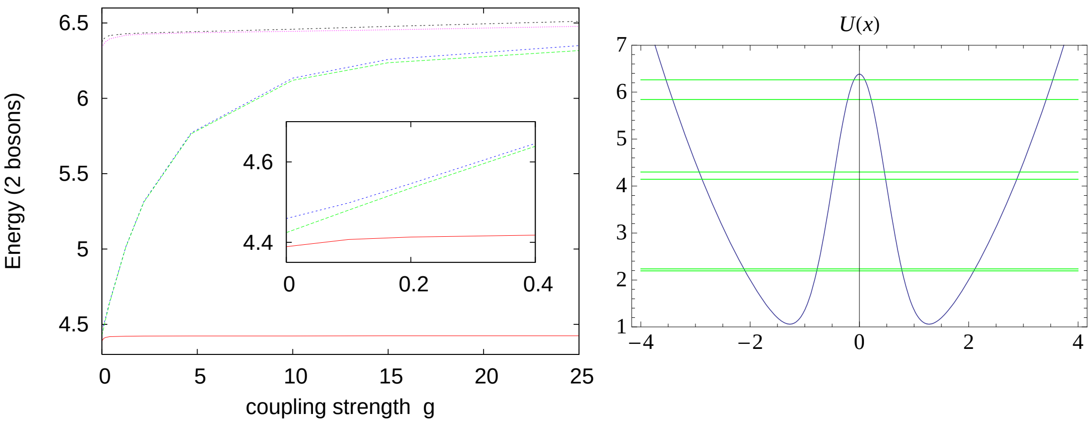

(a) (b)

Figure 5.3: (a) Two-particle spectrum as a function of the interaction strength g. *Inset*: Doublet formation with increasing g. (b) Corresponding single-particle spectrum of a double well with barrier height $h = 8$.

many-body eigenstates. Note that the term $(mn) = (02)$ vanishes since, by antisymmetry, only opposite-parity states are coupled. At $g = 0$, due to the levels' equidistance, only a single mode with Rabi frequency $\omega_{01} = \omega_{12} = \Delta^{(0)}$ contributes. For *very small* interaction energies compared to $\Delta^{(0)}$, the equidistance is slightly lifted, so that the Rabi oscillations are modulated by a tiny beat frequency $\omega_{01} - \omega_{12}$ (not shown). However, as the interaction is increased further, the two upper lines $E_{1,2}$ virtually glue to one another to form a doublet, whereas the gap to E_0 increases (Fig. 5.3a, inset).[1]

With these considerations on the weak-interaction behavior in mind, Eq. (5.2) asserts that for times $t \ll T_{12} \equiv 2\pi/\omega_{12}$, we only see an oscillation with period $T_{01} \ll T_{12}$, offset by $\delta^{(12)}$, which on a longer timescale modulates the *slow* tunneling of period T_{12}. For small initial imbalances, we have $\left|\delta^{(01)}/\delta^{(12)}\right| \propto |c_0/c_2| \gg 1$; so for short times we would observe the few-body analog of Josephson tunneling. In our case of an almost complete imbalance, in turn, $|\delta^{(12)}|$ dominates, which ultimately should correspond to *self-trapping*, viz., extremely long tunneling times. These considerations convey a simple yet *ab initio* picture for the few-body counterpart of the crossover from Rabi oscillations to self-trapping.

It is obvious that the two-frequency description above breaks down as the gap to higher-lying states melts (see Fig. 5.3a), even though for two atoms no actual crossings with higher states occur, as opposed to $N \geq 3$ (Sec. 4.1). The consequences for the spectrum are twofold: (i) the quasi-degenerate doublet will break up again, and (ii) states emerging from higher bands will be admixed. For the imbalance dynamics, (i) implies that the "self-trapping" scenario will give way to much shorter tunnel periods again, while (ii) signifies a richer multi-band dynamics. This most clearly manifests toward fermionization, $g = 25$.

---

[1] This level adhesion, already calculated for $N = 3, \ldots, 5$ in Sec. 4.1, may be understood from a naive lowest-band two-mode model (see [94] for details): As g is increased, the on-site interaction energy eventually overwhelms the tunneling energy $\Delta^{(0)}$, and the eigenstates evolve from number states $|N_0^{(0)}, N_1^{(0)}\rangle$ in the *delocalized* (anti-)symmetric orbitals $\phi_{a=0,1}^{(0)}$ into superpositions of number states $|N_{\mathrm{L}}, N_{\mathrm{R}}\rangle$ in the left/right-*localized* orbitals $w_{\mathrm{L(R)}}^{(0)} = \frac{1}{\sqrt{2}}\left(\phi_0^{(0)} \mp \phi_1^{(0)}\right)$. It goes without saying that any two such degenerate number states $|\nu, N-\nu\rangle \neq |N-\nu, \nu\rangle$ violate parity symmetry and only serve to form a two-dimensional energy subspace, which for nonzero $\Delta^{(0)}$ corresponds to the doublets in Fig. 5.3(a).

In the limit $g \to \infty$, the system also becomes integrable again via the Bose-Fermi mapping (Sec. 1.4.1). As an idealization, assume that at $t = 0$ we put two (noninteracting) fermions in the *right-hand* well, where they would occupy the lowest two orbitals, namely $w_{\mathrm{R}}^{(\beta)}$, $\beta = 0, 1$. Expressing this (fermionic) number state $\Psi(0) = \left(\prod_{\beta=0,1} C_{\mathrm{R}}^{(\beta)}\right)^{\dagger} |0\rangle$ through the single-particle eigenstates $|\boldsymbol{n} = (N_{a_\beta}^{(\beta)})\rangle_{-}$ via the annihilation operator $C_{\mathrm{R}}^{(\beta)} = \frac{1}{\sqrt{2}}(c_0^{(\beta)} + c_1^{(\beta)})$ leads to

$$\Psi(t=0) = \frac{1}{2} \sum_{a_0, a_1 \in \{0,1\}} |1_{a_0}^{(0)}; 1_{a_1}^{(1)}\rangle_{-},$$

where $1_{a_\beta}^{(\beta)}$ denotes occupation of the symmetric ($a_\beta = 0$) or antisymmetric ($a_\beta = 1$) orbital in band β. The frequencies $\omega_{\boldsymbol{n},\boldsymbol{n}'} = E_{\boldsymbol{n}} - E_{\boldsymbol{n}'}$ contributing to $\Psi(t)$ follow in a straightforward fashion:

$$\omega_{\boldsymbol{n},\boldsymbol{n}'} = \sum_{\beta, a_\beta} \epsilon_{a_\beta}^{(\beta)} \left(N_{a_\beta}^{(\beta)} - N_{a_\beta}^{\prime(\beta)}\right) = \sum_{\beta} \Delta^{(\beta)} \underbrace{\left(N_1^{(\beta)} - N_1^{\prime(\beta)}\right)}_{=0,\pm 1}. \tag{5.3}$$

Moreover, let us focus on the imbalance dynamics. Since $\delta^{(\boldsymbol{n}\boldsymbol{n}')} \neq 0$ only for opposite-parity states $\boldsymbol{n}, \boldsymbol{n}'$, the sum must contain only an *odd* number of terms. For the special case of two atoms, we obtain the simple result that the only participating frequencies are $\Delta^{(0)}$ (the lowest-band Rabi frequency, corresponding to the longer tunneling period) and $\Delta^{(1)}$ (the larger tunnel splitting of the first excited band). This links the strongly interacting dynamics to the noninteracting Rabi oscillations.

5.1.3 Role of correlations

In order to unveil the physical content behind the tunneling dynamics, let us now investigate the two-body correlations. Noninteracting bosons simply tunnel independently, as is reflected in the two-body density $\rho_2(x_1, x_2)$. As a consequence, if both atoms start out in one well, then in the *equilibrium point* of the oscillation (where $p_{\mathrm{L,R}}(t_*) \overset{!}{=} \frac{1}{2}$) it will be as likely to find both atoms in the same well as in opposite ones. This is illustrated in Fig. 5.4, which exposes snapshots $\rho_2(x_1, x_2; t_*)$ at the equilibrium points and visualizes the temporal evolution of the *pair* (or *same-site*) *probability*

$$\begin{aligned} p_2(t) &= \langle \Theta(x_1)\Theta(x_2) + \Theta(-x_1)\Theta(-x_2) \rangle_t \\ &= \int_{\{x_1 \cdot x_2 \geq 0\}} \rho_2(x_1, x_2; t) dx_1 dx_2. \end{aligned}$$

As we introduce small correlations, the pair probability does not drop to 0.5 anymore – in fact, at $g = 0.2$ it notably oscillates about a value near 100%. This signifies that both atoms can essentially be found in the *same* well in the course of tunneling, which is apparent from the equilibrium-point image of ρ_2. In plain words, *they tunnel as pairs*. At this point, it is instructive to revisit the eigenstate analysis above: While the $g = 0$ eigenstates $\Psi_{1,2}$ are *delocalized*, at intermediate $g = 0.2$ they have basically evolved into superpositions $|N_{\mathrm{L}} = 2, N_{\mathrm{R}} = 0\rangle \pm |0, 2\rangle$ of pair states *localized in each well*. In this light, the dynamics solely consists in shuffling the population back and forth between these two pair states.

Figure 5.4 in hindsight also casts a light on the fast (small-amplitude) modulations of p_{R}

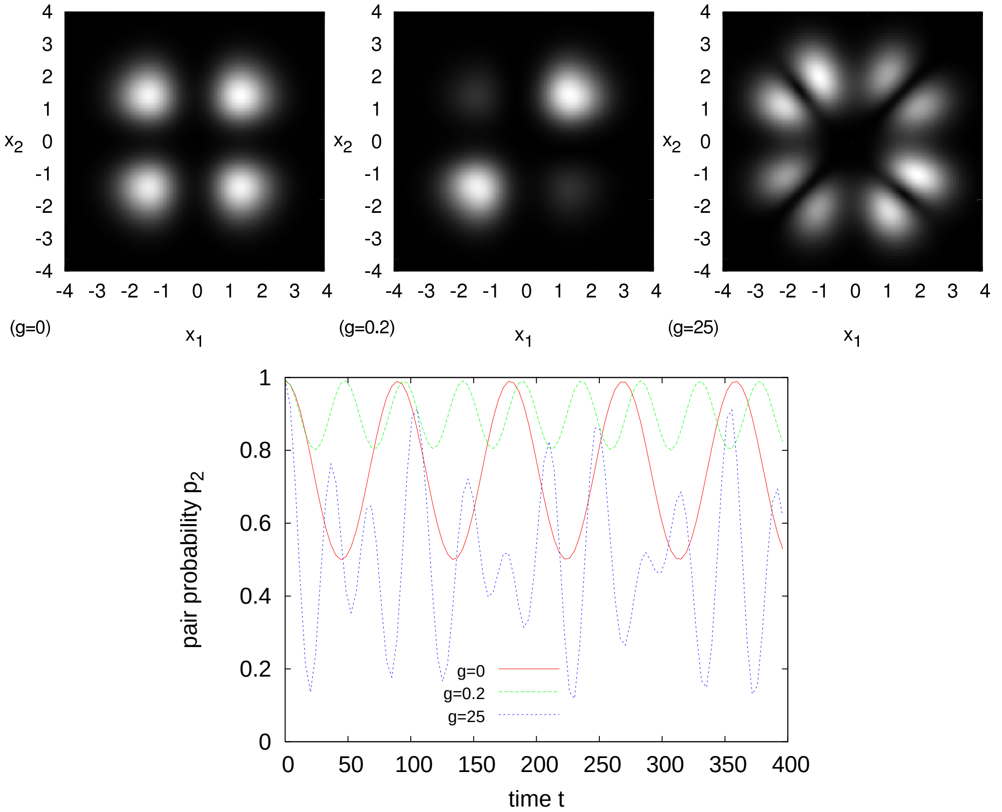

Figure 5.4: *Top*: Snapshots of two-body correlation density $\rho_2(x_1, x_2; t_*)$ at equilibrium points t_*, for $g = 0$ ($t_* = 44$), $g = 0.2$ ($t_* = 128$), and $g = 25$ ($t_* = 53$) from left to right. *Bottom*: Probability $p_2(t)$ of finding two atoms in the same well for $g = 0, 0.2, 25$.

encountered in Fig. 5.2(a), namely by linking them to temporary reductions of the pair number p_2. Thus it is fair to interpret them as attempted one-body tunneling. Along the lines of the spectral analysis above, this relates to the contribution from the ground state, in which the two atoms reside in opposite wells and which does *not* join a doublet. Since $\Theta(x_1)\Theta(x_2) + \Theta(-x_1)\Theta(-x_2)$ is parity symmetric, only equal-parity matrix elements contribute to p_2, which yields $p_2(t) \approx 1 - 2p^{(02)} \sin^2(\omega_{02}t/2)$.

It is clear that, as before, the time evolution becomes more involved as the interaction energy is raised to the fermionization limit (cf. $g = 25$). The two-body density pattern is fully fragmented not only when the pair is captured in one well (corresponding, e.g., to the upper right corner $x_1, x_2 \geq 0$), but also when passing through the equilibrium point $t = 53$. These contributions from higher-band excited states also reflect in the evolution of $p_2(t)$, which is determined by the two modes $\omega_\pm = \Delta^{(0)} \pm \Delta^{(1)}$. Over time, p_2 passes through just about any value from 1 (pair) to almost zero (complete isolation). In analogy to free fermions, it is again tempting to understand this involved pattern as two fermions tunneling independently with different frequencies.

5.1.4 Higher atom numbers

Although having focused on the case of $N = 2$ atoms so far, the question of higher atom numbers is interesting from two perspectives. For one thing, at stronger interactions many results become manifestly N-dependent, including distinctions between even/odd atom numbers, as seen in the preceding chapters. On the other hand, in an experimental setup consisting of a

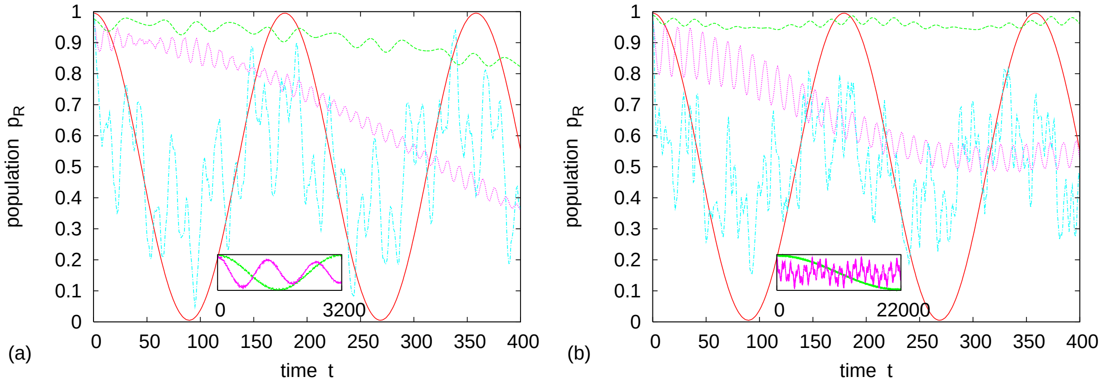

Figure 5.5: Time evolution $p_{\rm R}(t)$ of (a) $N = 3$, (b) $N = 4$ atoms initially in one well. Shown are the coupling strengths $g = 0$ (—), $g = 0.2$ (- - -), $g = 4.7$ (· · ·), and $g = 25$ (— · —). *Insets*: Long-time behavior for $g = 0.2$ (the longer period) and $g = 4.7$. (Observe the different time scales in both insets.)

whole *array* of 1D traps like in [14, 25, 103], number fluctuations may automatically admix states with $N > 2$.

Complete initial imbalance

For $N \geq 3$, the weak-interaction behavior does not differ conceptually. In fact, Eq. (5.2) carries over,

$$\delta(t) = \sum_{m<n} \delta^{(mn)} \cos(\omega_{mn} t),$$

but with the sum now running over $0 \leq m < n \leq N$. Strictly speaking, the dynamics is thus no longer determined by two but rather in principle $N(N+1)/2$ modes (mn) – although about half of these fail to contribute by symmetry. Nonetheless, the basic pattern can be understood from the two-atom case, as will become clear in a moment.

For $g = 0$, assume an ideal initial state with all atoms in the right-localized orbital $w_{\rm R} = \frac{1}{\sqrt{2}}(\phi_0 + \phi_1)$ of the lowest band. The weight coefficients $c_N(N_0) = \langle N_0, N - N_0 | \Psi(0)\rangle$ with respect to the eigenstates $|N_0, N_1\rangle$ have a binomial distribution

$$|c_N(N_0)|^2 = \frac{1}{2!^N}\binom{N}{N_0} \overset{N\to\infty}{\sim} \delta_{\Delta N_0}(N_0 - \bar{N}_0)$$

which for larger N asymptotically equals a Gaussian, with a sharp peak ($\Delta N_0 = \sqrt{N}/2$) near $\bar{N}_0 = N/2$. In this light, only these few states should contribute. Again, the equidistance of the levels guarantees a simple imbalance oscillation with $\Delta^{(0)}$. For interaction energies small compared to $\Delta^{(0)}$, the Rabi oscillations will again be modulated by beats, similar to the case $N = 2$.

As we move to larger values $g \sim 0.2$, the higher-lying of the $N + 1$ levels have again merged into doublets (Ch. 4). In particular, the highest eigenstate pair was conjectured to be roughly of the form $|N_{\rm L} = N, N_{\rm R} = 0\rangle \pm |0, N\rangle$ (in the limit $h \to \infty$). The idealized state distribution should be peaked at just these two vectors, whose energy splitting in the bare two-mode model has been estimated as $\omega \sim 2NU^{(0)}/(N-1)! \times (2\Delta^{(0)}/U^{(0)})^N$ [104], where $U^{(0)}$ denotes the on-site interaction energy. Thus the tunnel period is expected to grow exponentially as $N \to \infty$, a trend which may be roughly extrapolated from Fig. 5.5 (insets). Ultimately, this should connect to the condensate dynamics valid for $N \gg 1$ (Ng fixed) [94, 104–106], when tunneling becomes inaccessible for all intents and purposes. Of course, realistically, neighboring states will also be excited, which makes the time evolution richer. However, the separation of time scales leads to the characteristic interplay of fast, small-amplitude oscillations (related to attempted single-particle tunneling) and a much slower tunnel motion, as observed in Fig. 5.5.

Things become more intricate if we leave the two-mode regime, cf. $g = 4.7$. As demonstrated in Ch. 4, (anti-)crossings with higher-lying states (which connect to higher-band states at $g = 0$) occur for $N \geq 3$. Given our experience of the two-atom case, one might again expect a simplified behavior as we approach the fermionization limit. However, we will argue below that this has to be taken with a grain of salt because an initial state with N hard-core bosons in one well is highly excited.

In the spirit of the Bose-Fermi map, an idealized state with N fermions prepared in one well will have contributions from all excitations $|1^{(0)}_{a_0}; 1^{(1)}_{a_1}; \ldots; 1^{(N-1)}_{a_{N-1}}\rangle_-$ ($a_\beta = 0, 1\ \forall\beta$) in the N lowest bands, which is proven by induction on $N = 2$. In view of (5.3), many more frequencies are expected to be present: Besides the individual tunnel splittings $\Delta^{(\beta)}$ for each band, these should in principle be all four combinations $\Delta^{(0)} \pm \Delta^{(1)} \pm \Delta^{(2)}$ for $N = 3$, and 4×4 combinations $\{\Delta^{(l)} \pm \Delta^{(m)} \pm \Delta^{(n)} \mid 0 \leq l < m < n \leq N\}$ for $N = 4$ etc, taking into account parity-selection rules. However, in the fermionization limit with the idealized initial state above, things simplify even further. Since $\hat{N}_{\mathrm{R}} \equiv \sum_\beta C_{\mathrm{R}}^{(\beta)\dagger} C_{\mathrm{R}}^{(\beta)}$ —the Fock-space representation of $\Theta(x)$ in Eq. (5.1)— is a one-particle operator, an eigenstate $|\boldsymbol{n}\rangle_-$ is coupled only to "singly excited" states of the type $|\boldsymbol{n}'\rangle_- = a_1^{(\beta)\dagger} a_0^{(\beta)} |\boldsymbol{n}\rangle_-$ (for some β), with an excitation frequency $\omega_{\boldsymbol{n},\boldsymbol{n}'} = \Delta^{(\beta)}$. This yields an imbalance of

$$\delta(t) = \frac{1}{N} \sum_{\beta=0}^{N-1} \cos \Delta^{(\beta)} t \qquad (g \to \infty),$$

which relates to the intuitive picture of N fermions tunneling independently in the N lowest bands β, each with Rabi frequency $\Delta^{(\beta)}$.

This simple formula should be contrasted with the surprising complexity of the fermionization dynamics already for atom numbers as small as $N = 3, 4$, as shown in Fig. 5.5 (cf. $g = 25$). To be sure, for finite g and using a realistic loading scheme, a few more modes contribute, thus naturally rendering the dynamics more irregular. But even the innocuous formula above can account for the seemingly erratic patterns in Fig. 5.5: The key to see this is to consider the distribution of frequencies $\{\Delta^{(\beta)}\}$. In the unrealistic limit that $\Delta^{(\beta)} \approx \Delta^{(0)}$ $\forall\beta$, the imbalance would be a neat Rabi oscillation for any N, $\delta(t) \approx \cos \Delta^{(0)} t$. However, a realistic barrier likely has a Gaussian-type shape and a finite height; hence the splittings of higher bands tend to grow monotonically. As a consequence, only the *lower-band* frequencies $\Delta^{(\beta)}$ will contribute to the tunneling, whereas the higher-band splittings make for much faster modulations, which average out on a larger time scale. The gist is that for $N \gg 1$, those few lowest-band modes only have a weight of $O(1/N)$, which leads to quasi-equilibration around $p_{\mathrm{R}} = 1/2$.

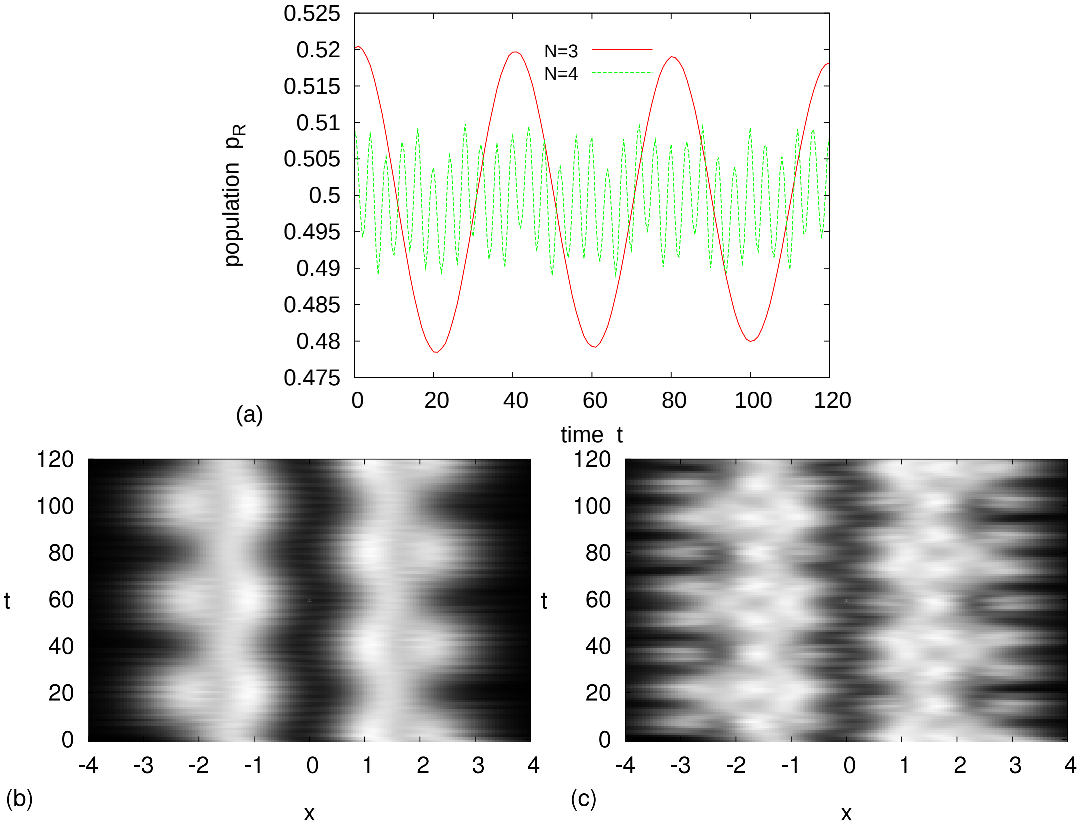

Figure 5.6: Partial-imbalance effects in the fermionization limit ($g = 25$). (a) Small-imbalance oscillations (Scenario 1.) for $N = 3, 4$ atoms. Plotted is the population of the right-hand well, $p_{\mathrm{R}}(t)$. *Bottom*: Density evolution $\rho(x; t)$ for $N - 1 = 2$ (b) and $N - 1 = 3$ atoms (c) initially in the right-hand well if exactly one atom is present on the left (Scenario 2.).

Partial imbalance

While we have so far assumed that all atoms are prepared in one well, it is natural to ask what the effect of *incomplete imbalances* $p_{\mathrm{R}}(0) < 1$ would be. For simplicity, we will focus on the fermionization limit (here $g = 25$). Two scenarios are conceivable, in principle:

1. Small imbalances $p_{\mathrm{R}} \approx 1/2$, i.e., small perturbations of the ground state;
2. Preparing, say, $N - 1$ atoms in one well and one in the other.

Case (1.) is plotted in Fig. 5.6(a) for $N = 3, 4$. We clearly observe Josephson-type oscillations in each case, but with markedly different time scales. This may be understood from the spectral structure near fermionization (cf. Sec. 4.1): For even N, the fermionic ground state $|1_0^{(0)}, 1_1^{(0)}, \ldots, 1_0^{(N/2-1)}, 1_1^{(N/2-1)}\rangle_-$ has all bands filled, so that the lowest excitation is created by moving one atom from band $\beta = N/2 - 1$ to $\beta = N/2$. Thus the "Josephson" frequency $\omega_{01} = \epsilon_0^{(N/2)} - \epsilon_1^{(N/2-1)}$ is a large *inter-band* gap, which for $N = 4$ gives a period of $T_{01} \approx 4$. For odd N, by contrast, the mechanism is a different one: Here the ground state leaves the highest band only *singly* occupied, so that the lowest excitation frequency is the small *intra-band* splitting $\omega_{01} = \Delta^{(N-1)/2}$. In Fig. 5.6(a) ($N = 3$), this may be identified as the rather long period $T_{01} \approx 40$.

Scenario (2.), paraphrased in the case $N = 3$, is the question of the fate of an atom pair if the target site (the left well) is already occupied by an atom. The striking answer, as evidenced in Fig. 5.6(b), is that the process can be viewed as single-atom tunneling on the background of the symmetric two-atom ground state. The tunneling frequency in the fermionization limit is $\Delta^{(1)} \approx 2\pi/40$, which has the intuitive interpretation of a fermion which—lifted to the band $\beta = 1$—tunnels independently of the two lowest-band fermions. From that point of view, it should come as no surprise that adding another particle destroys that simple picture. In fact, Fig. 5.6(c) reveals that if we start with $N - 1 = 3$ atoms on the right, then the tunneling oscillations appear erratic at first glance, and a configuration with three atoms per site becomes an elusive event (see, e.g., $t \approx 22, 44$ or 72). In the fermionic picture, this can be roughly understood as superimposed tunneling of one atom in the first excited band ($\Delta^{(1)}$) and another in the second band ($\Delta^{(2)} \approx 2\pi/15$), while the remaining zeroth-band fermions remain inactive.

5.2 Asymmetric double well

We have so far used the tilt d of the double well merely as a tool to load the atoms into one well. The question naturally arises whether the actual tunnel oscillations can be studied in *asymmetric* wells so as to manipulate the nature of the tunneling. Specifically, we consider a setup similar to Sec. 5.1: Two atoms are prepared in the right well (i.e., in ground state $\Psi_0^{(d_0)}$with a large initial asymmetry d_0). Subsequently, the asymmetry is ramped down to a final value $d \neq 0$, thus triggering the tunnel dynamics.

5.2.1 Tunneling resonances

In symmetric wells, pair tunneling is always resonant in the sense that an initial state with all atoms on one site is equal in energy to one with all atoms in the opposite well [96, 102]. Conversely, single-atom tunneling should only be likely so long as the repulsive interaction does not shift the pair state's energy off resonance with a target state of only a *single* atom on the left. This squares with our finding that the pair probability p_2 (Fig. 5.4) drops to 50% in the equilibrium points for $g = 0$, while in the correlated case ($g = 0.2$) it does not vary considerably from unity. To condense this insight into a single quantity, let us define

$$\bar{p}_1 = \max_{t>0}\{1 - p_2(t)\}$$

as the (maximum) *single-atom probability,* relating to the event of finding the atoms in *different* wells.

Figure 5.7 shows how $\bar{p}_1$ changes when the final asymmetry d between the wells is varied. For $g = 0$, $\bar{p}_1(d)$ has a plateau for $d \leq 0.011$. This relates to the transition from coexistence of single-atom and pair tunneling (at $d = 0$) to the point where the right-hand well is lowered such in energy that the initial pair state energetically matches a state with exactly *one* atom on the left. From the perspective of the two-body density in Fig. 5.4, the *final state* at $d = 0.011$ corresponds to the *equilibrium-point* snapshot for $d = 0$. For larger values of d, the energy difference between both wells is too large to transfer a substantial fraction of the population to the other well.

By contrast, at $g = 0.2$ the repulsion is sufficiently strong to drive the single-atom tunneling off resonance at $d = 0$ (Fig. 5.7). Lowering the right well so as to compensate for the

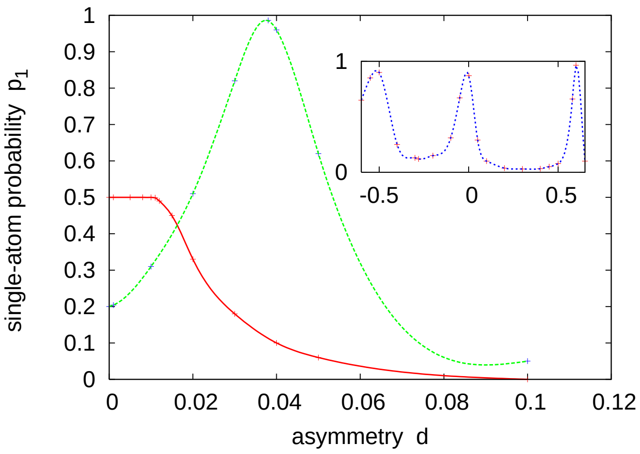

Figure 5.7: Maximum single-atom probability $\bar{p}_1$ as a function of the tilt parameter d. *Solid line:* uncorrelated tunneling, $g = 0$; *dashed line*: correlated tunneling, $g = 0.2$. *Inset*: Near the fermionization limit, $g = 25$. Note that the resonances are not symmetric in d owing to the unsymmetric initial state $\Psi(0)$.

interaction-energy shift leads to a dramatic increase of the tunnel amplitude near $d = 0.038$. The value of $\bar{p}_1 \approx 1$ confirms that this is pure single-atom tunneling: After half a tunnel period, both atoms are found precisely in opposite wells, until they return to the pair state on the right site.

Despite the more convolved dynamics that emerges as we go higher interactions, the one-atom tunnel resonance persists. However, in the fermionization limit $g \to \infty$, yet another resonance emerges at $d = 0$ already (Fig. 5.7). As in the uncorrelated case, this signifies coincident single-atom and pair tunneling. This resonance, however, is much more sensitive to symmetry breaking, which is intelligible from the picture of two fermions hopping simultaneously in different bands $\beta = 0, 1$. Skewing the double well ($d > 0$) thus attenuates both one- and two-atom tunneling until another, pure single-atom resonance is hit at $d = 0.58$. Conversely, energetically *lifting* the right-hand well ($d \approx -0.5$) makes tunneling to *excited* target states accessible.

5.2.2 Spectral analysis

To better understand the dependence of the tunnel dynamics on the tilt d, let us consider the two-body spectrum $\{E_m(d)\}$ at fixed coupling g. Since both the noninteracting and the fermionization limit can be deferred from the single-particle picture, we will first stop to review the spectrum of the tilted double well.

One-body spectrum

Figure 5.8 displays the spectrum $\{\epsilon_a(d)\}$ of the double well $U(x) = \frac{1}{2}x^2 + h\delta_w(x) - d \cdot x$ for variable asymmetries d. To get some insight, let us resort to a simple model (App. A.1) and expand the one-body Hamiltonian $h(p, x) = \frac{1}{2}p^2 + U(x)$ in terms of two modes $w_{s=\mathrm{L(R)}}$ localized on the left (right) site (tacitly assuming a fixed, isolated band β). We denote by

- $\langle w_s|h|w_s\rangle = \bar{\epsilon} \pm \varsigma/2$ the energies pertaining to *isolated* wells, where the left site has an energy offset ς
- $|\langle w_\mathrm{L}|h|w_\mathrm{R}\rangle| = \Delta/2$ the tunnel coupling.

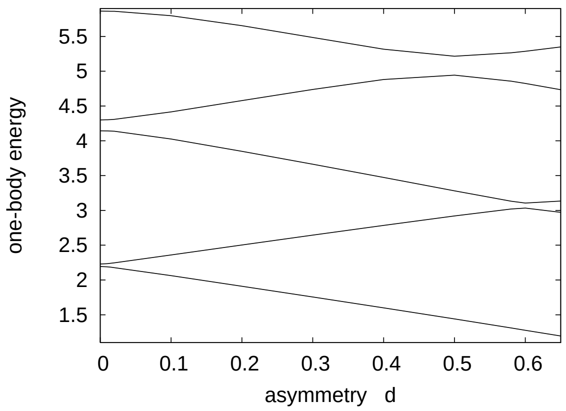

Figure 5.8: Single-particle spectrum $\{\epsilon_a(d)\}$ of the double well as a function of the asymmetry d.

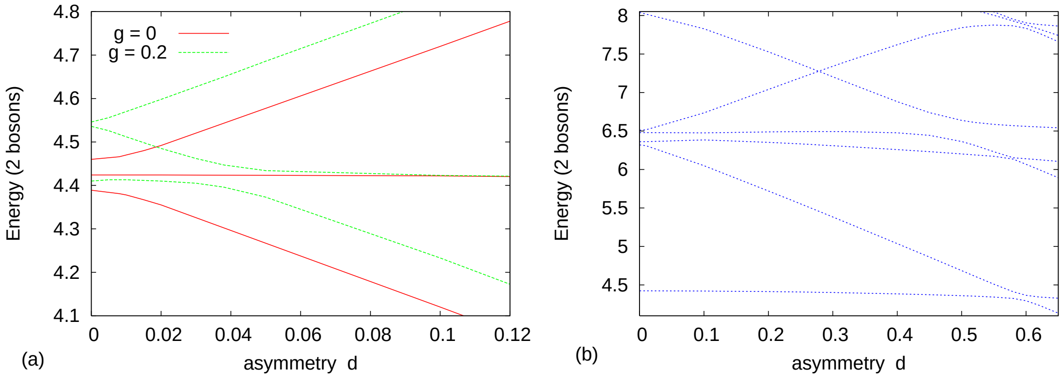

Figure 5.9: Two-body spectrum $\{E_m(d)\}$ in a tilted double well, $U(x) - d\cdot x$. (a) $g = 0,\ 0.2$ (b) $g = 25$.

Then a straightforward diagonalization yields

$$\begin{aligned}\phi_{a,\varsigma} &\propto \Delta\cdot w_{\mathrm{L}} + [\varsigma \pm \Delta(\varsigma)]\, w_{\mathrm{R}} \qquad (a = 0, 1)\\ \epsilon_{a,\varsigma} &= \bar{\epsilon} \mp \tfrac{1}{2}\Delta(\varsigma)\end{aligned}$$

where $\Delta(\varsigma) \equiv \sqrt{\Delta^2 + \varsigma^2}$ is the energy gap in the presence of the tilt. In the symmetric case, the states are simply given by the (anti-)symmetric orbitals $\phi_{a,\varsigma=0} \propto (w_{\mathrm{L}} \pm w_{\mathrm{R}})$, with the usual tunnel splitting $\Delta(0) \equiv \Delta$. As we switch on a tilt $\varsigma > 0$, parity is broken and the once delocalized states break up into one decentered on the left ($\phi_1 \approx w_{\mathrm{L}}$) and one on the right ($\phi_0 \approx w_{\mathrm{R}}$) as $\varsigma \gg \Delta$. This goes along with a level repulsion of $\epsilon_{0/1,\varsigma}$ about $\varsigma = 0$, where the ϕ_1 state pinpointed on the left site is energetically lifted, and vice versa. As the states decouple for $\varsigma \gg \Delta$, the energy approaches that of the isolated subsystem $\epsilon_{a,\varsigma} \sim \bar{\epsilon} \mp \varsigma/2$.

The above picture holds for each band β individually, provided their levels are well separated. In fact, Fig. 5.8 confirms that scenario for tilts small compared to the interband gap, $\varsigma \ll \bar{\epsilon}^{(\beta+1)} - \bar{\epsilon}^{(\beta)}$. For strong enough asymmetries d, though, states emerging from different bands mix, and new avoided crossings are observed in the plot.

Two-body spectrum

Noninteracting limit In the uncorrelated system, $g = 0$, the many-body spectrum $\{E_{\boldsymbol{n}} = \sum_a N_a \epsilon_a\}$ is obtained from the number states $|\boldsymbol{n}\rangle$ of the single-particle eigenstates ϕ_a. The energy shift of the levels $E_{\boldsymbol{n}}(d)$ with respect to $d = 0$ thus depends on the balance between contributions from symmetric orbitals $\phi_0^{(\beta)}$ and antisymmetric ones. Specifically, the $d = 0$ ground state exhibited in Fig. 5.9(a) is a coherently symmetric state $|20\rangle = [\phi_0^{(0)}]^{\otimes 2}$. Consistently, for perturbations $d > 0$ it localizes on the right, with its level shifting downward – contrary to the second excitation $|02\rangle = [\phi_1^{(0)}]^{\otimes 2}$. In between, $|11\rangle$ is a compromise between these two borderline cases in that both partial energy shifts cancel out, leaving a *delocalized* state. This gives us a new perspective on the tunneling dynamics reflected in Fig. 5.7. Imagine we start with all atoms prepared in the right well, viz., the ground state $\Psi_0^{(d\to\infty)}$, and then ramp down $d(t) \to 0$ so as to trigger the tunneling. If we follow the ground-state level nonadiabatically, then at $d = 0$ it finds three closely packed levels $E_{m=0,1,2}(0)$ it can couple to – in the sense that

$$\Psi(t) \approx \sum_{m=0,1,2} c_m(t)\Psi_m,$$

so that a nontrivial dynamics becomes possible. In fact, at $d = 0$, these correspond to Rabi oscillations. If we were to choose a final asymmetry $d < 0.01$ (in the notation above, $\varsigma^{(0)} < \Delta^{(0)}$), roughly the same levels would be available, confirming the plateau encountered in Fig. 5.7. However, for final values $d > 0.01$, the levels decouple, and no longer are there any target states at disposal for tunneling.

Intermediate regime These elementary thoughts also help us explore the nontrivial dynamics for intermediate couplings, as shown for $g = 0.2$ in Fig. 5.9(a). The $d = 0$ ground state, in the limit $\Delta^{(0)} \to 0$, has the Mott-insulator form $|1_\mathrm{L}1_\mathrm{R}\rangle$ and should be insensitive to symmetry breaking $d > 0$. By contrast, the quasi-degenerate excited pair $|2_\mathrm{L}0_\mathrm{R}\rangle \pm |0_\mathrm{L}2_\mathrm{R}\rangle$ only requires a minute perturbation to break up into two localized states. It is plain to see that, at $d \approx 0.04$, the lower excited curve anti-crosses the ground state, and the two states are virtually swapped. In the language of the simple two-mode model, the (avoided) crossing occurs for tilts $\varsigma^{(0)} = U^{(0)}$ matching the on-site repulsion energy.

The bearing this has on the tunnel dynamics is evident: Apart from the self-trapping scenario at $d = 0$, there is a fairly broad tunnel resonance at $d \approx 0.04$, where the fully imbalanced initial state $\Psi(0)$ couples to that with one atom on each site, $|1_\mathrm{L}1_\mathrm{R}\rangle$. This is but the one-body resonance encountered in Fig. 5.7. To come by a crude estimate for the critical value d_c, assume that the energy of initial and final states match, $\langle H_{d_c}\rangle_\mathrm{i} = \langle H_{d_c}\rangle_\mathrm{f}$. Modeling the initial pair state by the ground state $\Psi_0^{(d_0)}$ (at the initial $d_0 > 0$), and the final state with a single atom on the left by $\Psi_0^{(0)}$, yields the estimate

$$d_c = d_0 - \left(E_0^{(0)} - E_0^{(d_0)}\right)/N\left\langle x\right\rangle^{(d_0)}$$

in terms of the ground-state energies at the initial $d_0 > 0$ and $d = 0$, respectively, and the elongation $\langle x\rangle$ at time $t = 0$.

Fermionization limit Figure 5.9(b) shows the spectrum near fermionization, $g = 25$. The $d = 0$ ground state turns out to be widely robust against perturbations, which can be understood from the fact that its fermionic counterpart $|1_0^{(0)}1_1^{(0)}\rangle_-$ has balanced populations of right- and left-localizing orbitals. The only way to obtain a *right-localized* ground state is to lower one

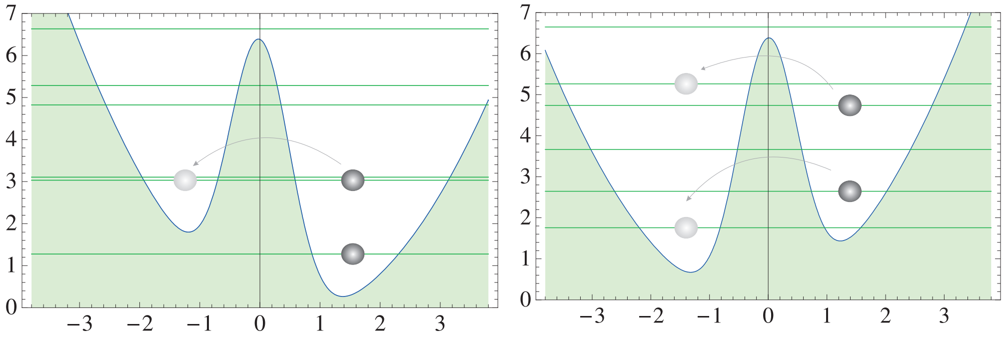

Figure 5.10: Visualization of the hopping processes in the fermionic picture. *Left*: Single-particle resonance for an asymmetry $d = 0.6$. *Right*: Suppressed two-particle tunneling as a sum of two highly off-resonant one-body processes ($d \approx -0.3$).

well enough for it to hit a localized state from the upper band $\beta = 1$.[2] This is what happens at $d \approx 0.6$, where the tilt energy $\varsigma^{(1)}/2 = \bar{\epsilon}^{(1)} - \bar{\epsilon}^{(0)}$ compensates the inter-band gap. That crossing marks exactly the one-body resonance seen in Fig. 5.7 at $d \approx 0.6$. In the fermionic picture invoked above, it may be thought of as one *excited* fermion tunneling to the *lowest* level on the left (illustrated in Fig. 5.10, *left*).

If we follow the localized state nonadiabatically, then at $d = 0$ we recover the mixed single-atom/pair resonance laid bare in Fig. 5.7. Further ramping up the right well to $d \approx -0.3$ (where the spectrum is mirrored at $d = 0$), we see yet another crossing. A closer look reveals that the partner state is entirely localized on the *left*, so that one might expect a pair resonance. However, as both states are localized in disjoint regions, they are not coupled by the perturbation $(-d \cdot x)$, and in practice no tunnel resonance is observed. It may be illuminating to look at this from the fermionic perspective. For $d \approx -0.3$, the initial state on the right is $\Psi(0) \approx |1_1^{(0)}; 1_1^{(1)}\rangle_-$, while the partner state emanating from $E(0) \approx 8$ in turn is given by $|1_0^{(0)}; 1_0^{(2)}\rangle_-$. In this light, the tunneling "resonance" in question refers to the following situation, shown pictorially in Fig. 5.10(*right*): Two fermions simultaneously hop from the zeroth (first excited) level on the right down to the zeroth level (up into the second level) of the energetically lower left site. While both processes individually are off resonance, the total energy is conserved. This reflects in the one-body spectrum (Fig. 5.8), where no avoided crossing is to be observed at $d \approx -0.3$ – rather, there is an accidental crossing of the sums $E_{\boldsymbol{n}} = \sum_a N_a \epsilon_a$. However, at $d \approx -0.6$, another *avoided* crossing emerges, which—in the fermion language—corresponds to multiple one-body resonances with the first and second excited level in the left well.

---

[2] In fact, this is what makes it so easy to prepare definite atom numbers in each well, as done in Sec. 5.1.4.

Chapter 6

Conclusion and outlook

Conclusion

In this thesis, we have studied few-boson systems in one-dimensional harmonic and double-well traps throughout the crossover from the non-interacting to the strongly repulsive *fermionization* limit. This was done from an *ab initio* perspective so as to capture few-body effects. To that end, we have both developed an exact-diagonalization approach—based on an expansion in terms of harmonic-oscillator states—and resorted to the multi-configurational time-dependent Hartree method.

In order to understand the basic mechanism of the fermionization transition, we have looked into the ground state in a simple harmonic trap. Its pathway leads via the formation of a correlation hole, signifying the reduced probability of finding two atoms at the same position, to a checkerboard pattern in the two-body density characteristic of the fermionization limit. Here each particle can be thought of as taking a discrete position isolated from all others – a feature that also reflects in the averaged one-body density profile, if washed out for larger atom numbers N. Furthermore, the fermionization crossover reduces the degree of coherence in the system, as indicated by the attenuation of the off-diagonal long-range order in the one-body density matrix. Concomitantly, much of the zero-momentum peak signaling Bose-Einstein condensation is redistributed toward higher momenta, culminating in a characteristic long-range tail of the momentum distribution, $\tilde{\rho}(k) \sim c/k^4$.

In general, the crossover depends nontrivially on the external potential. For a double-well trap, the coherence is reduced already for weak interactions due to on-site localization of the bosons. Toward fermionization, the interplay between inter-atomic and external forces leads to a qualitative difference between even and odd atom numbers: For even N, the expected localization persists, whereas an additional particle will delocalize over the two wells.

The role played by interactions has been illuminated by regarding an inhomogeneous interaction potential, in the sense that one side of the trap is more repulsive than the other. While the Bose-Fermi map remains valid for infinite repulsion, it is possible to displace the ground state to the less repulsive region for rather small interactions, especially in a double-well trap.

That investigation of the fermionization mechanism has been extended to the low-lying excitations. In a harmonic trap, the initially equidistant and multiply degenerate levels split up according to the degree of relative excitation. Near the fermionization limit, the lines merge again to the excitation spectrum of an ideal Fermi gas, suggesting a more regular dynamics for strong enough interactions. In a double well, the low-lying non-interacting spectrum is given by distributing all atoms over the lowest single-particle band. Increasing the interaction first leads to two-fold quasi-degeneracies associated with on-site localization of the underlying excited states. These are broken up again as higher-band states are admixed for larger repulsion, making for a complex level structure. However, a simplified pattern emerges toward the fermionization limit, which we have interpreted in terms of free fermions filling up the lowest bands up to the Fermi edge, and excitations thereof.

The understanding of the excitations has provided a base for the investigation of the few-boson tunnel dynamics in a double well. We have demonstrated that the tunneling first changes over from the familiar Rabi oscillations, in the uncorrelated limit, to a few-body counterpart of nonlinear self-trapping, where collective tunneling is strongly delayed and modulated by fast, small-amplitude oscillations interpreted as attempted one-body tunneling. As the fermionization limit is approached, a fragmented atom pair has been shown to tunnel coherently back and forth between the wells almost like a single-particle. This phenomenon has been analyzed in terms of multi-band Rabi oscillations of fermions, whose population imbalance is expected to quasi-equilibrate for larger N. Finally, by tilting the double well so as to compensate the energy offset due to on-site interactions, one-body tunneling can be tuned to be resonant.

Outlook While the investigation into the basic mechanism of the fermionization crossover can be regarded as more or less complete, there still is much uncharted territory in the area of ultracold few-atom systems. Even in the setup studied in this thesis, many intriguing time-dependent problems still await a solution. To name but a few examples: The tunneling resonances in biased double wells suggest a promising procedure of extracting single atoms experimentally; but also periodic modulations of the wells or nonadiabatically ramping the central barrier may reveal much new insight. This readily extends more complex, lattice-type setups or higher spatial dimensions, which would be numerically far more challenging, but also equally richer physically. An open question as of yet is the link to other areas such as quantum information, which may help illuminate longstanding issues from a few-body perspective.

While we have only considered repulsive short-range interactions, currently efforts are underway to study attractive interactions in few-boson systems. On the other hand, it may be interesting to explore the effect of long-range, e.g., dipolar interactions, which are nontrivial even in reduced dimensions. Finally, an up-and-coming line of research goes beyond the simple Bose gas – either by studying mixtures of different bosonic and/or fermionic species, or via including spin degrees of freedom. A first step into that direction is under preparation, and it surely will be part of a longer journey.

Appendix A

Simple models for double-well potentials

> *Nothing gives such weight and dignity to a book as an appendix.* (MARK TWAIN)

In this appendix, we shall review some basic properties of *double-well* potentials, i.e., single-particle potentials $U(x)$ characterized by two minima (for simplicity assumed to be symmetric about the origin, $\pm x_0$) separated by a sufficiently high energy barrier. This is an elementary model for the abstract situation of two distinct systems that are somehow coupled, and it represents the simplest nontrivial case of a (finite) lattice, as commonly regarded in solid-state physics. Borrowing from this picture, we will discuss the general structure of the single-particle problem (Sec. A.1) and, based on that, proceed with a simple many-body description, the two-site Bose-Hubbard model (Sec. A.2).

A.1 One-body problem

To get some intuition about the physics of a double-well system (and, by extension, multi-well potentials), we shall first resort to a solvable toy model of a harmonic well split by a central δ-function barrier. Equipped with this insight, we will make a two-mode expansion valid for double-well potentials of rather arbitrary shape.

A soluble model

Consider the following archetype of a double well: a harmonic trap split by a central barrier shaped as a delta peak [33]:

$$U(x) = \frac{1}{2}x^2 + h\delta(x).$$

This model has the appealing feature that it recovers the double-well model used in this thesis in the limit of an infinitely narrow barrier, $w \to 0$, and thus shares many basic features. There is yet another graceful property: We have already diagonalized the corresponding one-body Hamiltonian $h(p,x) = \frac{1}{2}p^2 + U(x)$ in Sec. 1.4.3, in the slightly different context of the *relative* motion of two atoms, $h_{\mathrm{rel}}(p,r) = p^2 + \frac{1}{4}r^2 + g\delta(r)$, interacting via a contact potential. Therefore, we can simply recast Eqs. (1.25-1.26) in terms of $x \equiv r/\sqrt{2}$, $h \equiv g/\sqrt{2}$. For the *even* solutions, this yields

$$\begin{aligned}\phi_\nu(x) &= c\,e^{-x^2/2}U\left(-\frac{\nu}{2},\frac{1}{2},x^2\right)\\ \nu(h)\in f_h^{-1}(0)\;:\;f_h(\nu) &= 2\frac{\Gamma\left(\frac{1-\nu}{2}\right)}{\Gamma\left(-\frac{\nu}{2}\right)}+h,\end{aligned}$$

while the odd eigenstates are simply given by the harmonic-oscillator states $\phi_{2n+1}\equiv u_{2n+1}$ ($n\in\mathbb{N}_0$) for any barrier value.

From this viewpoint, the process of continuously *splitting* a harmonic trap into two isolated wells ($h\to\infty$) corresponds exactly to the relative motion of two particles while increasing their *interaction* strength $g\to+\infty$ (and likewise for attractive interactions, not considered here). It is instructive to make that analogy explicit:

- To begin with, the *odd* states are completely unchanged by the central barrier. This is obvious since the barrier is supported solely at $x=0$ (cf. Figs. 1.1, 1.2), where the odd states are trivially zero. That relates to the problem for the *relative* motion r, where odd parity translates to permutational *anti*-symmetry, reinstating the common wisdom that *fermions* do not feel contact interactions.

- At $h=0$, the *even* states simply coincide with the harmonic-oscillator orbitals $\phi_{\nu(0)}=u_{2n}$. As h is increased, they acquire a dip at $x=0$, signifying their expulsion from the central-barrier region. As $h\to\infty$, this notch reaches down to $\phi_\nu(0)\to0$. More generally, in that limit the quantum number tends to the next higher *odd* value:

  $$\lim_{h\to\infty}\nu(h)=2n+1,$$

  while

  $$\lim_{h\to\infty}\phi_{\nu(h)}=Au_{2n+1},\quad A(x)\equiv\mathrm{sgn}(x).$$

  From the perspective of the pertinent *relative* problem, this is nothing but the *fermionization* of bosonic states for infinite repulsion.

Connecting the dots, we wind up with the following picture: As we ramp up the central barrier h, the initially equidistant harmonic spectrum $\epsilon_\nu=\nu+\frac{1}{2}$ gradually acquires the structure of *doublets*. These consist of (i) the even states, which are more and more notched at $x=0$ and (ii) the (unchanged) odd oscillator orbitals. Both become degenerate in the limit $h\to\infty$, at energies $\epsilon_n=n+\frac{3}{2}$ ($n\in\mathbb{N}_0$), and are separated from the next level pair by the gap $\Delta\epsilon=2$.

Two-mode description

The essence of the toy model treated above is as follows: For high enough barriers, the double-well spectrum arranges in isolated doublets, corresponding to pairs of anti-/symmetric orbitals. This comes as no surprise: After all, in the strict limit of an infinite barrier, the whole system decouples into two *isolated* subsystems “L” and “R”, whose configuration space is given solely by $\{x<0\}$ ($\{x>0\}$, respectively). It is only for finite barriers that these two are somehow coupled, which eventually leads to tunneling between the two wells.

We will now put the cart before the horse and extend the observations above to an expansion applicable to generic two-well systems. To this end, let us adapt the notation a little. Rather than counting all eigenstates $n = 0, 1, \ldots$, consider individual *bands* $\beta = 0, 1, \ldots$ consisting of a pair of symmmetric ($a_\beta = 0$) and antisymmetric ($a_\beta = 1$) eigenstates: $\phi^{(\beta)}_{a_\beta}$. Let us now look at a *fixed* (and well-isolated) band β, and consider the orthogonal transform

$$w_{s=\mathrm{L(R)}} = \frac{1}{\sqrt{2}} \left(\phi_0 \pm \phi_1 \right),$$

yielding unsymmetric states which are now *localized* in the left (right) well, respectively.[1]

We will now expand the one-body Hamiltonian $h(p, x)$ of a general double well in terms of these two localized orbitals and parametrize it by

- $\langle w_s | h | w_s \rangle = \bar{\epsilon} \pm \varsigma/2$ the energies pertaining to *isolated* wells, where the left site may have an energy offset ς
- $\langle w_\mathrm{L} | h | w_\mathrm{R} \rangle = -\Delta/2$ the coupling between two wells.

Then a straightforward diagonalization yields

$$\begin{array}{rcll} \phi_{a,\varsigma} & \propto & \Delta \cdot w_\mathrm{L} + [\varsigma \pm \Delta(\varsigma)]\, w_\mathrm{R} & \qquad (a = 0, 1) \\ \epsilon_{a,\varsigma} & = & \bar{\epsilon} \mp \frac{1}{2} \Delta(\varsigma) & \end{array}$$

where $\Delta(\varsigma) \equiv \sqrt{\Delta^2 + \varsigma^2}$ is the energy gap in the presence of the tilt.

In the symmetric case ($\varsigma = 0$), the states are simply given by the (anti-)symmetric orbitals $\phi_{a,\varsigma=0} \propto w_\mathrm{L} \pm w_\mathrm{R}$, with the usual *tunnel splitting*

$$\epsilon_{1,0} - \epsilon_{0,0} = \Delta(0) \equiv \Delta.$$

As we switch on a tilt $\varsigma > 0$, parity is broken and the once delocalized states break up into one decentered on the left (ϕ_1) and one on the right (ϕ_0) as $\varsigma \gg \Delta$, in which case the energy approaches that of the isolated subsystems, $\epsilon_{a,\varsigma} \sim \bar{\epsilon} \mp \varsigma/2$. The above picture holds for each band β individually, provided the bands are well separated, $\varsigma \ll \bar{\epsilon}^{(\beta+1)} - \bar{\epsilon}^{(\beta)}$.

A.2 Many-body problem

Let us now apply the above two-mode expansion to the Fock-space representation of the many-body Hamiltonian:

$$H = \sum_{a,b} \langle a | h | b \rangle c_a^\dagger c_b + \frac{1}{2} \sum_{ab,cd} \langle ab | V | cd \rangle c_a^\dagger c_b^\dagger c_d c_c,$$

---

[1] We use the term *band* in reference to the language of general S-site lattices with periodic boundary conditions known from solid-state physics [107]. There, the general solutions $\phi_q^{(\beta)}$ are *Bloch waves* parametrized in terms of the conserved quasimomentum q, while the orbitals $w_s^{(\beta)}$ *localized* on each site $s = 1, \ldots, S$ are termed *Wannier* functions. However, here we shall focus on two wells ($S = 2$), and we are not restricted to periodic boundary conditions.

where the single-particle basis is now $|a\rangle \equiv |\beta, s\rangle = w^{(\beta)}_{s=\mathrm{L,R}}$. With the nomenclature above, and for simplicity focusing on the symmetric case, this yields

$$H = \sum_{\beta,s} \bar{\epsilon}^{(\beta)} N_s^{(\beta)} - \sum_{\beta} \Delta^{(\beta)} \mathrm{Re}\left(c_{\mathrm{L}}^{\dagger} c_{\mathrm{R}}\right) + \frac{1}{2} \sum_{ab,cd} \langle ab|V|cd\rangle c_a^{\dagger} c_b^{\dagger} c_d c_c.$$

Now the (two-mode) *Bose-Hubbard* model makes the following assumptions:[2]

1. Only the lowest band $\beta = 0$ is included above. For the ground state, this is plausible if the energy to add a particle is small compared to the interband gap, $\mu \ll \bar{\epsilon}^{(1)} - \bar{\epsilon}^{(0)}$.
2. Only on-site interactions are considered, i.e., of all interaction integrals only $V^{(0)}_{\mathrm{LL,LL}} = V^{(0)}_{\mathrm{RR,RR}} =: U^{(0)}$ is retained. This is justified in the limit of an infinitely high barrier, when the *density overlap* between w_{L} and w_{R} tends to zero.

Obviously, the Bose-Hubbard model requires very small tunnel coupling and sufficiently weak interactions, so that virtual excitations of higher bands are strongly suppressed. Under these premises, though, this buys us the charmingly simple model (up to a constant shift)

$$\begin{aligned} H &= -\Delta^{(0)} \mathrm{Re}\left(c_{\mathrm{L}}^{\dagger} c_{\mathrm{R}}\right) + \frac{1}{2} U^{(0)} \sum_{s=\mathrm{L,R}} \left(c_s^{\dagger}\right)^2 {c_s}^2 \\ H/U^{(0)} &= -\frac{\Delta^{(0)}}{U^{(0)}} \mathrm{Re}\left(c_{\mathrm{L}}^{\dagger} c_{\mathrm{R}}\right) + \sum_{s=\mathrm{L,R}} \frac{1}{2} N_s (N_s - 1). \end{aligned}$$

This way, the whole Hamiltonian can be parametrized via the ratio $\Delta^{(0)}/U^{(0)}$ between the tunnel coupling and the on-site interaction energy. It is easy to read off the two limiting cases: For negligible interaction energy, $\Delta^{(0)}/U^{(0)} \gg 1$, delocalized eigenstates are favored, which are simply number states in the (anti-)symmetric orbital basis. By contrast, for dominant on-site interactions, $\Delta^{(0)}/U^{(0)} \ll 1$, $N_{s=\mathrm{L,R}}$ becomes a conserved quantity, so eigenstates tend to localize on each site s.

A more elaborate discussion on this can be found in Ref. [94], which considers the two-mode model in the hermitian operator basis

$$J_1 = \frac{1}{2}\left(c_{\mathrm{R}}^{\dagger} c_{\mathrm{R}} - c_{\mathrm{L}}^{\dagger} c_{\mathrm{L}}\right), \quad J_2 = -\mathrm{Im}\left(c_{\mathrm{R}}^{\dagger} c_{\mathrm{L}}\right), \quad J_3 = \mathrm{Re}\left(c_{\mathrm{R}}^{\dagger} c_{\mathrm{L}}\right)$$

satisfying the angular-momentum algebra $[J_\alpha, J_\beta] = i\varepsilon_{\alpha\beta\gamma} J_\gamma$. This leads to a Hamiltonian of the form (up to constants)

$$H = -\Delta^{(0)} J_3 + 2U^{(0)} J_1^2.$$

---

[2] The general Bose-Hubbard model [108, 109], and likewise the traditional fermionic Hubbard model [107], is derived in a totally analogous way, with the only additional assumption that only nearest-neighbor tunneling occurs, which is trivial in a two-site system. The extension to arbitrary dimensions $d > 1$ is straightforward.

Acknowledgments

First I would like to thank my adviser, Prof. Dr. Peter Schmelcher, for giving me the opportunity to work on a field that is both physically interesting and challenging. Professor Schmelcher was always available for engaging discussions. His scientific support has gone way beyond mere technical issues.

I am also greatly indebted to Prof. Dr. Hans-Dieter Meyer. As my co-adviser, he went out of his way to help me both with numerical problems and by his inspirational remarks. This work would not have been possible to this extent without his support.

Moreover, I am happy to thank Dr. Thomas Gasenzer, for being referee on my dissertation, as well as Profs. Selim Jochim, Markus Oberthaler, and Jochen Schirmer for many fruitful discussions. For that matter, it is a pleasure to mention Frank Deuretzbacher, Thomas Barthel, and Dr. Reinhold Walser.

My thanks also go out to the people in my group, for helpful and entertaining discussions. In particular, I thank Oriol Vendrell, Michael Brill, Kaspar Sakmann, and Emmerich Tempfli. It all helped provide the pleasant and productive atmosphere I could enjoy during my work.

Last, but by no means least, my family deserves my especial thanks for supporting me in any way conceivable.

List of abbreviations

The following list contains some *abbreviations* frequently used in this work:

nD n-dimensional

CM Center of mass

DVR Discrete variable representation, a method to represent wave functions and operators in a discrete basis

HO Harmonic oscillator

MCTDH Multi-Configuration Time-Dependent Hartree, a wave-packet propagation method (cf. 2.3)

Moreover, some mathematical *notations* are summarized below:

- $\oplus$: direct sum
- $\otimes$: tensor product (*also:* direct product)
- $\binom{a}{b}$: binomial coefficient of a over b
- $(f * g)(x) = \int f(x-y)g(y)dy$: convolution of two functions f, g
- $\sim$, $\overset{r\to\infty}{\sim}$ *etc.*: denotes asymptotic equivalence
- $\boldsymbol{a} = (a_1, \dots, a_N) \in \mathbb{Z}^N$: multi-index, with the following notations for "absolute value" $|\boldsymbol{a}| := \sum_{j=1}^N a_j$, factorial $\boldsymbol{a}! = \prod_j a_j!$, exponentiation $X^{\boldsymbol{a}} = \prod_j x_j^{a_j}$ and derivative $\partial^{\boldsymbol{a}} = \prod_j \left(\frac{\partial}{\partial x_j}\right)^{a_j}$ for $X = (x_1, \dots, x_N) \in \mathbb{R}^N$
- $\delta_\sigma(x) \equiv \frac{1}{\sqrt{2\pi}\sigma} e^{-x^2/2\sigma^2}$: normalized Gaussian of width σ
- $\mathbb{H}_N$: N-particle Hilbert space
- $|\boldsymbol{n}\rangle \equiv |N_0, N_1, \dots\rangle$: occupation-number (Fock) state
- $\mathrm{Re}(A) = \frac{1}{2}(A + A^\dagger)$, $\mathrm{Im}(A) = \frac{1}{2i}(A - A^\dagger)$: (anti-)hermitian operator decomposition
- $\Theta(\cdot)$, $\delta(\cdot)$: Heaviside's step function, and Dirac's 'delta function' (unless otherwise noted)
- $\mathrm{tr}_\Sigma\,(\cdot)$: (partial) trace over some subspace Σ
- $u_a(x) = H_a(x) e^{-x^2/2} / \sqrt{\sqrt{\pi} 2^a a!}$: harmonic-oscillator eigenfunctions

Bibliography

[1] C. J. Pethick and H. Smith, *Bose-Einstein condensation in dilute gases* (Cambridge University Press, Cambridge, 2001).

[2] L. Pitaevskii and S. Stringari, *Bose-Einstein Condensation* (Oxford University Press, Oxford, 2003).

[3] A. J. Leggett, Rev. Mod. Phys. **73**, 307 (2001).

[4] W. Ketterle, D. S. Durfee, and D. M. Stamper-Kurn, cond-mat/9904034 .

[5] R. Grimm, M. Weidemüller, and Y. Ovchinnikov, Adv. At., Mol., Opt. Phys. **42**, 95 (2000).

[6] T. Köhler, K. Góral, and P. S. Julienne, Rev. Mod. Phys. **78**, 1311 (2006).

[7] I. Bloch, J. Dalibard, and W. Zwerger, arXiv:0704.3011 .

[8] A. D. Cronin, J. Schmiedmayer, and D. E. Pritchard, arXiv:0712.3703 .

[9] *Quantum Information Processing*, edited by G. Leuchs and T. Beth (Wiley-VCH, Weinheim, 2003).

[10] S. Kuhr *et al.*, Science **293**, 278 (2001).

[11] S. Nussmann *et al.*, Phys. Rev. Lett. **95**, 173602 (2005).

[12] R. Folman *et al.*, Adv. At. Mol. Opt. Phys. **48**, 263 (2002).

[13] T. Gericke, C. Utfeld, N. Hommerstad, and H. Ott, Laser Phys. Lett. **3**, 415 (2006).

[14] T. Kinoshita, T. Wenger, and D. S. Weiss, Science **305**, 1125 (2004).

[15] V. Efimov, Phys. Lett. B **3**, 563 (1970).

[16] T. Kraemer *et al.*, Nature **440**, 315 (2006).

[17] T. Busch, B. G. Englert, K. Rzazewski, and M. Wilkens, Found. Phys. **28**, 549 (1998).

[18] Z. Idziaszek and T. Calarco, Phys. Rev. A **74**, 022712 (2006).

[19] M. Girardeau, J. Math. Phys. **1**, 516 (1960).

[20] E. H. Lieb and W. Liniger, Phys. Rev. **130**, 1605 (1963).

[21] M. Olshanii, Phys. Rev. Lett. **81**, 938 (1998).

[22] V. Dunjko, V. Lorent, and M. Olshanii, Phys. Rev. Lett. **86**, 5413 (2001).

[23] D. S. Petrov, G. V. Shlyapnikov, and J. T. M. Walraven, Phys. Rev. Lett. **85**, 3745 (2000).

[24] D. M. Gangardt and G. V. Shlyapnikov, Phys. Rev. Lett. **90**, 010401 (2003).

[25] B. Paredes *et al.*, Nature **429**, 277 (2004).

[26] M. D. Girardeau, E. M. Wright, and J. M. Triscari, Phys. Rev. A **63**, 033601 (2001).

[27] T. Papenbrock, Phys. Rev. A **67**, 041601 (2003).

[28] Y. Lin and B. Wu, Phys. Rev. A **75**, 023613 (2007).

[29] A. Minguzzi and D. M. Gangardt, Phys. Rev. Lett. **94**, 240404 (2005).

[30] A. del Campo and J. G. Muga, Europhys. Lett. **74**, 965 (2006).

[31] H. Buljan, R. Pezer, and T. Gasenzer, Phys. Rev. Lett. **100**, 080406 (2008).

[32] M. D. Girardeau and E. M. Wright, Phys. Rev. Lett. **84**, 5691 (2000).

[33] T. Busch and G. Huyet, J. Phys. B **36**, 2553 (2003).

[34] K. K. Das, M. D. Girardeau, and E. M. Wright, Phys. Rev. Lett. **89**, 170404 (2002).

[35] R. Pezer and H. Buljan, Phys. Rev. Lett. **98**, 240403 (2007).

[36] A. del Campo *et al.*, Phys. Rev. A **74**, 013605 (2006).

[37] G. E. Astrakharchik and S. Giorgini, Phys. Rev. A **68**, 031602 (2003).

[38] K. Sakmann, A. I. Streltsov, O. E. Alon, and L. S. Cederbaum, Phys. Rev. A **72**, 033613 (2005).

[39] M. A. Cirone, K. Góral, K. Rzazewski, and M. Wilkens, J. Phys. B **34**, 4571 (2001).

[40] D. Blume, Phys. Rev. A **66**, 053613 (2002).

[41] G. E. Astrakharchik and S. Giorgini, Phys. Rev. A **66**, 053614 (2002).

[42] O. E. Alon and L. S. Cederbaum, Phys. Rev. Lett. **95**, 140402 (2005).

[43] Y. Hao, Y. Zhang, J. Q. Liang, and S. Chen, Phys. Rev. A **73**, 063617 (2006).

[44] F. Deuretzbacher, K. Bongs, K. Sengstock, and D. Pfannkuche, Phys. Rev. A **75**, 013614 (2007).

[45] B. Schmidt and M. Fleischhauer, Phys. Rev. A **75**, 021601 (2007).

[46] S. Zöllner, H.-D. Meyer, and P. Schmelcher, Phys. Rev. A **74**, 053612 (2006).

[47] S. Zöllner, H.-D. Meyer, and P. Schmelcher, Phys. Rev. A **74**, 063611 (2006).

[48] S. Zöllner, H.-D. Meyer, and P. Schmelcher, Phys. Rev. A **75**, 043608 (2007).

[49] S. Zöllner, H.-D. Meyer, and P. Schmelcher, Phys. Rev. Lett. **100**, 040401 (2008).

[50] S. Zöllner, H.-D. Meyer, and P. Schmelcher, arXiv:0801.1090v1 .

[51] R. J. Jelitto, *Quantenmechanik II* (Aula-Verlag, Wiesbaden, 1988).

[52] F. Schwabl, *Quantenmechanik* (Springer, Heidelberg, 2002).

[53] J. J. Sakurai, *Modern Quantum Mechanics* (Addison-Wesley, New York, 1994).

[54] K. Huang, *Statistical Mechanics*, 2nd ed. (John Wiley & Sons, New York, 1987).

[55] K. Huang and C. N. Yang, Phys. Rev. **105**, 767 (1957).

[56] A. Derevianko, cond-mat/0507209 .

[57] D. Blume and C. H. Greene, Phys. Rev. A **65**, 043613 (2002).

[58] J. R. Taylor, *Scattering Theory* (John Wiley & Sons, Inc., New York, 1972).

[59] M. Block and M. Holthaus, Phys. Rev. A **65**, 052102 (2002).

[60] T. Cheon and T. Shigehara, Phys. Rev. Lett. **82**, 2536 (1999).

[61] I. V. Ovchinnikov and D. Neuhauser, Europhys. Lett. **74**, 785 (2006).

[62] M. D. Girardeau and A. Minguzzi, Phys. Rev. Lett. **99**, 230402 (2007).

[63] F. Deuretzbacher *et al.*, Phys. Rev. Lett. **100**, 160405 (2008).

[64] H. A. Bethe, Z. Phys. **71**, 205 (1931).

[65] M. Abramowitz and I. A. Stegun, *Handbook of Mathematical Functions* (Dover, New York, 1972).

[66] Z. Idziaszek and T. Calarco, Phys. Rev. A **71**, 050701 (2005).

[67] U. Schollwöck, Rev. Mod. Phys. **77**, 259 (2005).

[68] R. Guardiola, *Microscopic Quantum Many-Body Theories and Their Applications* (Springer, Berlin, 1998).

[69] *Computational Physics*, edited by K. H. Hoffmann and M. Schreiber (Springer, Heidelberg, 1996).

[70] O. Penrose and L. Onsager, Phys. Rev. **104**, 576 (1956).

[71] L. Erdos, B. Schlein, and H.-T. Yau, Phys. Rev. Lett. **98**, 040404 (2007).

[72] E. H. Lieb and R. Seiringer, Phys. Rev. Lett. **88**, 170409 (2002).

[73] E. H. Lieb, R. Seiringer, and J. Yngvason, Phys. Rev. Lett. **91**, 150401 (2003).

[74] W. Ketterle and N. J. van Druten, Phys. Rev. A **54**, 656 (1996).

[75] L. S. Cederbaum and A. I. Streltsov, Phys. Lett. A **318**, 564 (2003).

[76] T. Helgakar, P. Jørgensen, and J. Olsen, *Molecular Electronic-Structure Theory* (Wiley, New York, 2000).

[77] P. J. Roberts, J. Chem. Phys. **42**, 879 (1964).

[78] J. Zanghellini *et al.*, Laser Phys. **13**, 1064 (2003).

[79] O. E. Alon, A. I. Streltsov, and L. S. Cederbaum, Phys. Rev. A **77**, 033613 (2008).

[80] M. H. Beck, A. Jäckle, G. A. Worth, and H.-D. Meyer, Phys. Rep. **324**, 1 (2000).

[81] P. A. M. Dirac, Proc. Cambridge Philos. Soc. **26**, 376 (1930).

[82] G. A. Worth, M. H. Beck, A. Jäckle, and H.-D. Meyer, The MCTDH Package, Version 8.2, (2000). H.-D. Meyer, Version 8.3 (2002). See http://www.pci.uni-heidelberg.de/tc/usr/mctdh/.
[83] A. Jäckle and H.-D. Meyer, J. Chem. Phys. **104**, 7974 (1996).
[84] A. Jäckle and H.-D. Meyer, J. Chem. Phys. **109**, 3772 (1998).
[85] H.-D. Meyer and G. A. Worth, Theor. Chem. Acc. **109**, 251 (2003).
[86] H.-D. Meyer, F. L. Quéré, C. Léonard, and F. Gatti, Chem. Phys. **329**, 179 (2006).
[87] E. B. Kolomeisky, T. J. Newman, J. P. Straley, and X. Qi, Phys. Rev. Lett. **85**, 1146 (2000).
[88] K. Góral, L. Santos, and M. Lewenstein, Phys. Rev. Lett. **88**, 170406 (2002).
[89] T. Lahaye *et al.*, Nature **448**, 672 (2007).
[90] G. Theocharis, P. Schmelcher, P. G. Kevrekidis, and D. J. Frantzeskakis, Phys. Rev. A **72**, 033614 (2005).
[91] A. Minguzzi, P. Vignolo, and M. P. Tosi, Phys. Lett. A **294**, 222 (2002).
[92] C. N. Yang, Rev. Mod. Phys. **34**, 694 (1962).
[93] H. G. Vaidya and C. A. Tracy, Phys. Rev. Lett. **42**, 3 (1979).
[94] G. J. Milburn, J. Corney, E. M. Wright, and D. F. Walls, Phys. Rev. A **55**, 4318 (1997).
[95] R. W. Spekkens and J. E. Sipe, Phys. Rev. A **59**, 3868 (1999).
[96] D. R. Dounas-Frazer, A. M. Hermundstad, and L. D. Carr, Phys. Rev. Lett. **99**, 200402 (2007).
[97] M. Albiez *et al.*, Phys. Rev. Lett. **95**, 010402 (2005).
[98] A. Smerzi, S. Fantoni, S. Giovanazzi, and S. R. Shenoy, Phys. Rev. Lett. **79**, 4950 (1997).
[99] T. Anker *et al.*, Phys. Rev. Lett. **94**, 020403 (2005).
[100] J. Javanainen, Phys. Rev. Lett. **57**, 3164 (1986).
[101] K. Winkler *et al.*, Nature **441**, 853 (2006).
[102] S. Fölling *et al.*, Nature **448**, 1029 (2007).
[103] T. Kinoshita, T. Wenger, and D. S. Weiss, Nature **440**, 900 (2006).
[104] A. N. Salgueiro *et al.*, Eur. Phys. J. D **44**, 537 (2007).
[105] A. P. Tonel, J. Links, and A. Foerster, J. Phys. A **38**, 1235 (2005).
[106] C. E. Creffield, Phys. Rev. A **75**, 031607(R) (2007).
[107] N. W. Ashcroft and N. D. Mermin, *Solid State Physics* (Brooks Cole, USA, 1976).
[108] M. P. A. Fisher, P. B. Weichman, G. Grinstein, and D. S. Fisher, Phys. Rev. B **40**, 546 (1989).
[109] A. M. Rey, Ph.D. thesis, University of Maryland at College Park, 2004.